DIPARTIMENTO DI INGEGNERIA DELL'INFORMAZIONE

CORSO DI LAUREA MAGISTRALE IN BIOINGEGNERIA INDUSTRIALE

PATELLO-FEMORAL JOINT BIOMECHANICS DURING KNEE FLEXION:
AN IN-SILICO INVESTIGATION

Relatore: Prof.ssa Silvia Todros

Laureanda: Chiara Botte

Correlatore: Prof. Piero Pavan
Correlatore: Prof. Bernardo Innocenti

ANNO ACCADEMICO 2022 – 2023

Data di laurea 20/10/2023

ABSTRACT

The objective of this study was to develop a Finite Element (FE) model of the knee joint with different configurations of patella height to analyse the biomechanics of the patellofemoral joint (PF) during knee flexion.

The PF joint is of key importance in the biomechanics of the knee. The primary role of the patella is to evenly distribute the load of the quadriceps and facilitate efficient knee extension. When the patella deviates from its normal tracking, it causes elevated strains on the PF ligaments, potential damage to soft tissues, and knee pain. Furthermore, this misalignment can result in excessive joint reaction forces and elevated stress on the articular cartilage, increasing the probability of cartilage wear and the formation of bone abnormalities that contribute to the development of osteoarthritis.

An FE model of the knee joint was developed with 3D geometry reconstructed from patient-specific medical images and considering the mechanical behavior of bones (considering cortical and cancellous bone), cartilage, menisci, ligaments, and tendons in a healthy native condition. After the validation of the model under physiological conditions, the position of the native patella was modified to simulate the high-riding patella syndrome (patella alta) and the low-riding patella syndrome (patella baja). In the literature, the patellar height is considered a factor that could impair patellofemoral contact force, contact area and contact pressure.

Patella alta can occur as a consequence of sports-related trauma; however, it appears to be a predominantly congenital/developmental condition, not related to traumatic events. The exact pathophysiology remains unclear, but it is hypothesized that abnormally elongated patellar tendons represent one of the etiologic factors contributing to the development of high patella.

On the contrary, patella baja can be caused by a variety of factors, including surgical interventions, traumatic events, or congenital abnormalities. From a biomechanical perspective, it decreases the lever arm of the quadriceps tendon, requiring increased quadriceps force to achieve complete knee extension. This inefficiency in muscle function can result in modified joint loading and increased stress on the patellofemoral joint.

Different FE models are developed, based on the anatomy of a subject with physiological patellar height and modifying the anatomical structure of the knee joint by increasing or decreasing the patella height with respect to the reference case along a superior (alta) or an inferior (baja) axis to achieve a different Blackburne-Peel index, which measures various

anatomical relationships between the patella and the proximal tibia and is one of the most widely used methods of evaluating patella height. The flexion motion was performed for all three models within a knee flexion range of 0° to 90°.

The comparison between numerical results under different conditions, namely physiological and modified patellar heights, allows one to quantify the differences in contact pressure and areas in a healthy and pathological state. Specifically, it can be observed that the patella alta exhibits the highest overall contact area and the lowest force attributable to contact pressure. This phenomenon arises because the point of contact with the femur is located more distally than in the native and patella baja configurations, and because the patella engages with the trochlear groove at deeper degrees of flexion (beyond 90°).

The results contribute to our understanding of the underlying mechanisms of patellofemoral disorders and can guide the development of more effective diagnostic and treatment approaches. Furthermore, the FE models developed in this study can serve as a valuable tool for future research in patellofemoral biomechanics and related research areas.

RIASSUNTO

L'obiettivo di questo studio è stato quello di sviluppare un modello agli elementi finiti (FE) dell'articolazione del ginocchio in diverse configurazioni di altezza della rotula, per analizzare la biomeccanica dell'articolazione femoro-rotulea (PF) durante la flessione del ginocchio.

L'articolazione PF è di importanza fondamentale nella biomeccanica del ginocchio. Il ruolo principale della rotula è quello di distribuire uniformemente il carico del quadricipite e facilitare un'efficiente estensione del ginocchio. Quando la rotula devia dal suo normale posizionamento, provoca sollecitazioni elevate sui legamenti PF, potenziali danni ai tessuti molli e dolore al ginocchio. Inoltre, questo disallineamento può provocare forze di reazione articolare eccessive e sollecitazioni elevate sulla cartilagine articolare, aumentando la probabilità di usura della cartilagine e la formazione di anomalie ossee che contribuiscono allo sviluppo dell'osteoartrite.

È stato sviluppato un modello FE dell'articolazione del ginocchio con geometria 3D ricostruita da immagini mediche specifiche di un paziente e considerando il comportamento meccanico di ossa (osso corticale e trabecolare), cartilagine, menischi, legamenti e tendini in una condizione nativa sana. Dopo la validazione del modello in condizioni fisiologiche, la posizione della rotula nativa è stata modificata per simulare la sindrome della rotula alta e della rotula bassa. In letteratura, l'altezza della rotula è considerata un fattore che può compromettere la forza di contatto femoro-rotulea, l'area di contatto e la pressione di contatto.

La sindrome della rotula alta può verificarsi come conseguenza di un trauma legato allo sport; tuttavia, sembra essere una condizione prevalentemente congenita/sviluppata, non correlata a eventi traumatici. L'esatta fisiopatologia rimane poco chiara, ma si ipotizza che i tendini rotulei anormalmente allungati rappresentino uno dei fattori eziologici che contribuiscono allo sviluppo della rotula alta.

Al contrario, la rotula bassa può essere dovuta a diversi fattori, tra cui interventi chirurgici, eventi traumatici o anomalie congenite. Da un punto di vista biomeccanico, diminuisce il braccio di leva del tendine del quadricipite, richiedendo una maggiore forza del quadricipite per raggiungere la completa estensione del ginocchio. Questa inefficienza nella funzione muscolare può determinare una modifica del carico articolare e un aumento delle sollecitazioni sull'articolazione femoro-rotulea.

Sono stati sviluppati diversi modelli FE, basati sull'anatomia di un soggetto con altezza rotulea fisiologica e modificando la struttura anatomica dell'articolazione del ginocchio aumentando o

diminuendo l'altezza della rotula rispetto al caso di riferimento lungo un asse superiore (alta) o inferiore (bassa) per ottenere un diverso indice di Blackburne-Peel, che misura vari rapporti anatomici tra la rotula e la tibia prossimale ed è uno dei metodi più utilizzati per valutare l'altezza della rotula. Il movimento di flessione è stato eseguito per tutti e tre i modelli in un intervallo di flessione del ginocchio compreso tra 0 e 90°.

Il confronto tra i risultati numerici in condizioni diverse, ovvero altezza della rotula fisiologica e modificata, consente di quantificare le differenze di pressione e aree di contatto in uno stato sano e patologico. In particolare, si può osservare che la rotula alta presenta l'area di contatto complessiva più elevata e la forza più bassa attribuibile alla pressione di contatto. Questo fenomeno si verifica perché il punto di contatto con il femore è situato più distalmente rispetto alle configurazioni native e alla rotula bassa e perché la rotula si inserisce nel solco trocleare a gradi di flessione più profondi (oltre i 90°).

I risultati contribuiscono alla comprensione dei meccanismi alla base dei disturbi patello-femorali e possono guidare lo sviluppo di approcci diagnostici e terapeutici più efficaci. Inoltre, i modelli FE sviluppatu in questo studio possono servire come strumento prezioso per la ricerca futura nella biomeccanica femoro-rotulea e nelle aree di ricerca correlate.

CONTENTS

CHAPTER 1 ANATOMY OF THE KNEE

The knee is the most sophisticated joint in the body and the largest of the synovial condyloid joints[1] (shown in Figure 1.1). It combines a wide range of motion with great stability (Hansen J.T. et al., 2019).
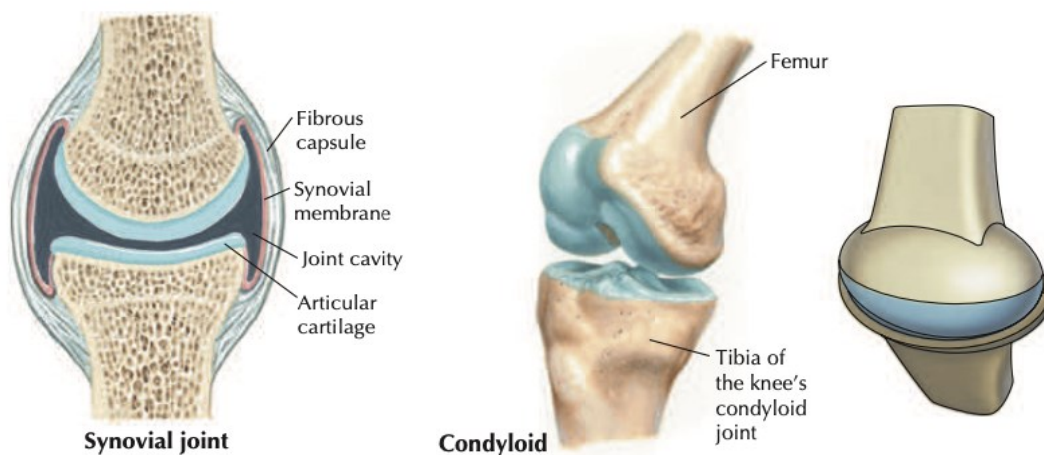
Figure 1.1 - Synovial condyloid joint of the knee (Hansen J.T.et al., 2019).

1.1 KNEE JOINT

The knee is a synovial joint of the human body that is subject to significant mechanical stresses during various daily activities. It is one of the most complex joints in the human body, consisting of multiple bones, ligaments, tendons, and muscles that work together to provide stability, mobility, and load transmission.

It is formed by the articulation of three bones: the femur, tibia, and patella. The femur is the bone of the thigh and is the largest bone in the body. The distal end of the femur has two rounded condyles (medial and lateral) that articulate with the tibial plateau. The tibia is located on the medial side of the leg. The proximal end of the tibia has two flat surfaces (medial and lateral tibial plateau) that articulate with the femoral condyles (Figure 1.2). The patella is located on the anterior aspect of the knee joint, is embedded in the quadriceps tendon, and acts as a fulcrum for knee extension.

The knee joint also involves the fibula bone, which is located on the outer side of the lower leg and helps stabilize the joint. The primary function of this bone is to be the distal attachment site of the lateral collateral ligament, and together with the lateral tibial condyle they form the tibio-

---

[1] It is the most prevalent form of joint, in which the bones are connected through a joint cavity containing a small quantity of synovial fluid. This cavity is enveloped by a capsule, and the bony surfaces that articulate with each other are coated with hyaline cartilage. Condyloid indicate that the joint permit biaxial movement.

fibular joint. However, this joint is usually not considered when dealing with the biomechanics of the knee (Innocenti B. & Galbusera F., 2022).

The bony components of the knee formed two joints: the tibio-femoral joint, between the distal part of the femur and the proximal part of the tibia, and the patellofemoral joint, between the distal part of the femur and the posterior part of the patella.

The knee joint is also supported by several ligaments, tendons, and muscles. The most important ligaments of the tibio-femoral joint include the anterior cruciate ligament (ACL), posterior cruciate ligament (PCL), medial collateral ligament (MCL), and lateral collateral ligament (LCL). The ligaments of the patellofemoral joint are the medial patellofemoral ligament (MPFL) and the lateral retinaculum (LR). More precisely the LR, it is not a real ligament, but is a net of soft tissue that keeps the link between the patellar tendon and the lateral side of the femur. The tendons surrounding the knee joint include the quadriceps tendon (QT), patellar tendon (PT), and hamstring tendons. The function of tendons is to transmit forces from muscles to bones, whereas muscles are responsible for applying forces. The muscles around the knee joint could be separate in two categories: extensors and flexors. The first group includes the quadriceps muscle, comprised of the rectus femoris, vastus medialis, vastus intermedius, and vastus lateralis. Instead, the second group includes gastrocnemius, semimembranosus, semitendinosus, and biceps femoris.
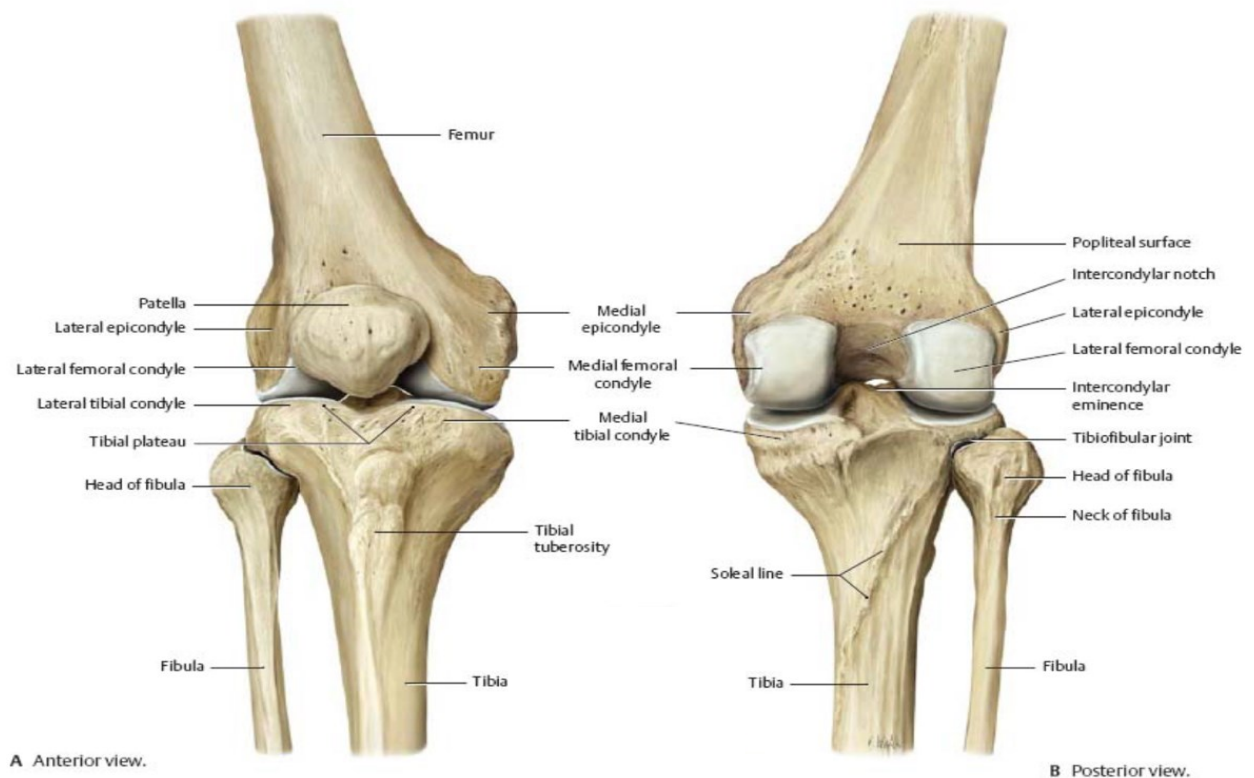
Figure 1.2 - Anatomy of right knee joint (Gilroy A. M. et al., 2008).

2

The tibiofemoral joint is a complex synovial joint. The tibial plateau, the proximal surface of the tibia, consists of medial and lateral articular surfaces that articulate with the corresponding femoral condyles. The congruence between the tibia and the femur is enhanced by the menisci, which create concave surfaces for articulation.

An important detail to note is that the continuity of the tibial plateau is interrupted by the presence of the so-called intercondylar eminence and two depressed areas, one anterior and one posterior to the eminence that accommodate the anterior and posterior horns of the lateral and medial menisci.

The longer oval-shaped medial articular surface is related to the medial meniscus along its anterior, medial, and posterior margins. The surface slopes upward in its anterior half and is flat in its posterior half. It forms a concave surface for the medial femoral condyle, and its lateral margin increases as it reaches the intercondylar region. The lateral articular surface is circular and adapted to its corresponding meniscus. In the sagittal plane[2], the surface is relatively flat in the central part, but slopes downwards anteriorly and posteriorly, creating a convex surface where the lateral femoral condyle fits.

As mentioned above, the anterior intercondylar area contains an anteromedial depression for the insertion of the anterior horn of the medial meniscus. Behind this depression, a smooth area provides attachment to the anterior cruciate ligament. The anterior horn of the lateral meniscus inserts in front of the intercondylar eminence, lateral to the anterior cruciate ligament. The eminence, with its medial and lateral tubercles, contributes to the stabilization of the femur. The posterior horn of the lateral meniscus is inserted into the posterior and downward sloping portion of the intercondylar area, while a depression behind the base of the medial intercondylar tubercle accommodates the posterior horn of the medial meniscus. The remaining area provides the insertion site for the posterior cruciate ligament (Standring S. et al., 2008).

The articulating surfaces of the tibia and femur are coated with a thin layer of hyaline cartilage, creating a smooth, low-friction surface for articulation and providing a certain level of shock absorption. The presence of the lateral and medial menisci between the two bones further contributes to shock absorption, aids in lubrication, and helps distribute force by improving the congruence of the joint surfaces.

---

[2] The sagittal plane is a vertical plane that extends longitudinally through the body, dividing it into two sections: a left section and a right section.

The four primary ligaments, already listed above, the anterior cruciate ligament, the posterior cruciate ligament, the medial collateral ligament, and the lateral collateral ligament, play crucial roles in maintaining the stability of the knee joint.
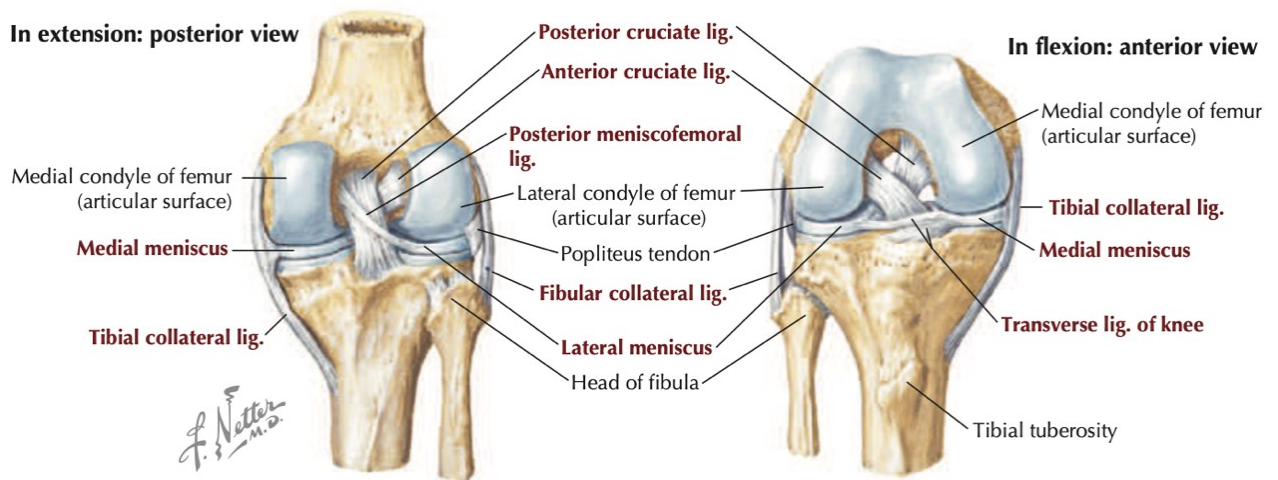
Figure 1.3- Ligaments of the tibio-femoral joint of the right knee (Netter F. H., 2019).

1.1.2 Patellofemoral Joint

The patellofemoral joint exhibits a high degree of complexity and research focused on this specific joint remains relatively limited (Ali A.A. et al., 2016; Baldwin M.A. et al., 2012; Fitzpatrick C.K. et al., 2010; Mizuno Y. et al., 2001; Baldwin M.A. et al., 2009).

The patellofemoral joint comprises the posterior surface of the patella and the trochlear surface of the distal anterior femur (Loudon J. K., 2016). The articular surface is located in the anterior front of the distal end of the femoral bone, centrally just above the femoral condyles and adjacent to the intercondylar fossa, which serves as the central groove that separates the femoral condyles in the inferior direction. In particular, this articulating surface is covered by hyaline cartilage.

On the contrary, the articular surface of the patella is located in the posterior aspect of the patella and is also protected by the articular cartilage. The articular surface of the patella aligns with the corresponding surface of the femur, which forms an inverted U-shaped intercondylar groove (or trochlear sulcus) with concave lateral and medical facets. When observed in the transverse plane[3], the entire region exhibits a concave contour, while in the sagittal plane it assumes a convex configuration. Collectively, these articulating surfaces generate an asymmetric saddle-like surface (Standring S. et al., 2008).

---

3 The transverse plane is a horizontal plane and it divides the body into an upper (superior) section and a lower (inferior) section.

The primary functions attributed to the patellofemoral joint include protecting the distal aspect of the femur from trauma and minimizing frictional wear to the quadriceps. Furthermore, it facilitates the transmission of quadriceps forces to the femur and patellar tendon, increases the lever arm of the quadriceps (a patellectomy can result in a reduction in force by up to 30%), reduces the magnitude of anterior-posterior tibio-femoral shear stress within the knee joint, and contributes to the aesthetic appearance of the knee (Innocenti B. & Galbusera F., 2022).

1.2 BONE: PATELLA, FEMUR, TIBIA,

1.2.1 PATELLA

The patella is a fully embedded sesamoid bone within the quadriceps tendon anterior to the distal part of the femur, providing an attachment point for the quadriceps tendon and the patellar tendon. It has a triangular shape with a flat and narrow distal end and a curved proximal region, featuring an anterior surface, a posterior surface, three sides, and an apex that forms its distal termination. When the knee is extended, the apex is positioned proximal to the knee joint line. The patella serves as a hard bone that articulates with the femur, covering and protecting the anterior articular surface of the knee joint.

The convex anterior surface of the patella appears corrugated due to longitudinal ridges and is separated from the skin by the prepatellar bursa. This surface is covered by an extension of the quadriceps femoris tendon that distally merges with the superficial fibers of the patellar tendon, representing a continuation of the quadriceps tendon. The posterior surface of the patella presents an oval smooth articular region in its proximal portion, intersected by a vertical edge that extends into the intercondylar incisura on the femoral surface of the patella. This edge divides the patellar articular surface into two facets, medial and lateral, usually the lateral facet being larger. In some cases, the posterior surface of the patella may have up to seven facets, three on the medial surface and four on the lateral surface. Below the articular surface, the apex of the patella is rough due to the insertion of the patellar tendon, while the area between the rough apex and the articular margin is covered by the infrapatellar fat pad. The articular cartilage that covers the patella is the thickest in the body due to the substantial amount of stress it encounters. The upper margin of the patella is thick and sloping anteriorly, and the medial and lateral margins are comparatively thinner and converge at the base.

In terms of structure, the patella consists predominantly of dense trabecular bone tissue covered by a thin layer of cortical bone. The trabeculae below the anterior surface run parallel to the

surface, while in other regions they radiate from the articular surface into the interior of the bone.

The primary functions of the patella are to improve the efficiency of the quadriceps by acting as a fulcrum, increasing the moment arm of the knee extensor mechanism, and protecting the quadriceps tendon from frictional forces by minimizing contact with the femur. Furthermore, it acts as a protective shield for deeper structures within the knee joint (Innocenti B. & Galbusera F., 2022, Standring S. et al., 2008, Cox C. F. et al., 2023).

1.2.1.1 Patella alta- Patella baja

The patellofemoral joint plays a crucial role within the intricate biomechanical network of the lower limb. It serves as a central pivot for the extensor mechanism, allowing efficient knee extension during various activities. The patella baja (inferior) and patella alta (superior) are two distinct anatomical variations that involve abnormal positioning of the patella within the trochlear groove of the femur. These conditions have biomechanical and kinematic implications that can affect knee function and potentially cause various problems (Cox C. F. et al., 2023).

The patella alta (shown in Figure 1.5a) is characterized by a high-riding patella that lies superior to the trochlear groove of the femur, causing the patella not to articulate with the trochlear groove until later in flexion. This places the patella at increased risk of dislocation or lateral patellar subluxation (Loudon J. K., 2016). Patella alta is present in $50 \div 60\,\%$ of primary patellar dislocations (Gao C. & Yang A. 2018). This condition is also associated with other patellofemoral abnormalities, including small patella, excessive patellar tilt, joint effusion, and ligamentous laxity. With a high-riding patella, the angle of the patellar tendon in relation to the tibia may be altered. This can affect the transmission of force from the quadriceps muscles to the tibia, potentially influencing joint stability and movement efficiency. The altered patellar position in patella alta can lead to an increased contact area between the patella and the femur during early knee flexion, and this can result in a decrease in contact stresses. The Blackburne-Peel index was used to define patellar height (Luyckx T. et al., 2009; Blackburne J. S. & Peel T. E., 1977) and measures the ratio of the perpendicular height from the tibial plateau line to the lower extremity of the patella articular surface (in Figure 1.4 named "A") and the length of the same articular surface of the patella (in Figure 1.4 named "B").
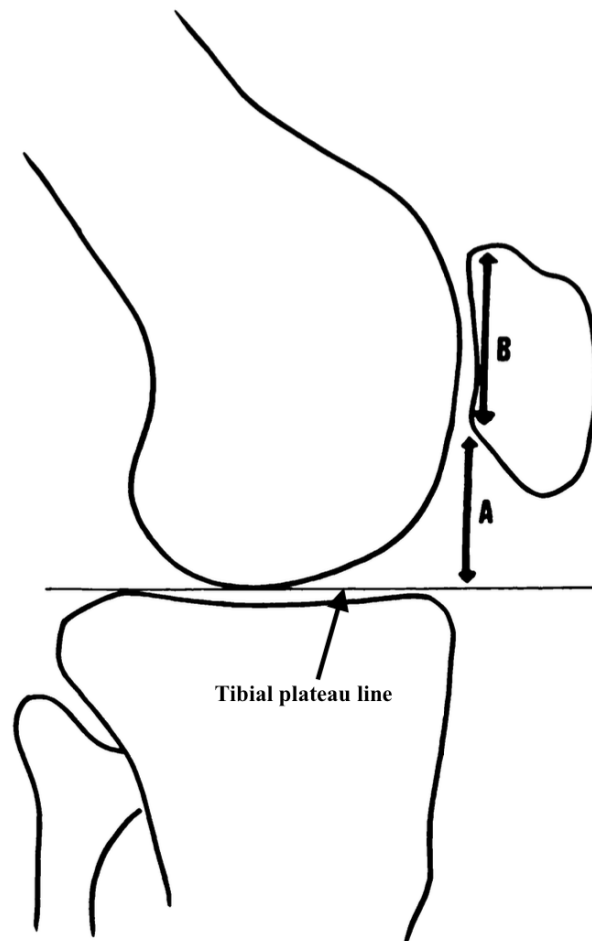
Figure 1.4 - Diagram showing the measurement method of "A" and "B".
(Blackburne J. S. & Peel T. E., 1977)

Generally, patella alta is diagnosed if the Blackburne-Peel index is greater than 1.

On the other hand, in patella baja (shown in Figure 1.5c), the patella is placed lower than its normal anatomical location within the trochlear groove of the femur. This can be due to various factors, including surgical procedures, trauma, or congenital conditions. Biomechanically, patella baja reduces the lever arm of the quadriceps tendon, requiring a greater quadriceps force to achieve full knee extension. This inefficiency in muscle function can lead to altered joint loading and stress on the patellofemoral joint. Furthermore, altered patellar tracking resulting from the patella baja can lead to irregular contact forces between the patella and the femur, contributing to cartilage wear, pain, and decreased joint stability. These changes are involved in the development of patellofemoral pain syndrome and other related conditions. Also patella baja can be defined by the Blackburne-Peel index; in particular, a ratio of 0.5 is a diagnostic of patella baja.

In conclusion, patella baja and patella alta are distinct variations in patellar positioning that result in differential biomechanics and kinematics within the patellofemoral joint. Understanding these variations is essential for diagnosing and managing related conditions, optimizing knee function, and devising effective rehabilitation strategies (Tecklenburg K. et al., 2006).
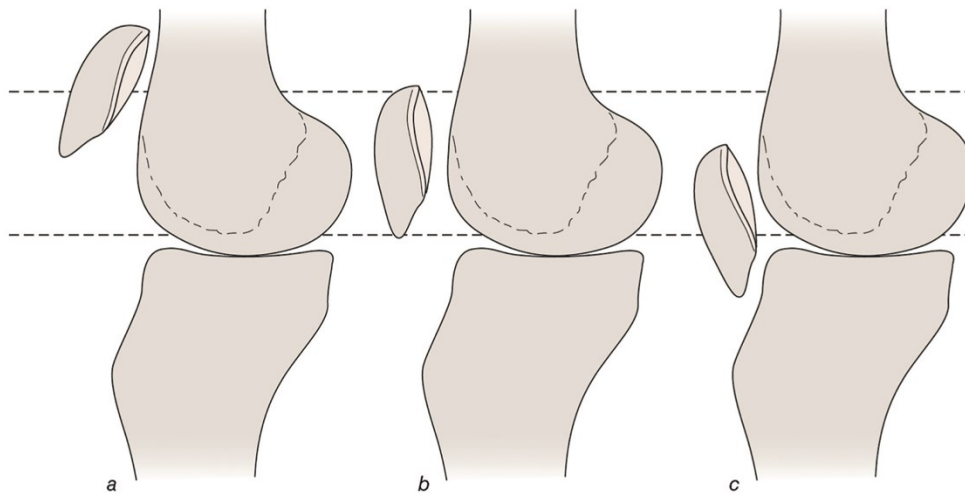
Figure 1.5- Patellar reference positions: a) patella alta; b) patellar normal position; c) patella baja (Loudon J. K., 2016).

1.2.2 FEMUR

The longest and strongest bone in the human body is the femur, which plays a crucial role in providing support and mobility. It has several anatomical features that contribute to its function and structure. The femoral diaphysis, which is mostly cylindrical, is bent forward. It has a rounded proximal head that projects medially from its neck. The distal extremity is wider and stronger, with a double condyle that articulates with the tibia.

In standing, the femoral diaphysis shows an inclination in the superior and external directions with respect to its articulation with the tibia, ensuring proper alignment with body weight. The degree of femoral obliquity varies between individuals, generally larger in women due to their relatively larger pelvic width and shorter femurs.

The femur involves a head, a neck, the greater trochanter, and the lesser trochanter. The head of the femur is spheroidal and faces anterosuperomedially to articulate with the acetabulum.

The femoral diaphysis, a cylinder of compact bony tissue, is surrounded by muscles and is not palpable. Its middle portion is relatively narrower and gradually widens towards the upper and lower ends. Its long axis forms an angle of approximately 10° with the vertical axis and diverges approximately 5-7° from the long axis of the tibia. This cylindrical structure comprises compact

bone tissue with a large medullary cavity. The wall of the femoral diaphysis is thick in the middle third and gradually thins as it extends proximally and distally. At the proximal end, dense trabeculae converge on a dense wedge, reinforcing the neck-body junction. Toward the distal end, the trabeculae descend perpendicularly to the articular surface, creating a series of cubic compartments.

The distal end of the femur acts as a load bearing surface to transmit weight to the tibia. It has two condyles (medial and lateral) that articulate with the tibial surface. The articular surface of the distal end is a wide area, similar to an inverted U, that accommodates the patella and tibia (Loudon JK., 2016). The patellar surface extends anteriorly on both condyles, with greater extension on the lateral condyle. The tibial surface is continuous with the patellar surface and divided by the intercondylar fossa. The femoral groove and condyles are covered by articular cartilage, allowing proper interaction with the patella and tibial condyles. The intercondylar fossa separates the two condyles distally and posteriorly. The lateral wall of the fossa presents a flat posterosuperior recess for the proximal insertion of the anterior cruciate ligament, while the medial wall presents a similarly large area for the proximal insertion of the posterior cruciate ligament.

These anatomical characteristics collectively contribute to the functionality and stability of the femur, allowing it to support weight, resist forces, and facilitate joint movement (Innocenti B. & Galbusera F., 2022, Standring S. et al., 2008).

1.2.3 TIBIA

The tibia, located on the inner side of the leg in relation to the fibula, is the second longest bone in the body after the femur. Its shaft has a triangular shape with expanded ends. The smaller distal end is projected downward as the medial malleolus. The front edge of the shaft is sharp and curves inward toward the medial malleolus.

The upper end of the tibia is also expanded and provides a weight-bearing surface for body weight transmitted through the femur. It consists of two plateaus, medial and lateral, an area between them called the intercondylar area, and the tibial tuberosity.

Both condyles have smooth, joint-shaped surfaces on top, separated by a non-articular area with an irregular shape known as the intercondylar area.

The tibial tuberosity is slightly raised and can be divided into a lower region with wrinkles and an upper region that is smooth and can be felt through the skin. A horizontal line across the

tuberosity of the tibia marks the lower limit of the upper cartilage of the tibia. The patellar tendon attaches to the smooth surface of the tuberosity. The distal portion of the tuberosity may have an oblique ridge, where the lateral fibers of the patellar tendon insert further down than the medial fibers.

The lower end of the tibia is slightly expanded and has five surfaces: front, medial, back, lateral, and bottom. Compared to the upper end, the lower end of the tibia rotates outward (tibial torsion). This torsion begins during fetal development and continues throughout childhood and adolescence until skeletal maturity (Standring S. et al., 2008, Koshi R., 2017).

In the front-to-back direction of the upper part of the tibia, the medial plateau of the tibia is concave, while the lateral plateau is convex, providing greater mobility on the outer side. Due to the greater force exerted on the inner side by the position of the femoral head, the medial plateau is larger than the lateral plateau, with up to 50% more surface area, and its articular surface is three times thicker (Innocenti B. & Galbusera F., 2022).

1.3 SOFT TISSUES: MENISCI, ARTICULAR CARTILAGE, LIGAMENTS AND TENDONS

There are several soft tissues that play a key role at the joint level. In the following, menisci, articular cartilage, tendons and ligaments will be discussed separately, describing their basic characteristics.

1.3.1 MENISCI

The menisci are two intracapsular fibrocartilaginous laminae, whose function is to make wider and deeper the articular surfaces of the tibia that accommodate the femoral condyles. Their outer edges are thick and convex, whereas their inner edges are thin and concave. The upper surfaces are smooth and concave, being in contact with the articular cartilage of the femoral condyles. The lower surfaces, flat and smooth, rest on the tibial articular cartilage. Approximately two-thirds of the articular surface of the tibia is covered by each meniscus. Two distinct structural regions are discernible within the menisci. The inner two-thirds comprise collagen bundles arranged radially, while the outer third is composed of thicker bundles arranged circumferentially. The innermost portion of the articular surfaces has thin bundles of collagen parallel to the surface, while the outermost portion is covered by the synovial membrane. This unique organization likely corresponds to specific biomechanical functions for

the two regions: the inner section is adapted to withstand compressive forces, while the outer section is designed to resist tensile forces (Standring S. et al., 2008, Koshi R., 2017).

The medial meniscus, which is wider towards the back, exhibits an almost C-shaped configuration. Its anterior horn attaches to the anterior tibial intercondylar surface in front of the ACL. The posterior horn is attached to the posterior tibial intercondylar surface between the insertions of lateral meniscus and PCL. Compared to the lateral meniscus, the medial meniscus is relatively stable and experiences less movement (Figure 1.6).

The lateral meniscus is round in shape and covers a larger area than its medial counterpart. The anterior horn is inserted ahead of the intercondylar eminence, positioned postero-laterally to the ACL. The posterior horn is linked to the area behind the eminence, in front of the posterior horn of the medial meniscus.
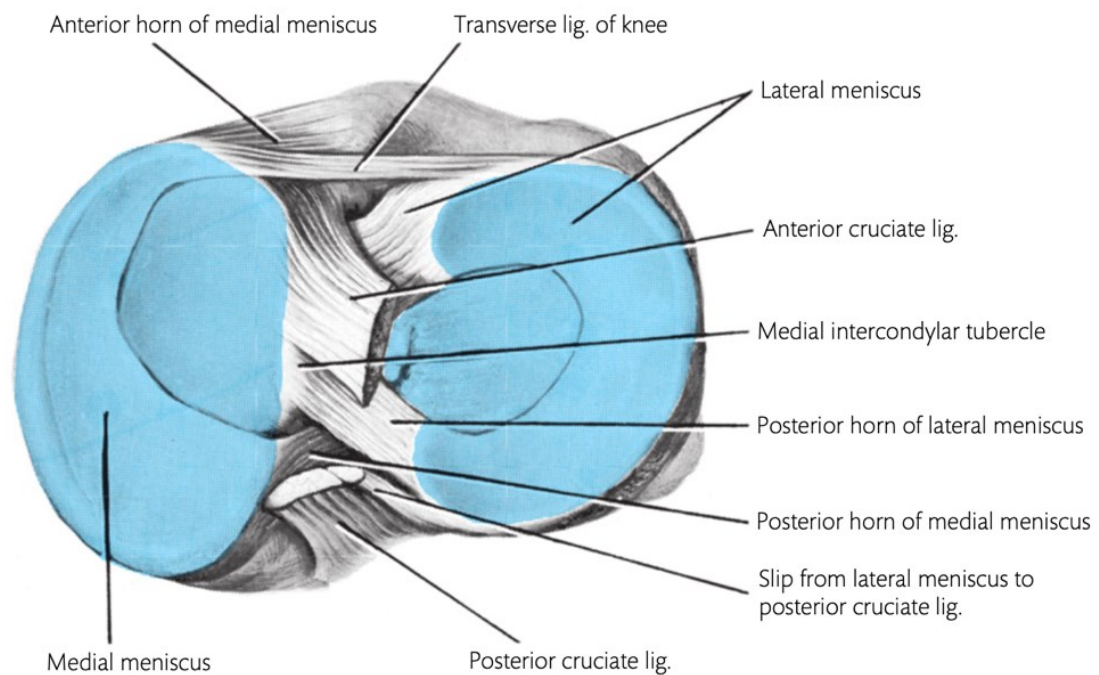
Figure 1.6 - Upper end of the tibia with menisci and portions of the cruciate ligaments (Koshi R., 2017).

The main role of the menisci, in conjunction with the articular cartilage, is to enlarge the contact area, thus reducing the pressure between the two articular surfaces within the knee joint (Innocenti B. et al., 2022).

1.3.2 ARTICULAR CARTILAGE

Articular cartilage is a thin layer of connective tissue that covers the surfaces of bones in joints, such as the knee, protecting bones from wear and allowing smooth movement with minimal friction. In the knee, the articular cartilage covers the lower surface of the femur (where the

femoral condyles are), the upper surface of the tibia (the tibial plateau), the patellar surface of the femur, and the posterior surface of the patella.

Articular cartilage consists of a dense extracellular matrix (ECM), composed of water, collagen, and proteoglycans, with a sparse distribution of cells, the chondrocytes. In addition to this solid matrix, it possesses a significant amount of water as a fluid component. Collagen provides mechanical strength to the solid matrix, while charged proteoglycans store water through osmosis, resulting in cartilage time-dependent behavior, i.e. creep and relaxation phenomena (Xia Y. et al., 2017).

Degenerative processes can lead to changes in the structure and composition of the ECM, affecting the biomechanical properties of the articular cartilage (Innocenti B. & Galbusera F., 2022).

1.3.3 *LIGAMENTS AND TENDONS*

Ligaments and tendons are fibrous connective tissues that interconnect various components of the musculoskeletal system, facilitating effective force transmission and facilitating movement in human joints. Ligaments establish connections between separate bones. Tendons, on the other hand, serve as bridges between muscles and bones, conveying the force generated by the muscles themselves. Both ligaments and tendons are composed of densely arranged and aligned collagen fibers embedded within a water-based matrix. Although water accounts for 60% to 80% of the wet weight, collagen, proteoglycans, and elastin constitute 65% to 85% of the dry weight.

Given their cordlike structure, most ligaments and tendons transmit forces along their main axis, while their response to bending and torsion is relatively minimal and often neglected (Innocenti B. & Galbusera F., 2022, Standring S. et al., 2008).

The role of the anterior cruciate ligament is to prevent excessive forward movement of the tibia relative to the femur, thus preventing hyperextension of the knee. On the contrary, the posterior cruciate ligament prevents excessive backward movement of the tibia relative to the femur.

The medial collateral ligament strengthens the inner side of the knee, preventing excessive forces from causing misalignment in the medial direction between the femur and the tibia or vice versa. It also adds stability to the medial meniscus due to its partial connection to this structure. On the other hand, the lateral collateral ligament fortifies the outer side of the knee.

Basically, the cruciate ligaments regulate stresses along the anteroposterior axis of the knee, while the collateral ligaments manage stresses in the lateral and medial directions.

The medial patellofemoral ligament plays an important role as the primary soft tissue restraint against lateral patellar displacement. The lateral retinaculum is not a clearly separate anatomical entity; rather, it consists of multiple layers of tissue on the front and side of the joint. The representation of the lateral retinaculum can be complex because it is made up of merging of tissue that has led to different understandings of these structures (Steensen R. N. et al., 2004; Shah K.N. et al., 2017).

The patellar tendon is a robust fibrous band that connects the lower patella to the tibial tuberosity. Its function involves stabilizing the patella for proper alignment and supporting the quadriceps femoris muscle in its action as a knee extensor.

The structure of the quadriceps muscle can be classified into distinct elements that run directly parallel to the femoral axis or diverge in different orientations. In particular, the vastus lateralis and medialis have smaller oblique segments near the lower end, contributing to a more significant transverse force vector. As a result, these elements play a crucial role in stabilizing the patella in the medial-lateral direction (Amis A.A. et al., 2003).

CHAPTER 2 KINEMATICS AND BIOMECHANICS OF THE KNEE JOINT

The knee joint is a very complex joint and fundamental for walking, which is why it is the subject of continuous research in therapeutic treatment and biomechanics modeling. In fact, several authors have proposed Finite Element (FE) models of the knee, but the transition from research to clinical application remains a challenge. Indeed, the problems of computational complexity, robustness to convergence, verification, and validation of these models are still being studied.

A deeper understanding of the biomechanics of the knee, including the kinematic mechanisms affecting the tissues of the joint, the responses of the biological system to external forces and the mechanical properties of the involved tissues, is fundamental to be able to develop a FE model that accurately describes the mechanical behavior of the joint.

2.1 THE GROOD-SUNTAY COORDINATE SYSTEM

The description by Grood & Suntay (1983) of an anatomical coordinate system has become one of the most widely used for delineating knee kinematics (Innocenti B. & Galbusera F., 2022). A coordinate system has the fundamental purpose of precisely defining the relative spatial relationship between two entities. The construction of this system for the knee involves the definition of three critical elements:

1) the Cartesian coordinate system fixed within each bone to elucidate its geometry;

2) the fixed axes of the body and the reference axes of the joint coordinate system, which delineate the interosseous motion;

3) the precise location of the translation reference point.

To explore the kinematics of the knee, the tibial coordinate system is firstly defined, as illustrated in Figure 2.1. A motion of clinical interest involves the internal-external rotation of the tibia around its mechanical axis. This axis, the z-axis in Figure 2.1, assumes the role of the fixed axis of the tibial body. Its positioning is equidistant between the proximal intercondylar eminences and crosses the center of the ankle distally. The reference direction is anterior and corresponds to the tibial y-axis. Operatively, the anterior tibial direction is defined as the cross product of the fixed axis with a line connecting the approximate center of each plateau.

The third axis, the x-direction, is defined through a right-hand coordinate system. The x-axis exhibits a positive orientation toward the right, resulting in a lateral orientation within the right knee and a medial orientation within the left knee.
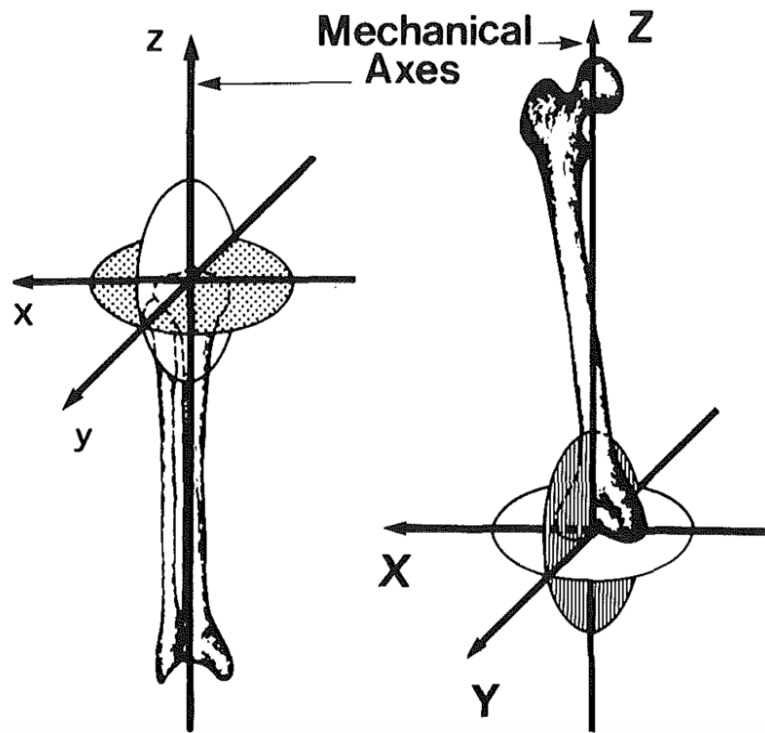

Figure 2.1 - In each bone, distinct Cartesian coordinate systems are established. The femoral system axes are denoted by capitalized letters X, V, Z, while the tibial system axes are represented by lowercase letters x, y, z. Common to both bones, the z-axis holds a positive orientation in the proximal direction, the y-axis is positively oriented anteriorly, and the x-axis assumes a positive orientation to the right (Grood E. S., & Suntay W. J. 1983).

Turning to the femur, the fixed axis of the body is chosen to align the rotations with the clinical flexion-extension motion. This means that the fixed axis must be perpendicular to the sagittal plane of the femur, thus aligning with the X axis of the femur in Fig. 2.1. To establish the flexion axis within the femur, it is necessary to start from the mechanical axis of the femur, the Z axis. This axis intersects the center of the femoral head proximally and the lowest point of the posterior surface of the femur between the medial and lateral condyles distally. From a practical point of view, the normal to the frontal plane (anterior axis) is defined through the cross product of the mechanical axis and a line connecting two points of the posterior femoral condyles. The direction of the flexion axis, embedded in the frontal plane of the femur, emerges through the cross product of the unit base vectors of the antero-posterior and mechanical femoral axes.

In summary, the fixed femoral axis governs flexion-extension, the fixed tibial axis is responsible for internal-external rotation, and the floating axis manages abduction-adduction motion (Grood E. S., & Suntay W. J. 1983).

16

2.2 THE TIBIO-FEMORAL JOINT KINEMATICS

The movements observed within most anatomical joints include three-dimensional motion, which can be defined by six independent coordinates or degrees of freedom. Among these, three coordinates correspond to translational motions, while the other three represent rotational movements using anatomical coordinate systems first described by Grood and Sunday, shown in the previous section.

From a functional and biomechanical point of view, the complex kinematics of the knee, in terms of tibio-femoral kinematics, is described by the following movements (Figure 2.2) (Innocenti B. et al., 2022):

- internal-external rotation (also known as axial rotation) and proximal-distal translation (or superior-inferior translation) are described along and about the tibial mechanical axis, respectively;

- flexion-extension and medial-lateral translation occur along and about the femoral epicondylar axis (flexion/extension axis), respectively;

- varus-valgus rotation and anterior-posterior translation occur, respectively, along and about a floating axis, obtained from the cross product of the previous tibial and femoral axes.
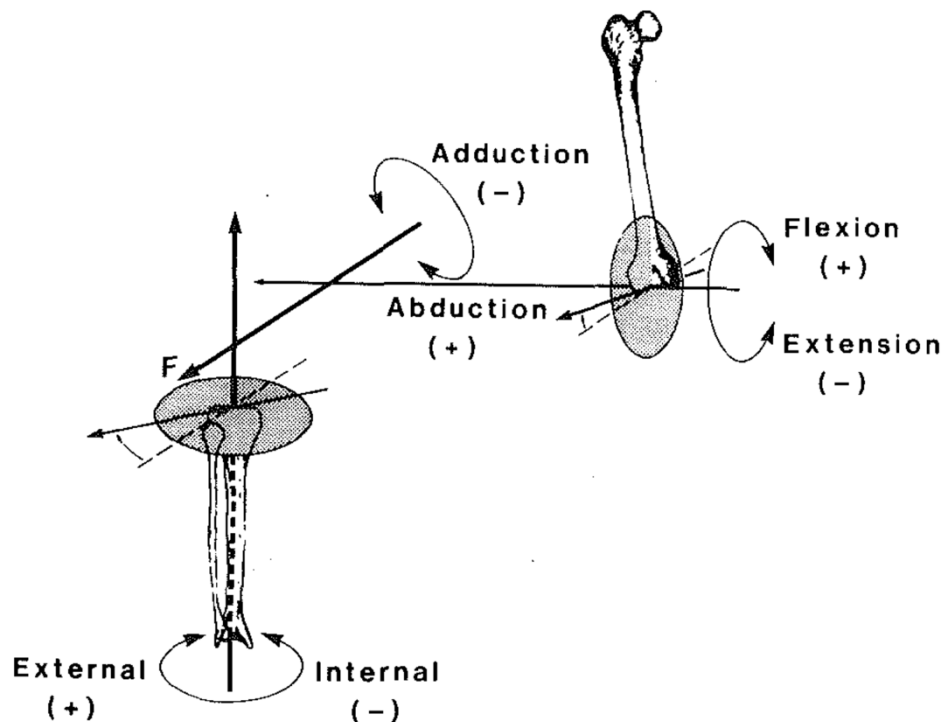

Figure 2.2 - Joint coordinate system of Grood and Suntay (Grood E. S., & Suntay W. J. 1983).

Among these motions, the flexion-extension one, occurring in the sagittal plane, clearly predominates over the others, with a range of motion from 0° in full extension to 140° in full flexion. In full extension, the femoral and tibial axes are aligned in the same plane. Instead, the range of motion in the other planes is much smaller and varies with the angle of flexion-extension. Rotational movements can manifest in any phase of flexion within the knee joint. During the end of extension, the femur undergoes medial rotation, while initiation of flexion leads to lateral rotation. During knee extension, the femoral condyles roll forward and slide backward on the tibial condyles (Standring S. et al., 2008). This backward sliding is crucial to allow the femur to maintain contact within the limited articulation area of the tibia. As the knee extends, the regions where the femur is in contact the tibia consistently shift forward in the femoral condyles. The extension of the lateral condyle reaches its peak before the extension of the medial condyle, and this extension is stopped by the tense ACL. Due to the flatter anterior curvature of the medial femoral condyle compared to the more spherical lateral condyle, the medial condyle continues to slide backward even after the lateral condyle is stopped. The maximum of extension involves medial femoral rotation, which effectively secures the femur to the tibia, tightening the ligaments, and achieving joint "locking". On the contrary, the sequence of movements for flexion mirrors these processes in reverse. The initiation of flexion is characterized by lateral femoral rotation, facilitated by differences in the shapes of the two condyles. This rotation effectively "unlocks" the knee joint and, after this, the knee flexors manage the process of flexion (Koshi R. 2017).

Several techniques have been used to investigate the kinematics of the human knee, and this remains an area of interest for industry professionals, clinicians, and biomechanics researchers.

A specialized two-dimensional representation of knee joint motion is called the "four-bar model" (Figure 2.3). This model considers motion within the sagittal plane, omitting tibial rotation, medial-lateral translations, and abduction and adduction. Assuming that the cruciate ligaments can be approximated as rigid connections ("bars") of constant length, and considering the other two "bars" formed by connecting the proximal tibial insertion points and the distal femoral points, it is evident that the instant center of rotation must consistently coincide with the intersection of the cruciate ligaments. Consequently, the knee is hypothesized to be a mechanism, allowing the position of the femur relative to the tibia to be deduced from a single variable. This principle reveals that the ACL, due to the increase in the radius of the femoral condyle during flexion, becomes progressively tense, pulling the femur towards the tibia.

However, this model has notable limitations, mainly treating the knee as symmetric and ignoring internal/external rotation.
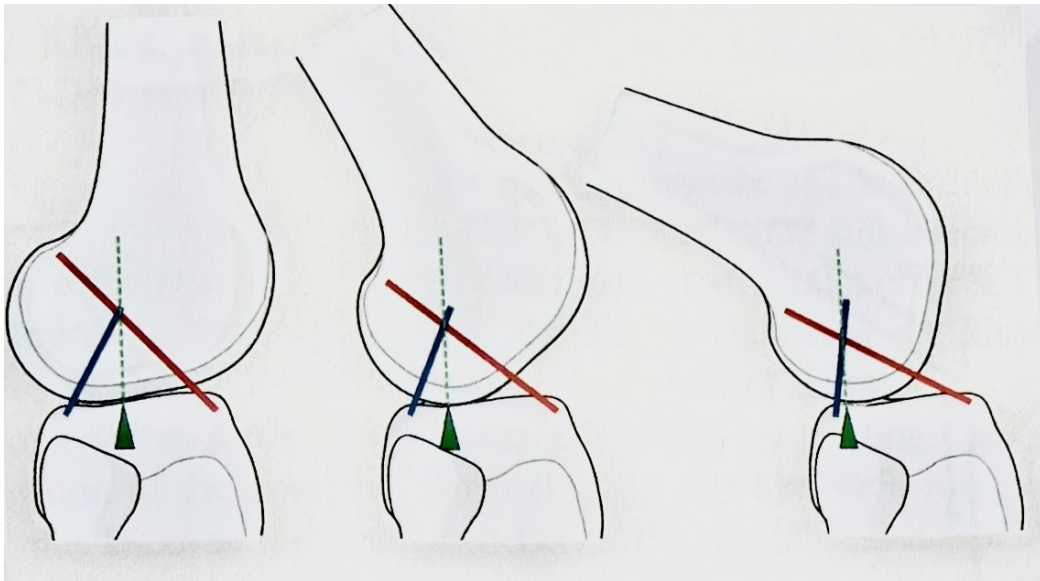

Figure 2.3 - The four-bar linkage model (Innocenti B. & Galbusera F. 2022).

In an effort to improve the knee model while maintaining a low number of degrees of freedom (DOFs), some researchers proposed an alternative approach. They divided the knee movement considering the kinematic analysis into the medial and lateral sides, avoiding the planar motion constraints of the earlier model. Using this refined model, the researchers studied the passive motion of the natural knee and were able to elucidate the medial pivoting knee motion and the roll-back behavior of the knee:

- The medial and lateral condyles exhibit different kinematics.

- In full extension, the center of the medial condyle aligns with the medial tibial condyle (slightly posterior), while the point of the lateral condyle is more anterior.

- During initial flexion, the medial condyle attempts to maintain its original position, limiting the anteroposterior translation. Meanwhile, the lateral condylar center moves posteriorly. This phase, in which the movement of the knee rotates around the medial condyle, is called the "medial pivot knee".

- Between 60° and 90° of flexion, the internal rotation of the femur decreases and both the medial and lateral condyles begin a posterior translation, known as "knee roll-back".

In summary, when applying a minor anteroposterior force, the lateral part initiates swift movement while the medial part remains stable (medial pivot). Only at considerable flexion

angles does the lateral part also move posteriorly in relation to the medial part, resulting in a posterior translation for both parts (roll-back) (Innocenti B. & Galbusera F., 2022).

The typical kinematic sequence of the external rotation of the human knee involves the tibia in relation to the femur as flexion increases. Furthermore, the lateral femoral condyle exhibits a more pronounced anterior translation compared to the medial femoral condyle. However, diverse patterns may arise based on joint health and individual anatomical attributes, in fact, the entities of these movements can significantly differ among individuals due to factors such as anatomy, age, and training.

2.3 THE PATELLOFEMORAL JOINT KINEMATICS

The patellofemoral articulation constitutes a complex joint in which the reaction forces are a function of quadriceps force, and the angle of flexion of the knee. Therefore, comprehending the biomechanics of the patellofemoral joint in physiological conditions is fundamental for the study of overall knee biomechanics.

The main role of the patella is to optimize knee extension by serving as a fulcrum that shifts the line of action of the quadriceps muscles anteriorly (Luyckx T. et al., 2009). This results in an increased lever arm for the quadriceps muscle moment relative to the knee's center of rotation. In particular, this mechanism contributes significantly to the knee extension torque, providing 31% of the total torque in full extension and reducing to 13% within the range of 90° to 120° of flexion. Furthermore, the patella serves as a protective shield for the anterior trochlea and minimizes friction between the quadriceps tendon and femoral condyles due to its position (Loudon JK., 2016). Functionally, the patella optimizes the distribution of the patellofemoral compressive forces, improving the contact area during flexion. It also acts as a guide for the extensor mechanism by coordinating the traction forces from various heads of the quadriceps and transmitting them to the patellar tendon. Lastly, the anatomical configuration of the patellofemoral joint functions as a safeguard against extensor apparatus dislocation. However, to accomplish these functions effectively, it is crucial to maintain proper patellar alignment and achieve optimal sliding during the dynamic process of knee flexion-extension (Innocenti B. & Galbusera F., 2022).

The relative motion between the patella and the distal femur, that determines the patella stability, is governed by four primary factors: joint geometry, the dynamic action of muscular structures that impact the patella, passive restrictions imposed by surrounding soft tissues, and alignment of the lower limb. From a kinematic perspective, the patellofemoral joint functions

as a sliding articulation, evidenced by the patella caudal movement of 7 cm during full flexion, coupled with concurrent internal-external rotation. In full extension, the patella remains unarticulated with the femur, allowing minor medio-lateral translation due to lateral retinaculum stiffness while in the standing position.

However, the comprehensive trajectory of this bone is three-dimensional. Additionally, antero-posterior translation is significant, since the patellar position during flexion causes a shift in the anteroposterior direction of the patellar tendon force. This force pulls the tibia anteriorly during lower flexion angles and pushes it posteriorly during higher flexion angles.

In a clinical context, the Q-angle serves as a widely used parameter to assess the alignment of the pull of the quadriceps muscle. Representing the angle between the quadriceps pull line (from the anterior superior iliac spine to the mid-patella) and a line connecting the patellar center with the tibial tuberosity (Figure 2.4), normal Q-angles are typically 10°-13° for men and 15-17° for women. In the frontal plane, the Q-angle introduces a lateral force on the patella due to the difference between the line of force of the quadriceps muscle and the patellar tendon. An increase in the Q-angle leads to an increase in the lateral force, translation, rotation, and lateral shift, increasing the risk of subluxation. On the contrary, a decrease in the Q-angle results in a decrease of the lateral force and translation (Loudon JK., 2016). Furthermore, an elevated Q-angle tends to amplify the lateral patellofemoral contact pressure, while a reduced Q-angle promotes an increase in the medial patellofemoral contact pressure (Mizuno Y. et al., 2001).
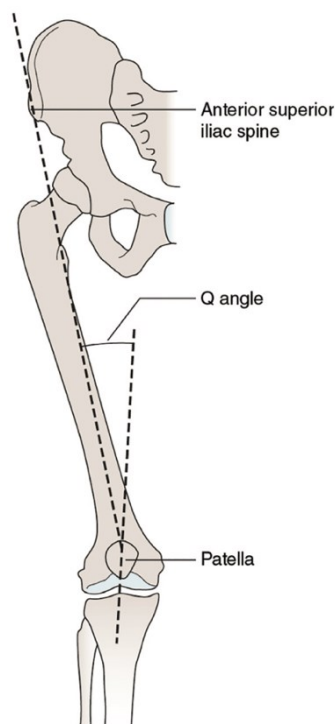

Figure 2.4 - Quadriceps Angle (Q-angle) (Loudon JK., 2016).

In conjunction with the interactions between the femur and tibia, during extension, the patella progressively elevates on the femur patellar surface. Given that the pull of the quadriceps on the patella aligns with the obliquity of the femur, the patella tends to deviate laterally during its ascent. This lateral deviation of the patella is countered by: (a) the greater anterior projection of the lateral femoral condyle; and (b) the horizontal insertion of the lowest fibers of the vastus medialis into the medial surface of the patella. Collectively, these factors ensure that the quadriceps force remains perpendicular to the axis of flexion and extension (Koshi R., 2017).

Functioning as a gliding joint, the patella manifests motion across multiple planes. These movements include superior/inferior glide, medial and lateral shift, medial and lateral tilt, as well as medial and lateral rotation (Figure 2.5). Termed patellar extension, superior glide occurs during tibio-femoral extension when the quadriceps contract, resulting in superior pull on the patella. On the contrary, patellar flexion corresponds to inferior glide and aligns with tibio-femoral flexion. Translations in the frontal plane drive lateral and medial shifts, mirroring tibio-femoral motion. In lateral shift, the lateral edge approaches the lateral side of the knee, whereas the medial shift pushes the medial side toward the medial edge of the knee. Tilt, which occurs along a longitudinal axis, involves the medial posterior facet moving closer to the medial femoral condyle in a medial tilt, and the lateral posterior patellar facet moving closer to the lateral femoral condyle in a lateral tilt.
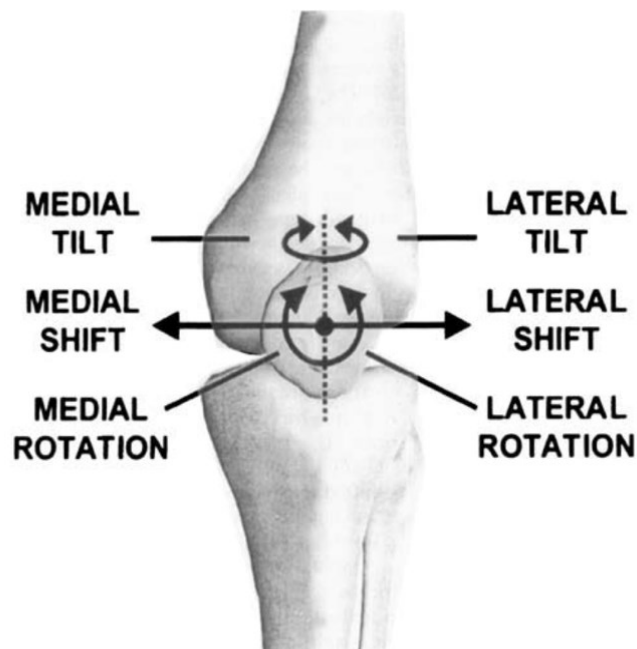

Figure 2.5 - The patellar kinematics are characterized by parameters such as patellar tilt, rotation, and shift. Tilt involves rotation around the patellar's long axis, rotation describes to movement around an anterior-posterior axis, and shift refers to medial-lateral translation (Mizuno Y. et al., 2001).

During knee flexion in a healthy knee, there is typically minimal lateral or medial movement, as the patella tends to maintain its central position on the trochlea. During extension of the knee from around 45° to full extension, the patella tilts medially, transitioning from an initially lateral tilt attributed to the geometry of the femoral trochlear groove. When flexed to approximately 30°, the patella reverts back laterally, retaining this lateralized position throughout the remaining flexion phase (Loudon JK., 2016).

Patellofemoral joint pain (PFP)

Patellofemoral joint pain (PFP) is prevalent in a variety of active individuals, biomechanical dysfunction is the primary factor underlying the development of this pathology. Furthermore, the optimal functioning of the patellofemoral joint depends on a delicate equilibrium within the surrounding soft tissue structures. Therefore, imbalanced tension from specific structures can induce an intensified force distribution between the patella and femur, inducing pain (Loudon JK., 2016; Standring S. et al., 2008). Anterior knee pain is often associated with malalignment and maltracking of the patella. During knee flexion, the lateral orientation of the quadriceps muscle generates a lateral force component that affects the patella. A maltracking toward the lateral side can increase the pressure between the lateral trochlear ridge and the patella, increasing the vulnerability to subluxation or dislocation of the patella. This increased pressure has the potential to generate patellofemoral pain and lead to degeneration of articular cartilage, even in the absence of instability episodes (Mizuno Y. et al., 2001).

Contact area

The patellar contact area undergoes a progressive expansion as knee flexion increases, effectively distributing joint forces across a larger surface. As the knee initiates flexion, the lower part of the patella engages with the upper section of the femoral condyles. This initial contact emerges between the lateral femoral condyle and the lateral facet of the patella, with an even distribution on both sides of the condyles by 30° of flexion. The contact region, initially compact, gradually enlarges as joint congruency improves (Innocenti B. & Galbusera F., 2022). Beyond 90° and up to 120° of knee flexion, the upper aspect of the patella interfaces with the femoral groove area. In deep flexion, there is only contact on the far medial and lateral edges of the patella. With progressive knee flexion, the patella articulating surface experiences continuous shifts. The contact point moves proximally along the patella and posteriorly-inferiorly along the femoral condyles (Loudon JK., 2016).

2.4 PATELLOFEMORAL FORCES

To comprehensively analyze the forces affecting the patellofemoral joint, it is necessary to focus on their action within the sagittal plane. We can introduce the notion of patellofemoral reaction force (PF), a combined effect generated on the patella, from both the quadriceps force (QF) and the patellar tendon force (TF) (depicted in Figure 2.6). These forces are intricately linked to patella change in the position in response to the varying flexion angles. These fundamental forces are derivated through the manipulation of different joint angular movements (Kumbhalkar M. A. et al., 2021). As flexion increases, the force magnitude grows; it is attributed to the progressive narrowing of the angle formed between the patellar tendon and the quadriceps, which leads to the increase of the resultant PF vector. Additionally, the elongation of both the tibial and femoral lever arms requires increased quadriceps strength to reduce the moment generated by the force of body weight (Innocenti B. & Galbusera F., 2022).
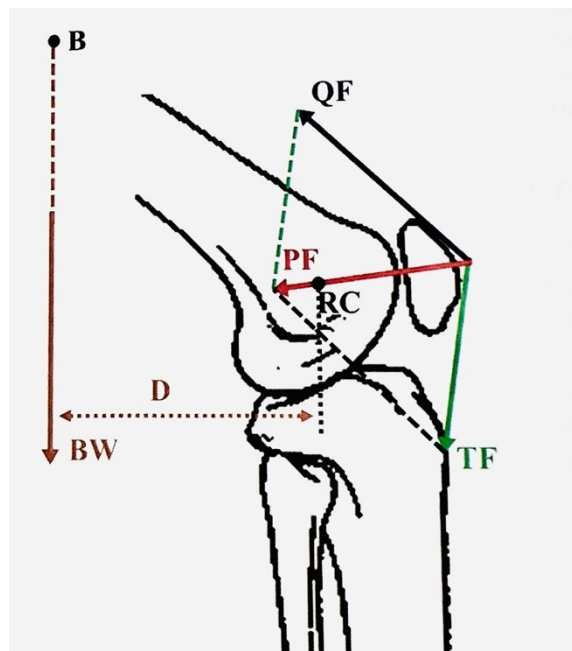

Figure 2.6 - The forces exerted on the patellofemoral joint within the sagittal plane. The patellofemoral reaction force (PF) results from the combined vector of the quadriceps muscle force (QF) and the patellar tendon force (TF). RC is the instantaneous rotation center of the knee. D represents the distance between RC and the vertical line extending through the body's center of gravity (B), where the force of body weight (BW) is exerted (Innocenti B. & Galbusera F., 2022).

The effective load exerted on the patellofemoral joint is calculated by PF divided by the contact area of the joint, denoting it as joint stress measured in terms of force per unit area. A larger interface between the patellar surface and the femur leads to a decrease in stress on the articular tissue. However, a combination of high PF and limited contact area results in elevated

patellofemoral joint stress, which could negatively affect joint cartilage. This stress can be aggravated by not optimal patellar positioning (Loudon JK., 2016). Excessive stress on the patellofemoral joint, as previously mentioned, appears to be the cause of PFP. This joint stress might arise due to irregular anatomy, misalignment, or deviant patellar tracking. Malalignment of the patella (lateralization) induces excessive compressive stress on the lateral facets of the patella, contributing to PFP. In general, it can cause undesired stress within the patellofemoral joint. Maintaining an equilibrium between medial and lateral stability is essential to preserve proper biomechanics of the patellofemoral joint (Loudon JK., 2016).

The primary inhibitor of lateral patellar displacement is the trochlear groove of the femur, especially the depth and inclination of the lateral femoral condyle. As the knee approaches extended flexion, the PF causes the patella posteriorly in the trochlear groove, exerting pressure along the sagittal plane, reducing its susceptibility to lateral dislocation (Innocenti B. & Galbusera F., 2022). On the contrary, this posterior force decreases during extension, whereas the lateral component increases due to external rotation of the tibia, a phenomenon known as the screw-home mechanism. In a normal patella, the lateral facet exceeds the medial facet in dimensions, facilitating the transmission of approximately 60% of the total force (Luyckx T. et al., 2009).

A crucial parameter in computing patellar forces is the distance "D" between the vertical line intersecting the body's center of gravity (barycenter) and the instant axis of joint rotation (RC in Figure 2.6). Adjusting posture in the sagittal plane (forward or backward) alters this distance, resulting in significant fluctuations in patellar force. For example, when body weight shifts posteriorly and away from the joint, the compressive force on the patella increases. In contrast, during activities that involve flexion under load, such as due to hip flexion during normal movements, the center of gravity moves forward, thus shortening the lever arm D. This phenomenon also accounts for variations in patellar force during actions like ascending stairs (forces ranging from 1.8 to 2.3 times body weight (BW)) and descending stairs (2.9 to 6.0 BW). Consequently, patellofemoral reaction forces exhibit considerable variability, mainly depending on the type of activity performed, with values ranging from 0.6 times body weight during walking to 7.7 times body weight while jogging and even up to 20 times body weight during jumping (Innocenti B. & Galbusera F., 2022; Loudon JK., 2016).

2.5 BONE

Bone is a complex and heterogeneous connective tissue that exhibits anisotropic[4], non-linear, and hierarchical properties (Innocenti B. & Galbusera F., 2022). Its mechanical characteristics are derived from geometry, density, microstructure, and material properties. Unlike other connective tissues, due to their greater stiffness and strength (Cowin S. C. & Doty S. B., 2007), bone's abundant mineral content makes it well-suited for structural and supportive rule. The bone shape dynamically adapts to varying environmental conditions, responding to the individual's activity and variations in applied loads. For this reason, biological remodeling continually renews bone tissue. Cortical and trabecular bone, the two main types of bone tissue, support significant stress during movement and activities such as weightlifting or rapid running and are strategically distributed within the bones, optimizing the properties of the tissue. The cortical bone forms the diaphysis and outer shell of long, short, flat, and irregular bones, whereas the trabecular bone exists in epiphyses and central regions of other types of bone. Given that bones experience both cyclic and static loading, their mechanical behavior is significantly influenced by fatigue and creep responses (Keaveny T.M. et al., 2005).

2.5.1 Mechanical properties and constitutive models

Although cortical and trabecular bones exhibit similar compositions and thus display comparable microscopic mechanical characteristics, variations in density and microstructure result in distinct macroscopic mechanical attributes. Cortical bone, as demonstrated by mechanical tests (Innocenti B. & Galbusera F., 2022), exhibits greater stiffness and reduced ductility compared to trabecular bone. These divergences in mechanical characteristics arise primarily from differences in the volume fraction[5] of the bone and the architectural arrangement. In particular, the porosities within these microstructures significantly influence their mechanical behavior. Cortical bone and trabecular bone exhibit linear strain-stress

---

[4] Anisotropy refers to the property or quality of a material exhibiting different characteristics or behaviors depending on the direction in which they are measured or observed. It signifies that the properties of the material are not uniform in all directions.

[5] It is the volume of mineralized bone per unit volume of the sample (bone volume/total volume).

relationships at the macroscopic level in the range of low strains (Figure 2.7). In addition, they show comparable elastic constants for both tensile and compressive loads.
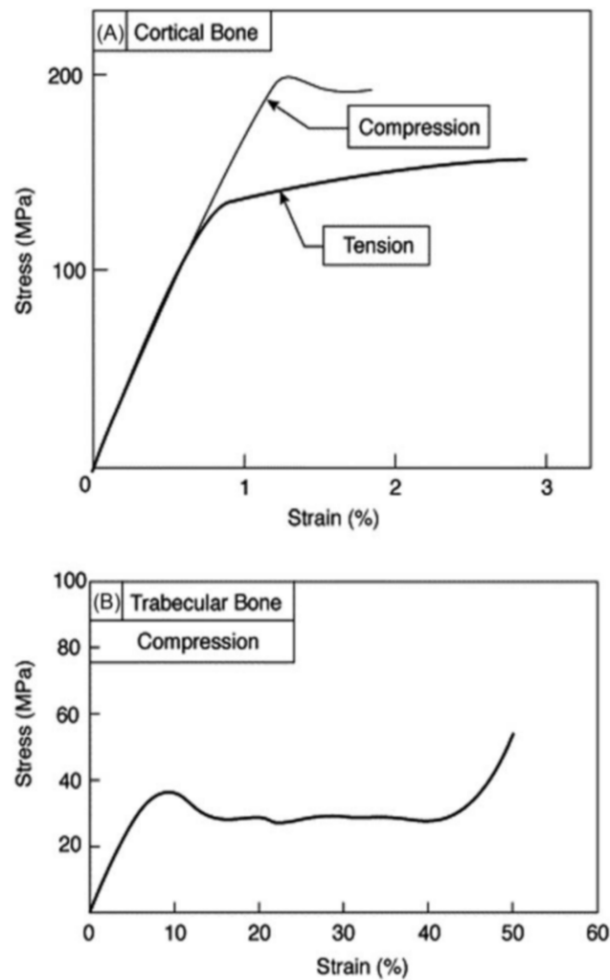

Figure 2.7 - Mechanical characteristics of cortical and trabecular bone. Common stress-strain curves representing cortical (A) and trabecular (B) bone samples subjected to compression or tension testing (Innocenti B. & Galbusera F., 2022).

Cortical bone

As said above, reflecting its microstructural anisotropy, the mechanical properties of human cortical bone exhibit anisotropy. A set of orthogonal directions can be defined. The first aligns with the longitudinal axis of the diaphysis, constituting the strongest and most rigid orientation. The second and third directions are mutually perpendicular within the plane orthogonal to the prior one. These are known respectively as the radial and circumferential directions, where mechanical properties are comparatively lower than the longitudinal direction, even though small differences in modulus and strength are noted between the radial and circumferential orientations. This tendency probably derivates from the evolutionary adaptation aimed toward resisting predominant uniaxial strains occurring along the diaphyseal axis during activities like walking (Keaveny T.M. et al., 2005). The presence of these three perpendicular planes of symmetry establishes cortical bone orthotropic material symmetry (ORTH) (Cowin S. C. &

Doty S. B., 2007) or transversely isotropic symmetry (TI)[6]. Furthermore, it is evident that the ultimate strength and strain in compression exceed the corresponding tension values (Innocenti B. & Galbusera F., 2022), providing the greater resistance of the cortical bone to compression loading. This divergence arises from the nonhomogeneous, anisotropic composite nature of bone. The level of anisotropy of bone tissue varies with anatomy and between individuals (Cowin S. C. & Doty S. B., 2007), while also being influenced by factors such as age, gender, load orientation, strain rate, and test conditions (dry or wet).

Cancellous bone

The cancellous bone, also known as trabecular or spongy bone, comprising short struts called trabeculae and interconnected elements, has a porous appearance. As a heterogeneous porous cellular solid, trabecular bone possesses anisotropic mechanical characteristics (Keaveny T.M. et al., 2005) influenced by both the porosity of the specimen and the spatial arrangement of individual trabeculae. Undergoing compression beyond its elastic threshold, unloading and then reloading, it exhibits a reduction in stiffness and the development of permanent strain. In compression, it yields at approximately 1% strain (Keaveny T.M. et al., 2005), after which it can support significant deformations, up to 50% strain, while retaining its load-bearing capacity. This makes the trabecular bone capable of absorbing considerable energy when mechanical failure. Its elastic and strength properties change depending on donor age, health, anatomical location, loading direction, and loading mode (Innocenti B. & Galbusera F., 2022).

Table 2.1 shows some references from the literature on the modeling of cortical and cancellous bone in the knee joint in a finite element analysis.

The selection of material symmetry for an elastic bone model is significantly dependent on the intended investigative application. Visual examination of cortical bone tissue reveals inherent orthotropic elastic symmetry (Cowin S.C. et al., 2007). The degree of anisotropy within bone tissue varies with the anatomical site and individual to individual, implying that some cortical bone tissue may possess transversely isotropic or even isotropic characteristics. Examined by Cowin and Doty (2007), the percentage divergence between elastic constants derived under ORTH and TI assumptions is minimal and has negligible effects on stress values. Thus, for stress analysis, a TI symmetry can be adequate. However, when considering the behavior of the physiological bone tissue composite material, the distinction between ORTH and TI

---

6 An orthotropic material is a type of anisotropic material that exhibits distinct mechanical properties along three mutually perpendicular axes.
A transversely isotropic material is a specific subtype of orthotropic material, characterized by having symmetry about one axis while having varying properties along the remaining two perpendicular axes.

assumptions may be notable. Despite this, numerous authors (Baldwin M.A. et al., 2009; Mesfar W., & Shirazi-Adl A. 2005; Baldwin M.A. et al., 2012; Blankevoort L. et al., 1991; Bendjaballah MZ. et al., 1995; Peña E. et al., 2006) regard cortical bone as a rigid body, implying the absence of deformation. In some cases, when joint kinematics is the focal point, treating the bone of the knee joint as rigid bodies is sufficient. On the contrary, for the analysis of bone stress and strain on contact surfaces, the development of a transversely isotropic linear elastic model for cortical bone becomes essential, a task undertaken by multiple authors (Innocenti B. et al., 2014; Cowin S.C. et al., 2007; Soenen M. et al., 2013; Kayabasi O. et al., 2007; Innocenti B. et al., 2016a).

Regarding cancellous bone, Cowin and Doty's examination (2007) suggests that it can be considered orthotropic or, in specific cases, transversely orthotropic. Despite often demonstrating nonlinear elastic properties even at low strains (Keaveny T.M., 2005), it is frequently modeled as linearly elastic material (Pianigiani S. et al., 2018; Kayabasi O. et al., 2007; van Jonbergen H.P. et al., 2012; Innocenti B. et al., 2009).

Authors	Constitutive model and mechanical properties
Innocenti, B. et al., (2014)	*Cortical bone* → Transversely isotropic • Young's Modulus [MPa]: $E_1 = 17,800$; $E_2 = 9,600$; $E_3 = 9,600$; • Poisson's Ratio: $\nu_{12} = 0.30$; $\nu_{13} = 0.30$; $\nu_{23} = 0.55$; *Cancellous bone* → Transversely isotropic • Young's Modulus [MPa]: $E_1 = 344$; $E_2 = 99$; $E_3 = 99$; • Poisson's Ratio: $\nu_{12} = 0.38$; $\nu_{13} = 0.38$; $\nu_{23} = 0.23$;
Soenen, M. et al., (2013) *Kayabasi O. et al., (2007)* *Innocenti, B. et al., (2016a)*	*Cortical bone* → Transversely isotropic • Young's Modulus [MPa]: $E_1 = 11,500$; $E_2 = 11,500$; $E_3 = 17,000$; • Poisson's Ratio: $\nu_{12} = 0.51$; $\nu_{13} = 0.31$; $\nu_{23} = 0.31$; *Cancellous bone* → Linear isotropic • Young's Modulus [MPa]: $E = 2,130$; • Poisson's Ratio: $\nu = 0.30$;
Innocenti, B. et al., (2009)	*Cortical bone* → Homogenous isotropic linear elastic • Young's Modulus [MPa]: $E = 16,600$;

	• Poisson's Ratio: $\nu = 0.30$; *Cancellous bone* → Homogenous isotropic linear elastic • Young's Modulus [MPa]: $E = 2{,}400$; • Poisson's Ratio: $\nu = 0.30$;
van Jonbergen, H. P. et al., (2012)	*Cortical bone* → Orthotropic • Young's Modulus [MPa]: $E_1 = 17{,}900$; $E_2 = 18{,}800$; $E_3 = 22{,}800$; • Shear Modulus [MPa]: $G_{12} = 5{,}710$; $G_{31} = 6{,}580$; $G_{23} = 7{,}110$; *Cancellous bone* → Homogenous isotropic linear elastic • Young's Modulus [MPa]: $E = 300$; • Poisson's Ratio: $\nu = 0.30$;

Table 2.1 - Constitutive model and mechanical properties of both cortical and cancellous bone.

2.6 LIGAMENTS AND TENDONS

Ligaments play a crucial role in governing proper joint kinematics by guiding normal movements and providing passive mechanical resistance to prevent abnormal movements. The anatomical configuration of the ligaments and the precise placement of the insertion site significantly influence joint stability and motion. Mostly, ligaments and tendons exhibit load transmission abilities along their main long axes (Innocenti B. & Galbusera F., 2022), with their responses to bending and torsion of less importance and often neglected. As these loads are transferred to the bones, the location of the insertion points dictates the orientation of the ligament-bone forces, thus substantially shaping the joint kinematics (Weiss J. A., & Gardiner J. C., 2001).

The LR and the MPFL play a vital role in maintaining patellar stability. Acting as static resistance against lateral forces, they prevent patellar subluxation from the trochlear groove into the transverse plane. In particular, the MPFL functions as the primary passive ligament restraint in the patellofemoral joint, contributing 50%-60% resistance to lateral displacement within the small flexion range (0-30 degrees) (Innocenti B. & Galbusera F., 2022). On the lateral side, the LR aids in stability (Loudon JK. et al., 2016; Standring S. et al., 2008). However, the LR remains poorly understood, with its precise anatomical landmarks yet to be exactly detailed (Shah K.N. et al., 2017). The intricate balance between the medial and lateral restraints represents a challenge for anatomical evaluation. Both LR tightness and patellar instability can

manifest as anterior knee pain. On the contrary, LR release has shown potential to improve patellar mobility and tracking (Unal B. et al., 2017).

In terms of the cruciate ligaments, the ACL experiences stretching during flexion, exerting a more pronounced influence on joint kinematics in the latter phase of flexion, and undergoes torsion during medial-lateral rotation. Anatomically, this ligament comprises two bundles (Hassebrock J. D. et al., 2020), which act together to give the ACL its biomechanical properties: the anteromedial bundle (aACL) and the posterolateral bundle (pACL). Each bundle is of importance at different points of knee flexion, contributing to a nonisometric behavior of the ligament. The load within the ligament changes between bundles as the knee progresses through its normal range of motion. Functionally, the ACL serves a dual purpose: acting as a primary restraint against anterior tibial displacement and a secondary restraint for tibial axial rotation, preserving the biomechanical integrity of the knee and mitigating meniscal damage (Hassebrock J. D. et al., 2020; Weiss J. A. & Gardiner J. C., 2001).

Similarly, PCL significantly influences joint kinematics, particularly in the initial degrees of flexion. Also this ligament consists of two nonisometric bundles named posteromedial bundle (pPCL) and anterolateral bundle (aPCL). These bundles exhibit complementary behaviors at all flexion angles, demonstrating reciprocal changes in length, tension, and fiber orientation. At full extension, the pPCL assumes tautness, providing substantial resistance to the posterior tibial translation force, and gradually shortening and adopting a more horizontal orientation during flexion. Conversely, the aPCL remains longer and taut at 90° of flexion, but assumes a more vertical orientation. The PCL primarily resists posterior tibial displacement and functions as a major secondary restraint against external tibial axial rotation (Weiss J. A., & Gardiner J. C., 2001).

In the same way as cruciate ligaments, MCL fibers can also be categorised into two functional bundles: deep MCL (dMCL) and superficial MCL (sMCL). The roles of the superficial and deep MCL are distinct (LaPrade R. F. et al., 2007). The sMCL serves as the primary restraint against the opening of the valgus at all flexion angles, while also cooperating with the ACL to counteract anterior translation and internal rotation. This contribution to tibial rotatory stability is most evident between 45° and 90° of knee flexion (Hassebrock J. D. et al., 2020). Both superficial and deep MCL serve as primary restraints against internal tibial rotation and secondary restraints against anterior tibial displacement (LaPrade R. F. et al., 2007; Weiss J. A., & Gardiner J. C., 2001).

The lateral collateral ligament (LCL) acts as the primary stabilizer, preventing varus rotation of the knee, particularly between 5° and 25° of knee flexion, while also resisting external tibial rotation. Additionally, it acts as a secondary restraint against anterior and posterior tibial displacement (Weiss J. A., & Gardiner J. C., 2001).

The patellar tendon is an essential component of the knee's extensor mechanism. Understanding the function of PT under physiological loading conditions is necessary to understand knee biomechanics. Despite numerous studies on this structure biomechanics, there are limited data on three-dimensional (3D) PT deformation (alterations in both length and orientation) during *in vivo* weight-bearing flexion (Defrate L. E. et al., 2007). The length of the patellar tendon is not uniform, predominantly increasing from full extension to 30° of knee flexion, with minimal alterations between 30° and 110° of flexion. Furthermore, the patellar tendon orientation shifts from anterior to posterior as flexion angles exceed 60° (Defrate L. E. et al., 2007). This tendon contributes to correct patellar alignment and knee extension.

The force ratio of the extensor mechanism (Lee D. et al., 2013) provides a way to comprehend the force distribution across the quadriceps and patellar tendon at different degrees of flexion. The highest PT forces occur at 60 degrees of flexion. At flexion angles below 45 degrees, the ratio of PT force to QT force exceeds 1.0. Within this range, the patellofemoral contact point is located distally on the patella, giving the quadriceps tendon a mechanical advantage. On the contrary, the force ratio drops below 1 at flexion angles beyond 45 degrees, with the patellofemoral contact point moving proximally on the patella, giving the patellar tendon a mechanical advantage.

2.6.1 Mechanical properties and constitutive models

Ligaments and tendons have similar mechanical behavior (Cowin S. C. & Doty S. B., 2007); however, due to their different compositions, their mechanical properties are different (Figure 2.8).
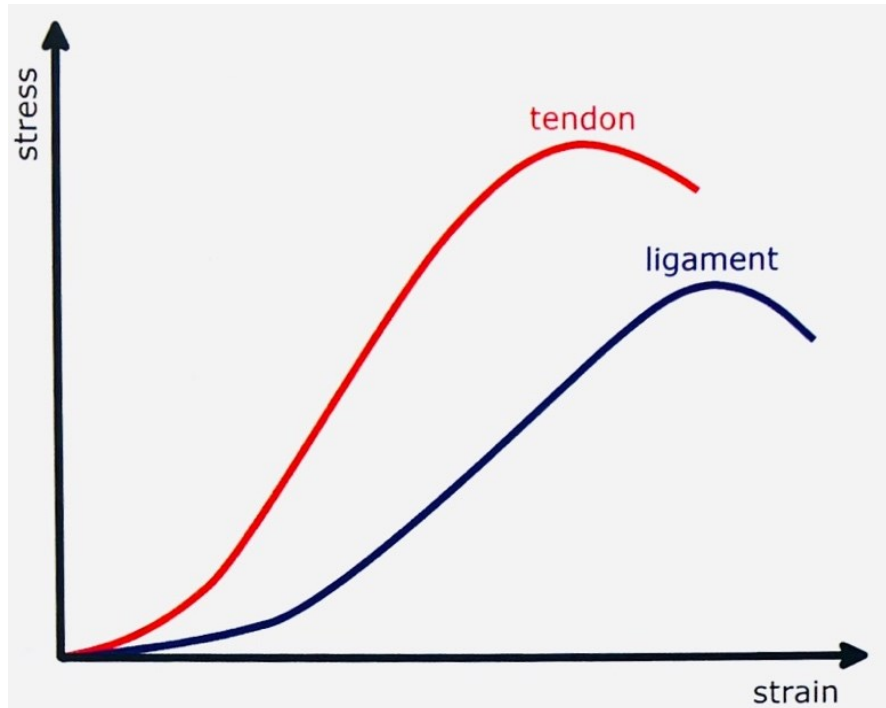

Figure 2.8 - The unique stress-strain profiles of tendons and ligaments emphasize the higher stiffness and strength exhibited by tendons (Innocenti B. & Galbusera F., 2022

These structures exhibit a clearly time-dependent response (Cowin S. C. & Doty S. B., 2007), implying their viscoelastic nature. The loading process induces microstructural rearrangements that require time for development. Therefore, the mechanical response of these tissues is strongly influenced by the rate of strain and the duration of loading. Ligaments and tendons also exhibit characteristic viscoelastic behaviors of creep and stress relaxation; under constant loads, the samples undergo elongation over time, whereas under constant strain, the load needed to sustain deformation decreases together with internal stresses. Over time, viscoelastic effects decrease until they reach equilibrium. Their mechanical characteristics are strongly dependent on the properties of collagen fibers.

To study the mechanical properties of these structures, it is necessary to study their mechanical response by performing different experimental tests, which reveal different material properties. The most common tests include uniaxial tensile tests to failure, creep tests, and relaxation tests. From uniaxial tests performed along multiple directions, significant anisotropic behavior

emerges in both ligaments and tendons, predominantly due to the unidirectionally orientated collagen fiber structure (Cowin S. C. & Doty S. B., 2007).

Tensile tests in tendon or ligament tissues are typically align along the collagen fiber axis. This procedure yields characteristic nonlinear load-displacement curves, which are similar for ligaments and tendons, but exhibit a distinct contrast between tension and compression responses (Figure 2.9). Collagen fibers, in fact, provide primary resistance to tensile loading (Weiss J. A., & Gardiner J. C., 2001), while offering minimal resistance to compression and bending.
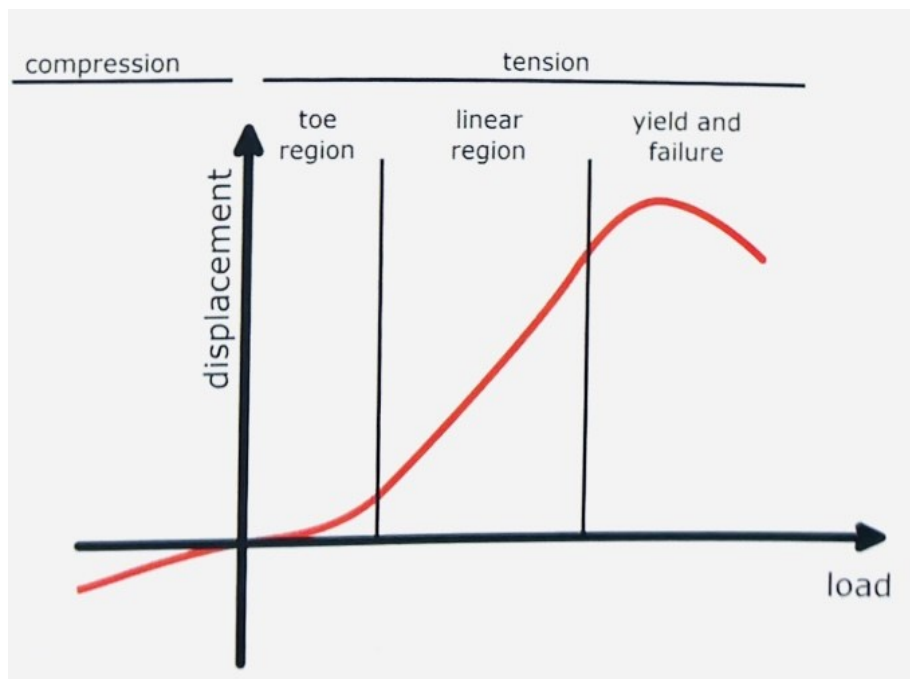

Figure 2.9 - An illustrative uniaxial load-displacement graph of ligaments and tendons, demonstrating the toe region, the linear region, and the segments where yield and failure occur (Innocenti B. & Galbusera F., 2022).

Under tension, the load-displacement curve delineates three distinctive regions. The toe region, which exhibits an exponential or quadratic shape (Weiss J. A., & Gardiner J. C., 2001), highlights the low stiffness, attributable to progressively straightening crimped fibers during elongation. Consequently, initial minimal force levels induce substantial deformations and elongation. Due to a higher collagen content (up to 85%) and lower elastin content, tendons generally exhibit greater stiffness and strength; the ligament's toe region is longer due to its less aligned collagen fibers. Generally, they can be stretched up to 5% - 7% without damage, while failure strains typically range around 12% - 15% and are elastin content dependent (Innocenti B. & Galbusera F., 2022). As the crimps diminish, entering the linear region, the fibers start to offer substantial resistance to tension, resulting in increased stiffness and progressively increasing force requirements for equivalent elongation (Cowin S. C. & Doty S. B., 2007). The

transition from the toe to linear regions typically occurs at 1.5% - 3% strain, although marked inter-specimen variability exists (Cowin S. C. & Doty S. B., 2007). The biomechanical significance of the toe region remains somewhat elusive; ligaments and tendons are typically preloaded in vivo, aligning their response with the linear region. In this phase, collagen molecules are aligned along the loading direction and are tensioned. The slope of the linear region describes the elastic modulus of the tissue, generally ranging between 0.2 and 2 GPa with considerable variability dependent on the biomechanical role and location of the tissue. Subsequently, in the last phase, the response remains predominantly linear until failure; under higher loads, collagen fibers start to undergo damage and failure (Weiss J. A., & Gardiner J. C., 2001), ultimately leading to yielding and failure of the specimen; the ultimate load and stress denote the condition of complete tissue sample failure (Innocenti B. & Galbusera F., 2022).

Ligament pre-strain

The estimation of reference strains, also known as pre-strains or in situ strains, presents significant experimental challenges (Galbusera F. et al., 2014), often leading to assumptions being made to address this issue and to correctly simulate the initial state of knee extension. Experimental measurement of pre-strain in knee joint ligaments has been shown to be nonuniform throughout individual ligaments and to vary depending on joint position (Weiss J. A., & Gardiner J. C., 2001). Determining in situ stress and strain involves substantial experimental complexities. Weiss et al. (2001) have measured changes in ligament stress and strain from an unknown reference configuration due to the difficulty in establishing a unique zero-stress reference length. Optical and video-based measurement techniques have been employed to establish a reference state of zero stress, allowing for the measurement of in situ strain. Unfortunately, there are limited data quantifying in situ strain levels, so many researchers have neglected in situ strain or assumed a uniform initial strain for all ligaments.

Baldwin et al. (2012) took an alternative approach, focusing on optimising mechanical properties for tibio-femoral soft tissue structures on a specimen-specific basis, with consistent results with previous findings from other authors.

Blankevoort et al. (1991a) developed a method for applying non-uniform initial strains to individual ligament elements within their 3D knee model. Using an iterative procedure, they minimized deviations between predicted and experimentally measured flexion movements. The algorithm adjusted the initial strain of each ligament until the model's reproduced kinematics closely matched the previously measured experimental data.

Table 2.2 presents commonly used pre-strain values found in the literature.

Ligaments	Pre-strain
aACL	-0.05
pACL	0.07
aPCL	-0.29
pPCL	-0.14
MCL	0.04
LCL	0.05
MPFL	0.06
LR	0.04

Table 2.2 - Ligaments reference strain at full extension finds in literature (Shu, L., et al. 2022; Innocenti, B. et al., 2014; 2011; Akbar, M., 2012; 2019).

Ligament wrapping

The knee ligaments exert forces that extend beyond the insertion areas, not only in the direction that connects the insertion and origin points. They demonstrate wrapping behavior among themselves or with bones (Galbusera F. et al., 2014; Weiss J. A., & Gardiner J. C., 2001). For example, ligaments such as ACL and PCL wrap around each other, whereas MCL wraps around the bones. This phenomenon causes the transfer of soft tissue load at locations different from the insertion sites and alters the direction of load transmission at these insertion points (Weiss J. A., & Gardiner J. C., 2001). Additionally, tendons that wrap around structures experience notably elevated friction forces in these wraparound sections (Cowin S. C. & Doty S. B., 2007).

A significant number of studies that use 1D elements to model ligaments have neglected this phenomenon of wrapping. Blankevoort et al. (1991b) were among the first to investigate whether the wrapping effect of the MCL, represented by straight-line elements, could be overlooked. In certain specific scenarios where wrapping significantly alters force distribution and direction, this omission might considerably compromise result accuracy. However, the overall impact of neglecting ligament wrapping was assessed to be less dramatic in other cases.

Classification of ligament models

Creating an accurate constitutive model for knee ligaments is a challenge due to the complex mechanical behavior of these structures. They exhibit nonlinearity, anisotropy, inhomogeneity, viscoelasticity, and undergo substantial deformations. A wide variety of

element types and constitutive models have been employed to represent knee ligaments, from simple one-dimensional elastic elements to complex three-dimensional hyperplastic structures with anatomically realistic geometries (Galbusera F. et al., 2014).

In the literature, one-dimensional (1D) models (Bendjaballah MZ. et al., 1995; Blankevoort L. et al., 1991a, 1991b; Innocenti B. et al., 2014; Baldwin M. A. et al., 2012) use line elements such as springs, trusses, and beams. Two-dimensional (2D) models (Baldwin M. A. et al., 2009; Shu L. et al., 2022; Fitzpatrick C. K. et al., 2010) employ elements such as shells or membranes, while three-dimensional (3D) models (Peña E. et al., 2005; 2006) use solid elements.

Line elements offer advantages including easy implementation, low computational cost, and the potential to represent ligaments through load-elongation relationships from experimental tests and pre-strain. However, they lack information on the behavior of the transverse plane, require special techniques to simulate ligament wrapping, and cannot predict stress distributions throughout the ligament (Weiss J. A., & Gardiner J. C., 2001). On the contrary, 3D structures can predict quantities inaccessible with 1D elements, provide improved anatomical realism, and address wrapping limitations. However, they require a more complex model formulation, significantly increasing computational costs (Galbusera F. et al., 2014).

In conclusion, when the main interest is the prediction of joint kinematics, linear ligament models offer a quicker option with acceptable outcomes (Weiss J. A., & Gardiner J. C., 2001). However, when the focus is on the ligament's biomechanics or its interaction with surrounding tissues, a 3D model is essential to accurately capture the mechanical behavior of knee ligaments. Developing a computational model requires consideration of all these aspects, and the choice of an appropriate modeling approach should be based on the specific application (Galbusera F. et al., 2014).

Ligaments as one-dimensional elements

Nonlinear one-dimensional (1D) elements remain a recommended and prevalent approach for simulating the comprehensive behavior of the knee (Galbusera F. et al., 2014). The first mechanical tests revealed the nonlinear nature of force-elongation curves for all knee ligaments. These early insights influenced the development of initial numerical models for the knee joint, employing elements capable of representing nonlinear force-strain or force-elongation relationships. These models used functions that included quadratic behavior or were quadratic only within the toe region, transitioning to linearity afterward. Within these options, the formulation presented by Blankevoort et al. (1991b) (Function 2.1) is particularly notable, being one of the most frequently used (Figure 2.10).

$$f(\varepsilon) = \begin{cases} \dfrac{1}{4}k\dfrac{\varepsilon^2}{\varepsilon_l}, & 0 \leq \varepsilon \leq \varepsilon_l \\[2ex] k(\varepsilon - \varepsilon_l), & \varepsilon > \varepsilon_l \\[2ex] 0, & \varepsilon < 0 \end{cases} \qquad (2.1)$$
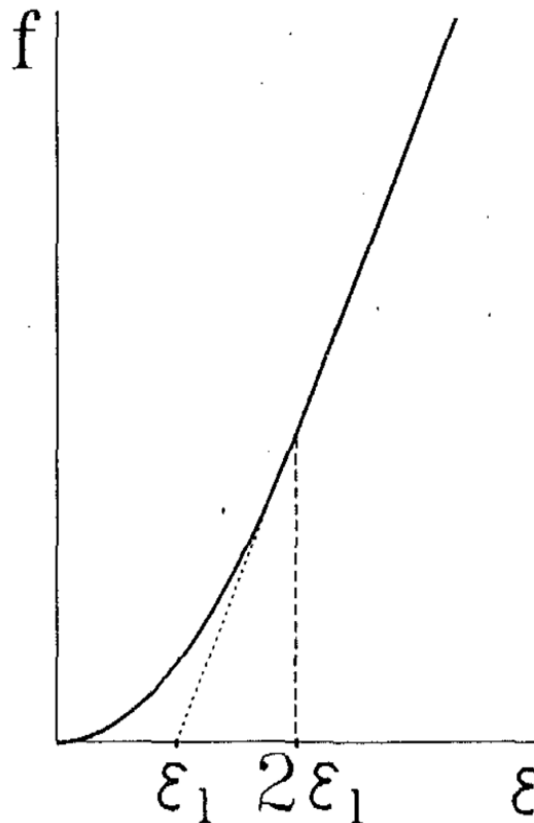

Figure 2.10 - Force–strain relationship of a generic ligament. ε_l is the threshold strain, which indicates the change from the toe to the linear regions (Blankevoort L., & Huiskes R., 1991).

The function $f(\varepsilon)$, the current tensile force in ligaments or tendons, is assumed to be nonlinear for low strains and linear for strains higher than a certain level (Figure). The scalar k is the transversal section axial stiffness, representing the force per unit strain generated in the ligament. The value $2\varepsilon_l$ is the threshold strain that indicates the change from the toe to the linear region (the linear strain εl limit was set at 0.03). The parameter ε is the strain in the ligament calculated from its length L and the zero-load length L_0:

$$\varepsilon = \frac{L - L_0}{L_0}$$

At the joint reference position, the initial strain in a bundle is given by the parameter ε_r. This parameter determines the zero-load length of a ligament bundle starting from the reference length L_r:

$$L_0 = \frac{L_r}{(\varepsilon_r - 1)}$$

2.6.1.1 Cruciate ligaments

As mentioned above, (Peña E. et al., 2006; Blankevoort L. et al., 1991b; Shu L. et al., 2022), a prevailing approach involves employing two distinct structures to simulate the ACL, corresponding to its anatomically distinguishable bundles that exhibit different mechanical functions. However, for the sake of simplification, certain studies documented in the literature opted for a single-bundle ligament model. Similarly to the ACL, a multi-bundle ligament model is also commonly adopted for the PCL. The representations of the ACL and PCL in finite element models of the knee joint, as encountered in the literature, are summarized in Table 2.3.

Authors	Model type and mechanical properties
Pianigiani S. et al., (2018)	1D model, single bundle for each ligament. Linear elastic material model *ACL:* • Young's Modulus [MPa]: E = 169; • Poisson's Ratio: ν = 0.45; *PCL:* • Young's Modulus [MPa]: E = 177;

	• Poisson's Ratio: $\nu = 0.45$;
Blankevoort L., & Huiskes R. (1991)	1D model, two bundles for each ligament. Quadratic stress-strain behavior in the toe region and linear behavior for strains higher than $2\varepsilon_l$ (Function 2.1); • aACL and pACL stiffness: 5,000 [N]; • aPCL and pPCL stiffness: 9,000 [N];
Peña E. et al., (2006)	3D model, two bundles for each ligament (aACL, pACL, aPCL, pPCL). Transversely isotropic hyperelastic model
Mesfar W., & Shirazi-Adl A. (2005)	1D model, multiple bundles for each ligament. Non-linear material properties
Shu L. et al., (2022)	1D axial connecters with no compressive stiffness, two bundles for each ligament.

Table 2.3 - Model type and mechanical properties of ACL and PCL; a = anterior bundle, p = posterior bundle.

2.6.1.2 Collateral ligaments

For the sake of modeling simplicity in knee joint analyses, the MCL is often treated as a single bundle. In contrast, certain researchers (Innocenti B. et al., 2014) have introduced a distinction between the anterior and posterior bundles in their models, while others (Bendjaballah MZ. et al.,1995; Peña E. et al., 2006; Blankevoort L., & Huiskes R., 1991b) have represented it as comprising three distinct segments: an anterior, a medial, and a posterior portion. Regarding the LCL, due to anatomical challenges in differentiating multiple bundles within this ligament, 1D computational models typically adopt a single linear element to represent it. However, in some investigations (Bendjaballah MZ. et al. ,1995; Peña E. et al., 2006; Blankevoort L., & Huiskes R., 1991b; Shu L. et al., 2022), the LCL has been partitioned into three segments, namely, anterior, posterior and medial, to provide a more detailed description of the joint's mechanical behavior. A comprehensive overview of these findings is presented in Table 2.4.

Authors	**Model type and mechanical properties**
Pianigiani S. et al., (2018))	1D model, single bundle for each ligament. Linear elastic material model

	MCL: • Young's Modulus [MPa]: E = 362; • Poisson's Ratio: ν = 0.45; *LCL:* • Young's Modulus [MPa]: E = 228; • Poisson's Ratio: ν = 0.45;
Blankevoort L., & Huiskes R. (1991)	1D model, five bundles for MCL (superficial part: aMCL, iMCL, pMCL; and deep part: aCM, pCM), and three bundles for LCL. Quadratic stress-strain behavior in the toe region and linear behavior for strains higher than $2\varepsilon_l$ (Function 2.1); • aMCL, iMCL and pMCL stiffness: 2,750 [N]; • aCM and pCM stiffness: 1,000 [N] • aLCL, mLCL and pLCL stiffness: 2,000 [N];
Peña E. et al., (2006)	3D model, three bundles for each ligament (aMCL, mMCL, pMCL, aLCL, mLCL, pLCL). Transversely isotropic hyperelastic model
Innocenti, B. et al., (2014)	1D model, two bundles for MCL and one for LCL. Linear elastic material model *MCL (aMCL and pMCL):* • Young's Modulus [MPa]: E = 196; • Poisson's Ratio: ν = 0.45; *LCL:* • Young's Modulus [MPa]: E = 111; • Poisson's Ratio: ν = 0.45;
Innocenti, B. et al., (2011)	1D model, two bundles for MCL and one for LCL. Quadratic stress-strain behavior in the toe region and linear behavior for strains higher than $2\varepsilon_l$ (Function 2.1); • aMCL and pMCL stiffness: 2,750 [N]; • LCL stiffness: 4,000 [N];
Mesfar W., & Shirazi-Adl A. (2005)	1D model, multiple bundles for each ligament. Non-linear material properties

Shu L. et al., (2022)	1D axial connecters without compressive stiffness, three bundles for each ligament (aMCL, mMCL, pMCL, aLCL, mLCL, pLCL).

Table 2.4 - Model type and mechanical properties of MCL and LCL; a = anterior bundle, p = posterior bundle, i = intermediate bundle, m = medial bundle.

2.6.1.3 MPFL and lateral retinaculum

MPFL and LR are two much-discussed anatomical structures, and certain researchers in cadaveric examinations face challenges in identifying these ligaments within specific anatomical specimens after dissection. This situation has created debates about both the functionality and the existence of the MPFL and the LR.

Consequently, the available literature on these two ligaments remains quite limited. Biomechanical investigations have revealed that the primary static stabilizer on the medial side of the patella is the MPFL (Criscenti G. et al., 2016), effectively preventing subluxation of the lateral patellar. Similarly, the LR serves as a lateral stabilizer for the patella.

Table 2.5 shows a summary of what has been found in the literature.

Authors	Model type and mechanical properties
Baldwin M. A. et al., (2009)	Nonlinear, tension-only springs embedded in a low-modulus, hyper-elastic deformable 2D model
Akbar M. et al., (2019)	1D model, three-bundle nonlinear tensile spring each
Mesfar W., & Shirazi-Adl A. (2005)	1D model, four bundles for MPFL, and three bundles for LR. Non-linear material properties
Shu L. et al., (2022)	1D axial connecters without compressive stiffness, single bundle for each ligament.
Baldwin M. A. et al., (2012)	3D fiber-reinforced structures

Table 2.5 - Model type and mechanical properties of MPFL and LR.

2.6.1.4 Patellar tendon

If the focus of the study does not interest the patellofemoral joint, computational models in the literature often exclude the patella and the patellar tendon. However, when the patellofemoral joint is a subject of interest, it can be represented using a variety of element types, including 1D, 2D, or 3D elements (Table 2.6).

Authors	Model type and mechanical properties
Pianigiani S. et al., (2018)	1D model, three bundles. Linear elastic material model: • Young's Modulus [MPa]: E = 507; • Poisson's Ratio: $\nu = 0.45$;
Peña E. et al., (2006)	3D model, one bundle. Transversely isotropic hyperelastic model
Baldwin M. A. et al., (2009)	Nonlinear, tension-only springs embedded in a low-modulus, hyper-elastic deformable 2D model
Akbar M. et al., (2019)	1D model, 10-bundle linear tensile spring
Mesfar W., & Shirazi-Adl A. (2005)	1D model, nine bundles. Non-linear material properties
Shu L. et al., (2022)	2D fiber-reinforced structures

Table 2.6 - Model type and mechanical properties of PT.

2.7 MENISCUS

The menisci are important elements within the intricate knee system, serving as vital multifunctional components. Their biomechanical complexity involves pivotal roles, such as load distribution, shock absorption, stability enhancement, and facilitation of lubrication. The way the menisci execute these diverse tasks is deeply linked in their macroscopic and microscopic anatomy (Markes, A. R. et al., 2020; Fox A. J. et al., 2015). Their behavior is entirely dynamic, efficiently fulfilling these functions. When the contact surface of the joint is expanded, they effectively disperse contact forces across the articular surfaces. In essence, they redistribute the load distribution across incongruent joint surfaces while preserving maximal congruency (Peña, E. et al., 2005). Menisci show a complex three-layer arrangement of collagen fibers, strategically designed to transform vertical compressive loads into circumferential stresses (Markes A. R. et al., 2020). Specifically, the inner layer presents circumferentially oriented fibers to respond to circumferential stresses, while the intermediate layer contains radially oriented collagen fibers, even if in smaller quantities. The outermost layer, the surface layer, comprises fibers aligned parallel to the surface at various angles (Markes A. R. et al., 2020).

Biomechanical investigations (Fox A. J. et al., 2015) have underlined the crucial contribution of the menisci to knee function: a substantial portion, approximately 40-60%, of the load impacting the extended knee joint is transmitted to the menisci (65–70% lateral and 40–50% medial). This transmission increases to approximately 90% during flexion. Under weight-bearing conditions, axial forces compress the menisci, leading to circumferential stresses. These stresses are based on the conversion of axial force into tensile strain, facilitated by the circumferential collagen fibers of the meniscus. As shown in Figure 2.11 the meniscus is compressed by the force transmitted from the femur and the force transmitted from the tibia, F_{fem} and F_{tib}. It deforms radially, being also anchored by the force transmitted through the anterior and posterior meniscal horns, F_{ant} and F_{post}. This causes a complex stress state. The vertical and horizontal projections F_v and F_h are determined by the compression imposed by the femur, while radial deformation induces circumferential forces F_{circ}. Thus, part of the axial contribution is transformed by processes related to the horn shape and anchorage, and the response is through a radial force F_{rad}.
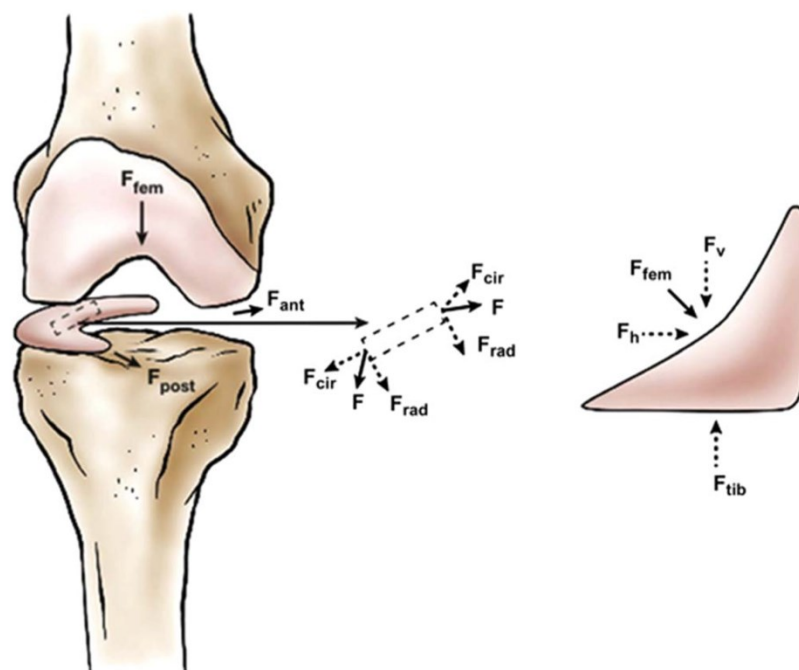

Figure 2.11 - Diagram of the forces acting on the meniscus in the loading phase (Fox A. J. et al., 2015).

2.7.1 Mechanical properties and constitutive models

The microstructure of the meniscus affects its mechanical properties, which determines the mechanical response of the tissue. The knowledge on the compressive behavior of the meniscal tissue is limited; compression tests can be performed under conditions of creep (maintaining constant force while deformation changes) or relaxation (maintaining constant

deformation while force changes) to distinguish the time-dependent viscoelastic characteristics of the meniscus. It emerges that the meniscus is approximately 1000 times stiffer in tension than in compression (Innocenti B. & Galbusera F., 2022), which allows for easy deformation during application of axial load, accommodating the adjacent femoral condyles and the tibial plateau. Furthermore, this underscores the propensity of the meniscus to counter circumferential tensile stress more effectively than compressive stress.

A summary of some constitutive models of menisci findings from the literature is presented in Table 2.7. In mathematical knee model formulation, for simplicity, the menisci are occasionally omitted (Blankevoort L. et al., 1991; Blankevoort L., & Huiskes R., 1991). Conversely, they are sometimes considered as linear, isotropic elastic materials (Peña E. et al., 2006; Pianigiani S. et al., 2018; Innocenti B. et al., 2014), or in other cases (Guess T. M. et al., 2010; Zielinska B., & Donahue T. L., 2006; Bolcos P. O. et al., 2018; Vaziri A. et al., 2008; Kwon O. S. et al., 2014), they have been characterized as transversely isotropic materials.

Authors	Constitutive model and mechanical properties
Peña E. et al., (2006)	Single-phase linear elastic and isotropic material: • Young's Modulus [MPa]: E = 59; • Poisson's Ratio: ν = 0.49;
Pianigiani S. et al., (2018)	Linear elastic and isotropic material: • Young's Modulus [MPa]: E = 53; • Poisson's Ratio: ν = 0.49;
Innocenti, B. et al., (2014)	Linear elastic and isotropic material: • Young's Modulus [MPa]: E = 8; • Poisson's Ratio: ν = 0.45;
Guess T. M. et al., (2010); Zielinska B., & Donahue T. L., (2006)	Linear elastic transversely isotropic: • Young's Modulus [MPa]: E_{circ} = 150; E_{axl} = 20; E_{rad} = 20; • Poisson's Ratio: ν_{circ} = 0.20; ν_{axl} = 0.30; ν_{rad} = 0.20;
Kwon O. S. et al., (2014)	Linear elastic transversely isotropic: • Young's Modulus [MPa]: E_{circ} = 150; E_{axl} = 20; E_{rad} = 20; • Poisson's Ratio: ν_{circ} = 0.20; ν_{axl} = 0.30; ν_{rad} = 0.30;

Bolcos P. O. et al., (2018)	Linear elastic transversely isotropic: • Young's Modulus [MPa]: $E_{circ} = 159.6$; $E_{axl} = 20$; $E_{rad} = 20$; • Poisson's Ratio: $\nu_{circ} = 0.5$; $\nu_{axl} = 0.0015$; $\nu_{rad} = 0.0015$;
Vaziri A. et al., (2008)	Transversely isotropic poroelastic: • Young's Modulus [MPa]: $E_{circ} = 100$; $E_{axl} = 0.075$; $E_{rad} = 0.075$; • Poisson's Ratio: $\nu_{circ} = 0.20$; $\nu_{axl} = 0.30$; $\nu_{rad} = 0.20$; Transversely isotropic elastic: • Young's Modulus [MPa]: $E_{circ} = 140$; $E_{axl} = 20$; $E_{rad} = 20$; • Poisson's Ratio: $\nu_{circ} = 0.30$; $\nu_{axl} = 0.20$; $\nu_{rad} = 0.20$;

Table 2.7 - Constitutive model and mechanical properties of menisci.

2.8 ARTICULAR CARTILAGE

The articular cartilage is a viscoelastic substance composed of two distinct phases (Cowin S. C. & Doty S. B., 2007): the solid phase (extracellular matrix) and the fluid phase (interstitial water). The significant fluid content within cartilage arises from the hydrophilic nature of its proteoglycans, which also contributes to its swelling behavior as a result of high internal osmotic pressure. Consequently, the biphasic nature of cartilage plays a crucial role in shaping its mechanical properties and its load-bearing capability; also serves to decrease matrix pressure when subjected to loads, safeguarding it (Innocenti B. & Galbusera F., 2022).

Typically, the thickness of articular cartilage can be divided into four primary zones, distinguished by varying collagen fiber arrangements and orientations, which leads to dissimilar mechanical responses, necessitating various tests to scrutinize the mechanical traits of this material (Innocenti B. & Galbusera F., 2022). Typically, indentation tests are used to evaluate the behavior of the superficial tangential zone, while the analysis of the deep zone behavior requires compression tests.

2.8.1 Mechanical properties and constitutive models

The articular cartilage shows a time-dependent behavior that can be approximately described assuming viscoelastic properties. If the loading time remains considerably shorter than the recovery time, viscoelastic materials behave like elastic materials. Compression of the articular cartilage leads to changes in pressure and interstitial fluid flow through the porous permeable extracellular matrix (ECM). This flow leads to frictional resistance, primarily

attributing to the viscoelastic property of cartilage during compression (Innocenti B. & Galbusera F., 2022). To summarize, the mechanical characteristics of articular cartilage are nonlinear and time-dependent, qualifying it as a poro-viscoelastic material.

Table 2.8 outlines the predominant model types and material parameters developed for the knee joint articular cartilage. Initially, a linear continuum model was used, coupled with poroelastic models that assumed the fluid and matrix components to be incompressible (the biphasic theory). These models of articular cartilage presumed the collagen-proteoglycan matrix to be an incompressible, porous-permeable solid matrix, and the interstitial fluid to be incompressible as well (Cowin S. C. & Doty S. B., 2007), and it was necessary for providing a comprehensive representation of this complex material's behavior. However, linear models (DeVries Watson N. A. et al., 2015; Mesfar W., & Shirazi-Adl A. 2005; Pianigiani S. et al., 2018; Zielinska B., & Donahue T. L., 2006; Bendjaballah MZ. et al., 1995; Innocenti B. et al., 2014; Guess T. M. et al., 2010; Peña E. et al., 2005) offer notable advantages due to their capacity to solve the problem with fewer parameters to be evaluated.

Authors	Constitutive model and mechanical properties
DeVries Watson N. A. et al., (2015) *Innocenti, B. et al., (2014)*	Linear elastic and isotropic material: • Young's Modulus [MPa]: E = 12; • Poisson's Ratio: ν = 0.45;
Mesfar W., & Shirazi-Adl A. (2005)	Homogeneous isotropic material: • Young's Modulus [MPa]: E = 12; • Poisson's Ratio: ν = 0.45;
Peña E. et al., (2005)	Single-phase linear elastic and isotropic material: • Young's Modulus [MPa]: E = 5; • Poisson's Ratio: ν = 0.46;
Guess T. M. et al., (2010);	Linear elastic and isotropic material: • Young's Modulus [MPa]: E = 15; • Poisson's Ratio: ν = 0.475;
Pianigiani S. et al., (2018)	Linear elastic and isotropic material: • Young's Modulus [MPa]: E = 13;

	• Poisson's Ratio: $\nu = 0.475$;
Zielinska B., & Donahue T. L., (2006)	Linear elastic isotropic and homogeneous material: • Young's Modulus [MPa]: $E = 15$; • Poisson's Ratio: $\nu = 0.475$;
Bendjaballah MZ. et al., (1995)	Linear elastic and isotropic material: • Young's Modulus [MPa]: $E = 12$; • Poisson's Ratio: $\nu = 0.45$;

Table 2.8 - Constitutive model and mechanical properties of menisci.

CHAPTER 3 - MATERIALS AND METHODS

Finite Element Analysis (FEA) represents a widely employed approach that enables the prediction and examination of an object's behavior across various physical conditions through calculations, models, and simulations. It facilitates the optimization of components of a complex structure during the design phase, allowing one to reduce the number of physical prototypes to build and the number of experiments.

FEA is based on the Finite Element method, a numerical technique that subdivides the complex object under testing into a finite number of subdomains, called finite elements, interconnected at points denoted as nodes. This method allows engineering problems described by partial differential equations (PDEs), providing an approximate solution. The analysis is performed by creating a mesh made of a number of small elements which form the shape of the structure. Computation is performed on each individual element to arrive at the ultimate result for the entire structure.

3.1 RESEARCH AND ANALYSIS OF DICOM IMAGE DATA

As a starting point, DICOM (Digital Imaging and Communications in Medicine) images related to a lower limb CT scan were searched. Indeed, even though our focus is only on the knee joint (specifically, the left knee has been chosen for study), certain examinations and references concerning the entire limb are required for the selection of the native physiological knee. Therefore, it was necessary to select the DICOM file of interest, since most of CT scans were from patients with varus or valgus[7] issues.

The selection was carried out by measuring the femoral mechanical angle (FMA) and the tibial mechanical angle (TMA), referring to the values found in the literature for a neutral knee alignment (Marques Luís N. et al., 2021; Moser L. B. et al., 2022; Hirschmann M. T. et al., 2019).

DICOM images were uploaded and displayed using a 2D image processing program for subsequent design and development of three-dimensional models. An approximate segmentation of the 2D images was performed to calculate the angles of interest (FMA and TMA).

---

[7] Varus is an angulation of the knee joint where the lower leg deviates inward, while valgus is an angulation where the lower leg deviates outward. These terms describe specific knee joint alignment deviations.

According to the existing literature, a knee with neutral alignment has a joint line inclined by 3° (3° varus alignment in the tibia and 3° valgus alignment in the femur). This simplified approach assumes parallel orientation of joint lines, with the FMA at 93° and the TMA at 87°. Furthermore, only a small portion of the population appears to have a 3° oblique joint line (Hirschmann M.T. et al., 2019).

The FMA represents the angle on the medial side between the femoral mechanical axis and a tangent drawn to the distal femoral condyles. Similarly, the TMA is the medial angle formed between the tibial mechanical axis and a tangent drawn to the tibial plateau (Figure 3.1).
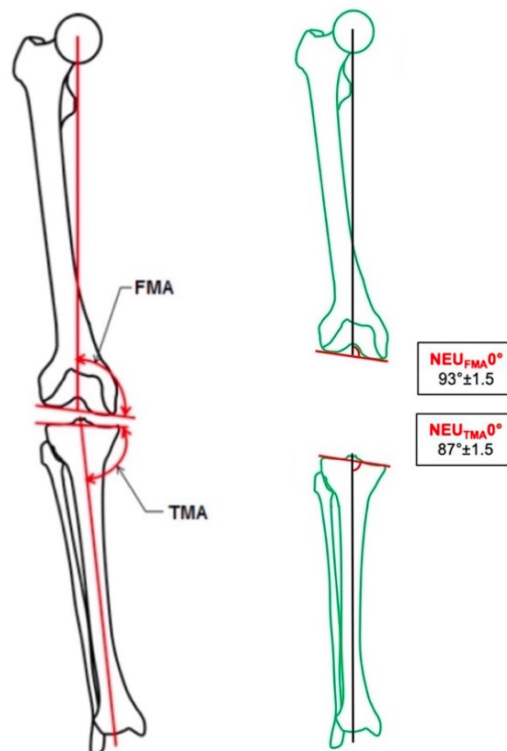
Figure 3.1 - Measurements of the femoral mechanical angle (FMA) and tibial mechanical angle (TMA). $NEU_{FMA}0°$ ranges from 91.5° to 94.5°. $NEU_{TMA}0°$ ranges from 85.5° to 88.5° (Hirschmann M. T. et al., 2019).

The selected DICOM file shows an FMA of 93.5° and a TMA of 87.4°.

3.2 IMAGE SEGMENTATION, 3D MODEL CREATION, AND POST-PROCESSING

At this point, the 2D images were segmented to create the main structures of interest (femur, tibia, patella, menisci, and articular cartilages).

With the *thresholding* command, the segmentation phase was developed; it was possible to highlight the structures of our interest by manually editing the *thresholding* ranges and creating appropriate *masks* (shown in Figure 3.2).
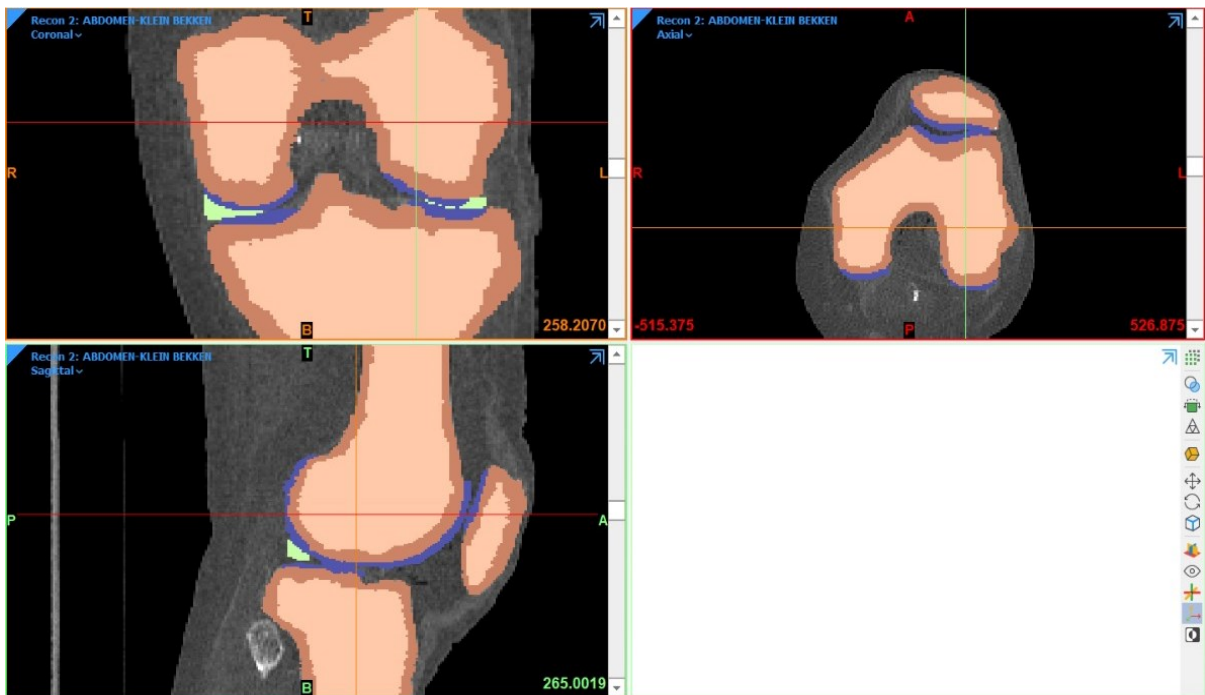

Figure 3.2 - The software's graphical interface consists of three different views of the same image: frontal (top left), axial (top right), and lateral (bottom left). The following are represented: cortical bone of femur, tibia, and patella in light brown; cancellous bone of the same bone components in light pink; their corresponding articular cartilages in blue; and finally the menisci in green.

Generating 3D from these *masks*, it became apparent that the volume was not free of noise and imperfections, and therefore needs to be corrected. To eliminate the problems, it was necessary to operate on the *masks* through commands that allow one to remove parts of the image that are not of interest to the component in question or, in the opposite case, to select and add areas that belong to that district. The models created still have numerous errors and incongruencies. For this reason, a post-processing operation had to be performed. This process is a key step for visualization and operations on the model; *smoothing* was then performed, and any holes that were present have been filled in. Next, a *Boolean* subtraction had to be performed, in cases in which the various geometries were about to compenetrate, in order to avoid problems during the following finite element analysis. A representation of the complete 3D model is shown in Figure 3.3.
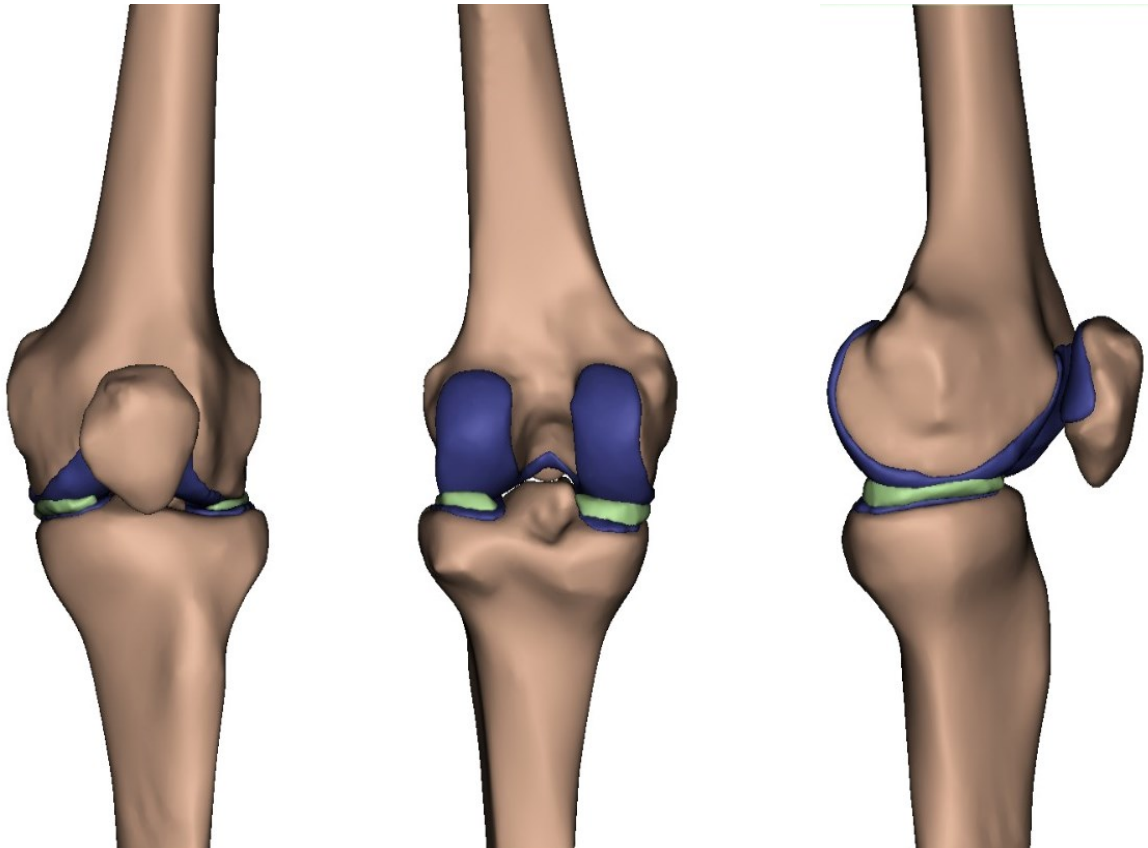
Figure 3.3 - Representation of the 3D model in the anterior, posterior and lateral views, respectively.

3.3 FINITE ELEMENT MODEL

The structures included in this work are subsequently listed:

- distal part of the femur;
- proximal part of the tibia;
- patella;
- articular cartilage of the femur, tibia, and patella;
- menisci;
- patellar tendon (PT);
- quadriceps tendon (QT);
- anterior cruciate ligament (ACL);
- posterior cruciate ligament (PCL);
- medial collateral ligament (MCL);
- lateral collateral ligament (LCL);
- medial patellofemoral ligament (MPFL);
- lateral retinaculum (LR).

The fibular bone, as in most of the work found in the literature, was not taken into account.

Software Abaqus was used to perform all the Finite Element simulations. Abaqus/CAE is an interactive environment that is used to create FE models, submit analyses, monitor and diagnose jobs, and evaluate results. The 3D model of the knee joint was imported into the FEM analysis environment, where the necessary setups were arranged to run the simulations. In Abaqus/CAE it is possible to define material properties, interactions and constraint, boundary and loading conditions, and to mesh the different parts of the model. Then, to perform the analysis, Abaqus/Explicit was used, an explicit dynamics finite-element solver that is well-suited to simulate brief transient dynamic events. This solver has the ability to effectively handle severely non-linear behavior, suitable for models that can undergo large rotations and large deformations. It is computationally efficient for the analysis of large models with relatively short dynamic or quasi-static response.

In the case of the explicit method, there is no enforcement of equilibrium, but this does not mean that it is not accurate. It is possible to minimize its deviation from equilibrium to almost zero by increasing the number of solution steps, i.e. reducing the time-step size. Abaqus/Explicit determines the solution to a nonlinear problem without iterating, but by explicitly advancing the kinematic state from the previous increment (Abaqus Analysis User's Guide, Abaqus/CAE User's Guide).

3.4 PART MODULE

Parts serve as the foundational elements of an Abaqus/CAE model, and through the Part module, it is possible to generate, modify, and oversee these components within the present model.

In addition to the components obtained from segmentation, tendons, and ligaments are also considered in the model.

Cruciate ligaments are represented as 1D elements, shaped by spring elements that represent the different fiber bundles of the ligament, assumed to be nonlinear elastic. Collateral ligaments, MPFL, LR, PT, and QT, were discretized with 2D shell elements.

The selected geometric attributes for this investigation, as derived from data from the literature (Innocenti B. et al., 2014; Stäubli H. U. et al., 1999; Hassebrock J. D. et al., 2020; Hashemi J. et al., 2005; LaPrade R. F. et al., 2007; Amis A.A. et al., 2003; Mesfar W. & Shirazi-Adl A. 2005), are detailed in Table 3.1. In the context of the cruciate ligaments, the cross-sectional

area, width, and the thickness of the bundles have been excluded, as they are not essential for the implementation of the model.

Ligaments/ Tendons	Length at full extension [mm]	Width [mm]	Cross sectional area [mm^2]	Thickness [mm]
aACL	34.5	-	-	-
pACL	36.1	-	-	-
aPCL	29.9	-	-	-
pPCL	31.2	-	-	-
MCL	108.6	10.8	14	1.3
LCL	69.6	4.6	18	2.6
MPFL	65.9	16.8	42.7	2.5
LR	45.9	13	28.5	2.1
PT	67.2	35 (patella) 26 (tibia)	36.8	1.2
QT	68	25	64.6	2.7

Table 3.1 - *Geometric sizes found in the literature of ligament and tendon bundles.*

3.4.1 Reference Coordinate System

Following the methodology outlined by Grood and Sunday (1983), two separate and distinct reference systems were defined for the femur and tibia parts.

Reference system of the femur

The reference system (Figure 3.4) was established with the following components:

- an axis aligned with the mechanical axis of the femur (z-axis);

- an axis aligned with the anatomical transepicondylar axis, which runs through the medial epicondyle and the lateral epicondyle of the femur, representing the flexion-extension axis (x-axis);

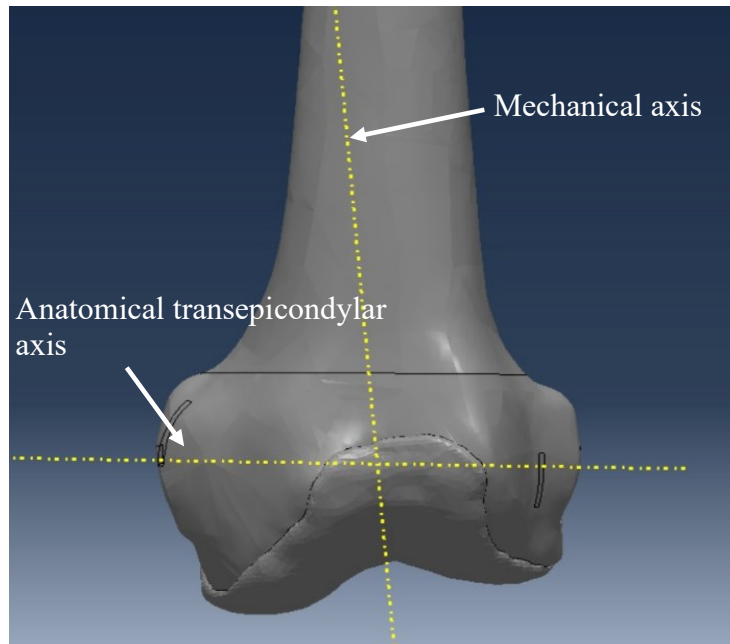- an axis that is perpendicular to the two axes mentioned above (y-axis).

Figure 3.4 - Femur coordinate system

Reference system of the tibia

The tibial reference system (Figure 3.5) was created with the following components:

- an axis aligned with the mechanical axis of the tibia, representing the axis of internal-external rotation (z-axis);

- an axis aligned with a line connecting the approximate center of each plateau (x-axis);

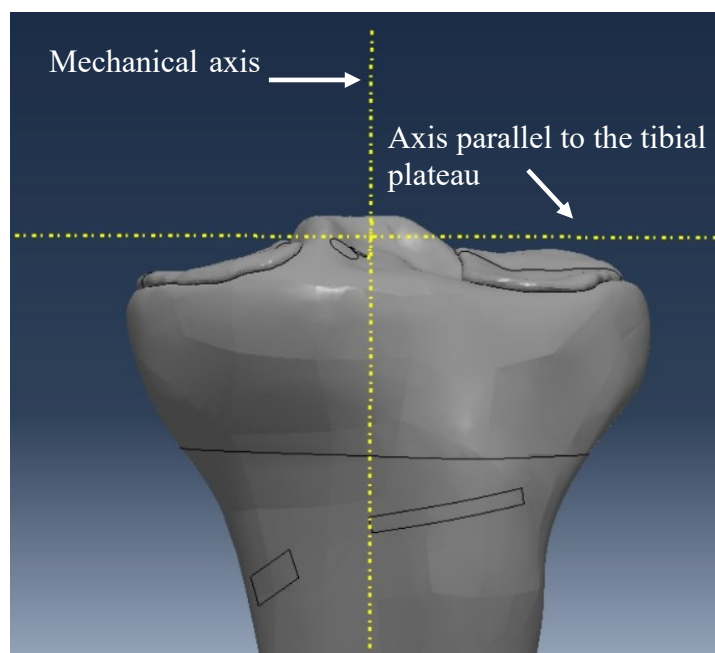- an axis that is perpendicular to the two axes mentioned above (y-axis).

Figure 3.5 - Tibia coordinate system

3.5 ASSEMBLY MODULE

When a part is created, it maintains its own coordinate system, which is independent of other parts within the model. On the contrary, the Assembly module is used to generate instances of these parts and to position these instances in relation to one another within a global coordinate system. This process results in the creation of the assembly.

3.5.1 *Positioning and partitioning on the bone for insertion*

In the current model, information from literature studies (Hassebrock J. D. et al., 2020; Innocenti B. et al., 2016b; Victor J. et al., 2009a; LaPrade R. F. et al., 2007; Steensen R. N. et al., 2004; Amis A.A. et al., 2003) was combined to identify the tibial, femoral, and patellar attachment sites for each ligament and tendon. The knee model was constructed based on the documented anatomical positions of the primary soft tissue insertions, as outlined in various sources from the literature. This process was designed to determine the precise location of the attachment for the origin and insertion points of the individual ligaments and tendons.

Specifically, following the methodology developed by Innocenti et al. (2016b), the insertion points of the cruciate and collateral ligaments were identified in the software used for segmentation. Once the origin and insertion points of each tendons and ligaments were established, these points were imported into the Abaqus model to facilitate subsequent positioning of the model components.

After placing the tendons and ligaments, the bony parts were partitioned at the insertions. This procedure was performed to facilitate the subsequent definition of the constraints and interaction properties between the soft tissues and the bone component.

3.5.1 *Illustration of the total model*

In Figure 3.6, the comprehensive model, comprising all elements, is shown in the full extension reference configuration. Bony components are shown in pink, articular cartilage in brown, tendons and ligaments in grey, and menisci in white.
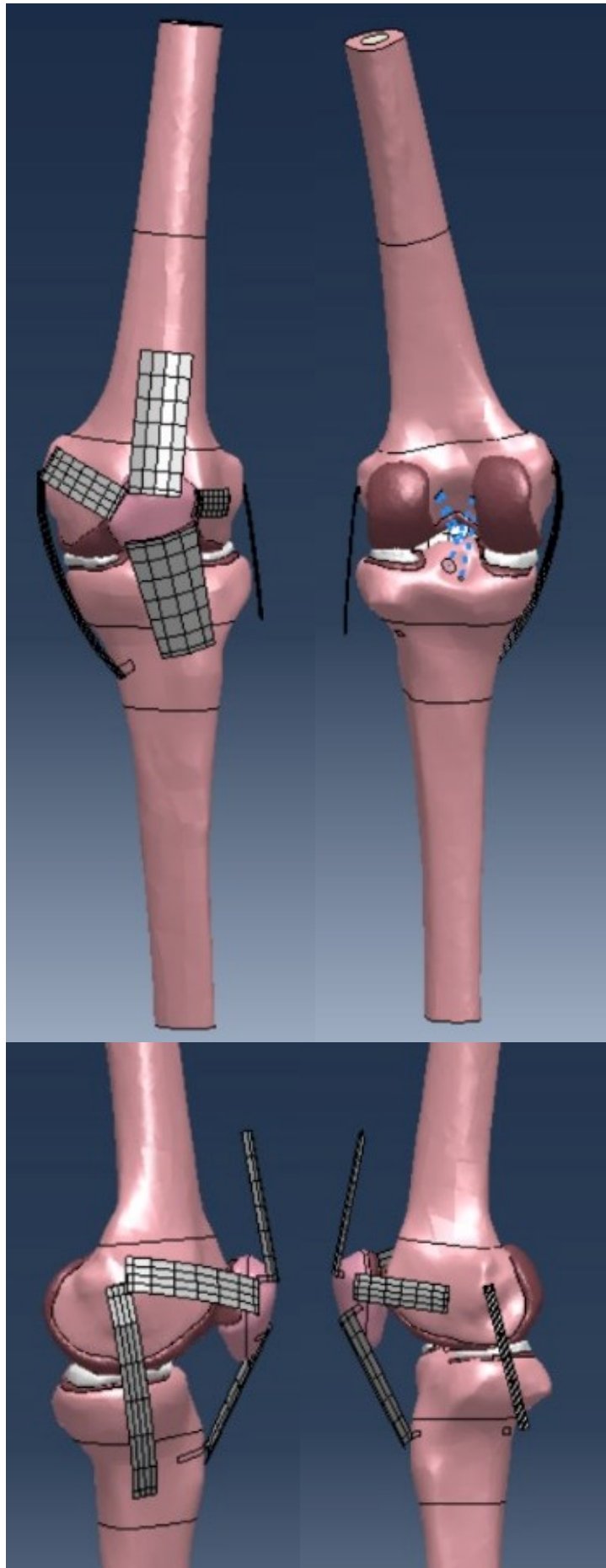
Figure 3.6 – Top left: anterior view; top right: posterior view; bottom left: medial view; bottom right: lateral view

3.6 MATERIAL PROPERTIES

To begin with, each component was assigned an appropriate material.

3.6.1 Bone - cancellous, cortical, patellar

Cortical bone and cancellous bone, both present in the tibia and femur, exhibit distinct properties. According to the findings in the literature (Kayabasi O., et al., 2007), cancellous bone is characterized as a linear elastic isotropic material, while cortical bone is considered transversely isotropic to accurately represent its capacity to support greater stress in the longitudinal direction. The patella, consisting only of cortical bone, is assumed to be linear elastic and isotropic (Jonbergen H. P. et al., 2012).

The properties and behaviors of the selected materials for cortical, cancellous bone, and patellar bone are detailed in Table 3.2.

	Material behavior	Young's Modulus [MPa]	Poissons' ratio	Shear Modulus [MPa]	Density [g/cm^3]
Cortical bone	Transversely isotropic linear elastic	$E_1 = 11{,}500$; $E_2 = 11{,}500$; $E_3 = 17{,}000$;	$\nu_{12} = 0.51$; $\nu_{13} = 0.31$; $\nu_{23} = 0.31$;	$G_{12} = 3{,}600$; $G_{13} = 3{,}300$; $G_{23} = 3{,}300$;	$d = 1.85$
Cancellous bone	Homogeneous isotropic linear elastic	$E = 2{,}130$;	$\nu = 0.30$;	-	$d = 1$
Patellar bone	Homogeneous isotropic linear elastic	$E = 15{,}000$;	$\nu = 0.30$;	-	$d = 2$

Table 3.2 - Material properties of tibia, femur, and patella.

3.6.2 Articular Cartilage and Menisci

The menisci and the articular cartilage were assumed to exhibit linear elastic isotropic behavior. Parameters consistent with Mesfar W., & Shirazi-Adl A. (2005) and Kwon O. S. et al. (2014) were used for the cartilage layer. However, to model the material properties of both menisci, the approach outlined in the studies by Pianigiani et al. (2018) and Guess T. M. et al. (2010) was chosen.

The material properties and behaviors of these components are described in Table 3.3.

	Material behavior	Young's Modulus [MPa]	Poissons' ratio	Density [g/cm³]
Articular cartilage	Linear elastic isotropic	E = 12;	ν = 0.45;	d = 1
Menisci	Linear elastic isotropic	E = 53;	ν = 0.49;	d = 1.1

Table 3.3 - Material properties of the tibia, femur, and patella.

3.6.3 Ligament and Tendon

To avoid neglecting the effect of wrapping between the ligaments and between the ligaments and the bone component, it was decided to represent the collateral ligaments, MPFL, LR, PT, and QT as 2D shell elements.

However, considering that in healthy conditions and without applied loads, ligaments and tendons are never completely unloaded, rendering the toe region almost negligible, a decision was taken to represent them as linear elastic isotropic materials.

In any case, it is essential to consider a nonzero pre-strain value for these ligaments, as they are already under load in the extended position. This consideration does not apply to the patellar tendon and the quadriceps tendon. The values of these pre-strain are shown in Table 2.2 (Chapter 2).

A comprehensive summary of the properties of these ligaments and tendons can be found in Table 3.4 (Pianigiani et al., 2018; Innocenti B. et al., 2014; Stäubli, H. U. et al., 1999; Criscenti G. et al., 2016).

	Material behavior	Young's Modulus [MPa]	Poissons' ratio	Density [g/cm³]
MCL	Linear elastic isotropic	E = 362;	ν = 0.45;	d = 1.67
LCL	Linear elastic isotropic	E = 228;	ν = 0.45;	d = 1.67
MPFL	Linear elastic isotropic	E = 211;	ν = 0.45;	d = 1.67

LR	Linear elastic isotropic	E = 30;	ν = 0.45;	d = 1.67
PT	Linear elastic isotropic	E = 507;	ν = 0.45;	d = 1.67
QT	Linear elastic isotropic	E = 344;	ν = 0.45;	d = 1.67

Table 3.4 - Material properties of MCL, LCL, MPFL, LR, PT, and QT.

3.6.3.1 Cruciate ligaments

Cruciate ligaments are shaped by nonlinear spring elements, simplified as 1D axial connectors without compressive stiffness.

The stiffness-force relationship of ligaments, which exhibits nonlinear elastic characteristics with respect to the zero-load region (Shu L. et al., 2022), was modeled in accordance with the approach proposed by Blankevoort et al. (1991b), using Function 2.1 described in Chapter 2.

This function allows the representation of the nonlinear force-strain behavior of the ligaments, as illustrated in Figure 3.7. Instead, the material parameters used for the cruciate ligaments are provided in Table 3.5 (Blankevoort et al.,1991b; Shu L. et al., 2022; Galbusera F. et al., 2014).
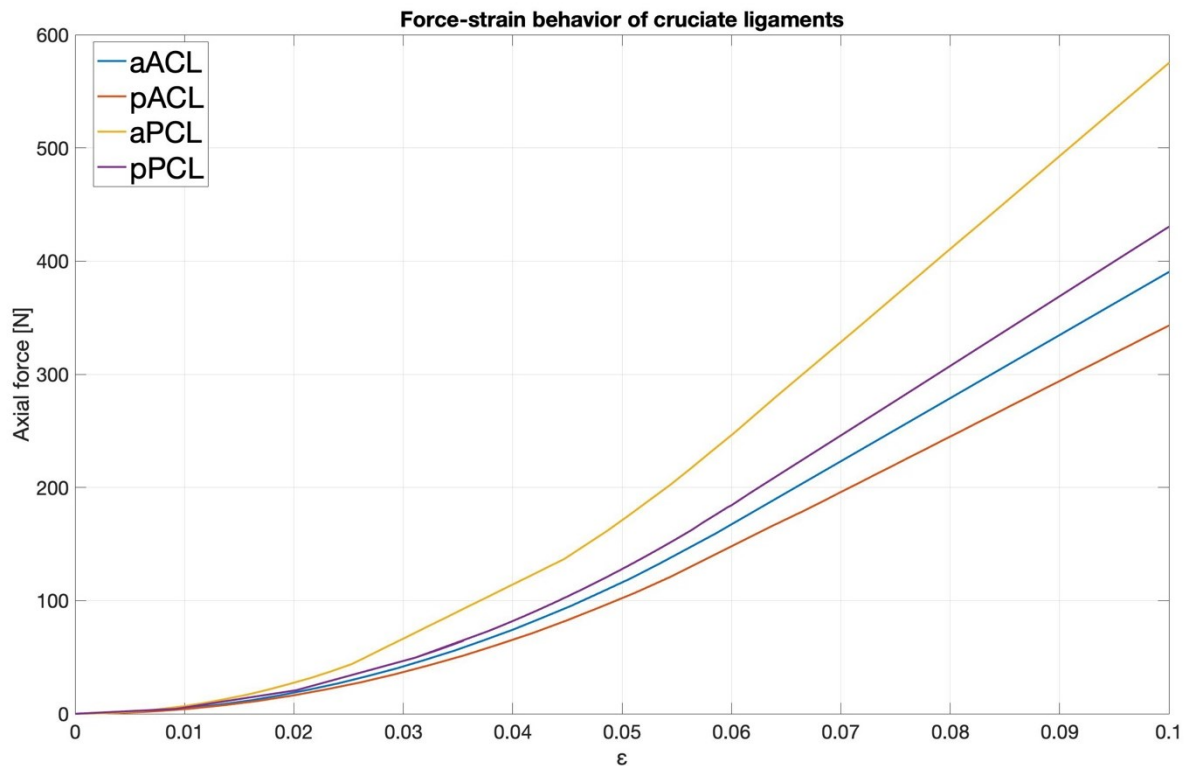
Figure 3.7 – Force-strain curve of cruciate ligaments; a: anterior, p: posterior.

	Stiffness k [N]	Reference strain or pre-strain ε_r	Reference length L_r [mm]
aACL	5,576	-0.05	35.9
pACL	4,901	0.07	34.1
aPCL	8,214	-0.29	36.7
pPCL	6,146	-0.14	39.2

Table 3.5 - Material properties for the cruciate ligaments: k is the linear stiffness used in Function 2.1, ε_r is the reference strain and L_r is the reference length of the ligaments in full extension.

3.6.3.2 Pre strain

Thermal expansion was applied to model the initial deformation of the ligaments by assigning a negative expansion coefficient in the material assignment of each ligament.

In Abaqus/CAE the expansion is modeled as follows (Abaqus/CAE User's Guide):

$$\varepsilon^{th} = \alpha(\theta - \theta_0)$$

- ε^{th} is the thermal strain;

- α is the coefficient of thermal expansion, coincident with the initial strain εr (values shown in the Table 2.2, Chapter 2);

- θ e θ_0 are the current chosen temperature of 1 K and the reference temperature of 0 K, respectively.

3.7 MESH GENERATION

Femur, tibia, and patella were partitioned to create a finer mesh in the regions of interest, that is the region near the articular cartilage and the partitions for ligament insertions. Instead, a coarse mesh was created in the proximal femur and distal tibia, respectively.

To partition the tibia, two planes perpendicular to its mechanical axis were identified. The first plane is located 35 mm from the most proximal point of the tibia, while the second plane is located 75 mm from the same reference point, resulting in three distinct bone partitions.

Similarly, the femur was partitioned into three sections using two planes perpendicular to its mechanical axis. These planes were located at distances of 57 and 157 mm from the femur's most distal point of the femur.

The resulting mesh of the total model is shown in Figure 3.8, and has 242,301 elements and 48,109 nodes. The type and shape of the elements chosen for each part and the total number of elements can be found in Table 3.6.
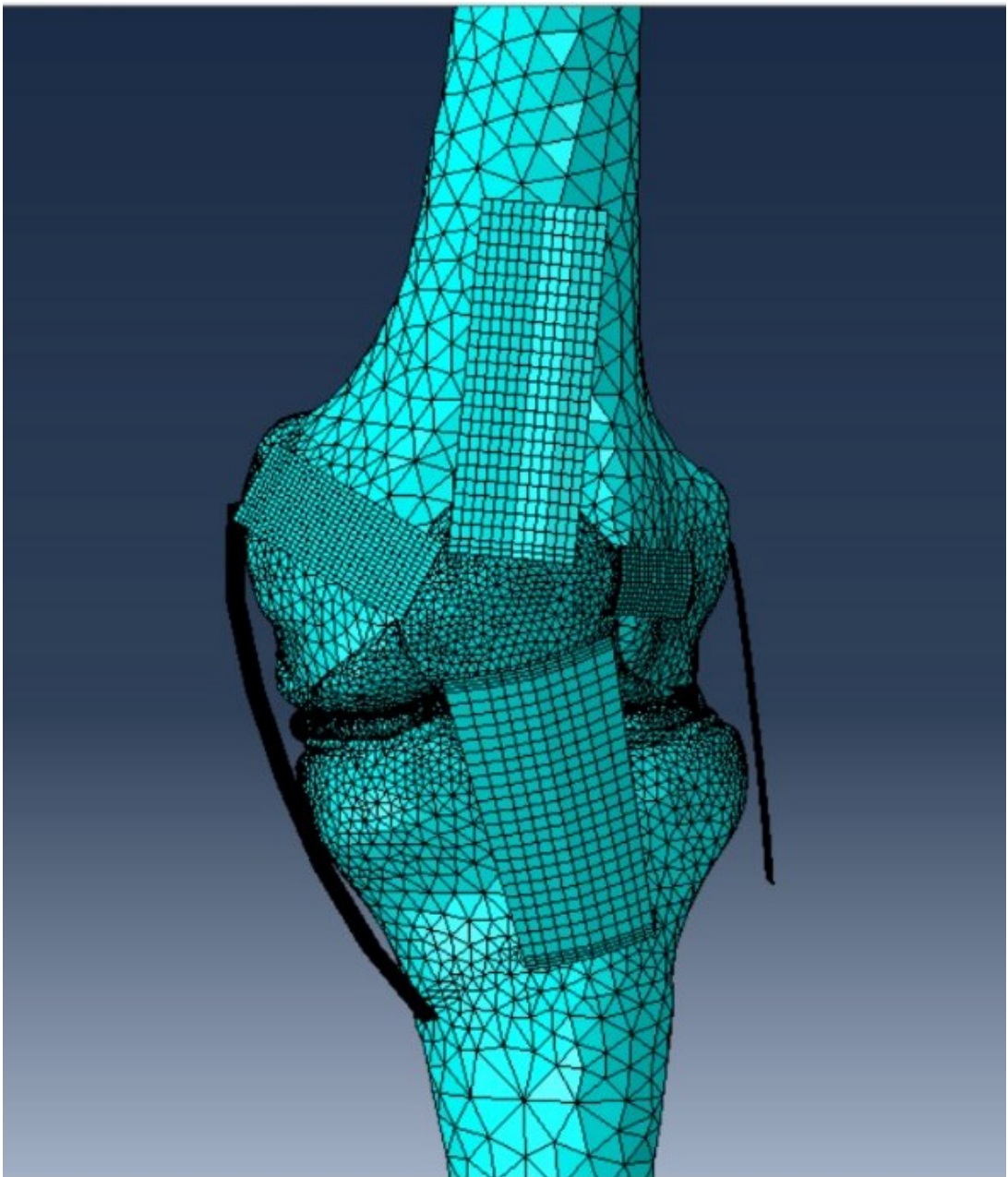
Figure 3.8 – Zoom of the total model mesh.

Parts	Number of elements	Element type and shape
Femur	145,583	C3D4 – a 4-node linear tetrahedron
Femur articular cartilage	19,223	C3D4 – a 4-node linear tetrahedron
Tibia	38,843	C3D4 – a 4-node linear tetrahedron
Tibia articular cartilage	6,353	C3D4 – a 4-node linear tetrahedron
Patella	12,428	C3D4 – a 4-node linear tetrahedron
Patella articular cartilage	6,262	C3D4 – a 4-node linear tetrahedron
Lateral meniscus	6,685	C3D4 – a 4-node linear tetrahedron
Medial Meniscus	4,961	C3D4 – a 4-node linear tetrahedron
MCL	456	S4R – a 4-node doubly curved thin shell, linear quadrilateral
LCL	208	S4R – a 4-node doubly curved thin shell, linear quadrilateral
MPFL	480	S4R – a 4-node doubly curved thin shell, linear quadrilateral
LR	240	S4R – a 4-node doubly curved thin shell, linear quadrilateral
PT	280	S4R – a 4-node doubly curved thin shell, linear quadrilateral
QT	300	S4R – a 4-node doubly curved thin shell, linear quadrilateral

Table 3.6 – Number, type and shape of elements used for each part of the model.

3.8 INTERACTIONS

Once the materials were assigned, the contact relationships between the surfaces of the components belonging to the model were defined.

All the interactions between the cartilage-bone, cartilage-cartilage, cartilage-menisci, and ligament-bone interfaces were established according to previous studies (Innocenti B.et al., 2014; 2011; Pianigiani S. et al., 2018; Markes A. R. et al., 2020).

In detail, at the tibial cartilage-menisci interfaces and the femoral cartilage-menisci interfaces, a general contact was used, with a coefficient of friction equal to 0.01. The same type of contact was used between ligaments and bone interfaces, but with a friction coefficient equal to 0.04.

Instead, a surface-to-surface contact definition was used as an alternative to general contact to model contact interactions between cartilage-cartilage interfaces, such as tibial cartilage-femoral cartilage and femoral cartilage-patellar cartilage, with a coefficient of friction equal to 0.001.

3.9 CONSTRAINTS

Bones

The distal portion of the tibia was coupled to a reference point situated 371 mm from the top surface of the tibial plateau, located at the ankle joint, and aligned with the tibial mechanical axis. For the femur, the rotation center along the transepicondylar axis was determined. The proximal part of the femur was coupled to this point, where flexion of the femur was applied. In Figure 3.9 are shown the constraints of the bony components.
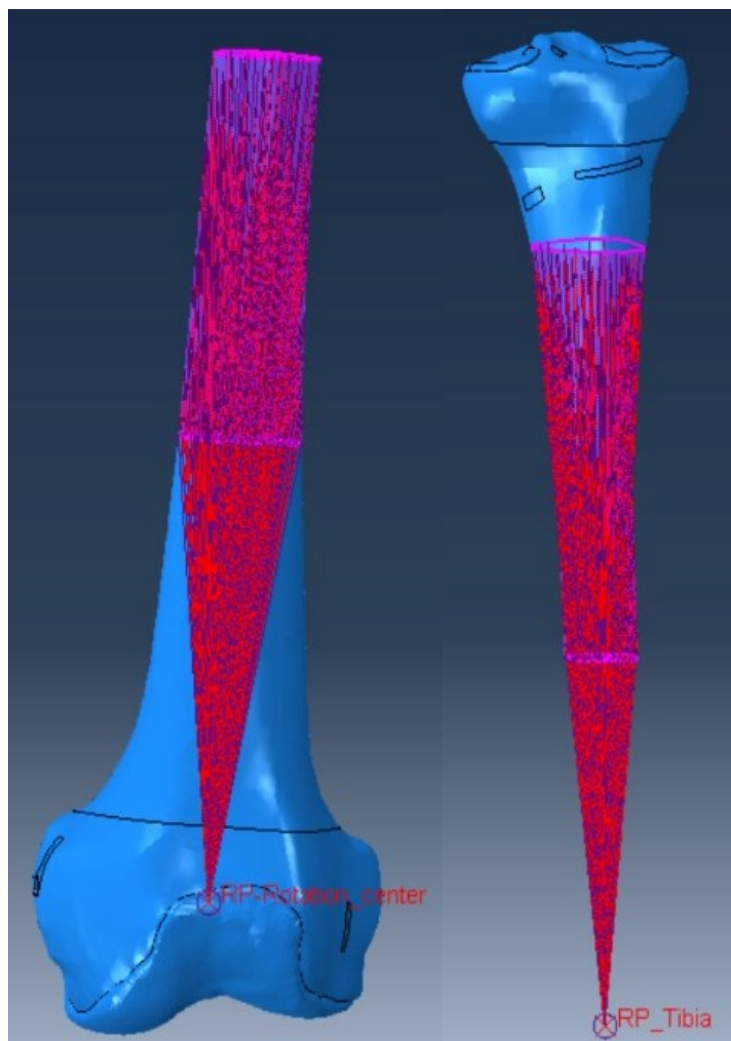
Figure 3.9 – Femur coupling on the left; tibia coupling on the right.

Soft tissues

To determine the constraints more precisely, the ligaments were divided into three parts: the two extreme parts represent one the origin and the other the insertion of the ligament on the bony components.

For all ligaments and tendons, a coupling constraint was applied between their insertion and origin surfaces and the insertion areas on the bony components. The coupling constraints allow one to constrain the motion of a surface to the motion of one or more points. In detail, the insertion area of the ligaments in the femur, tibia, and patella was considered as the surface area; while the nodes of the partitions made on the ligaments were taken as control points (as an example in Figure 3.10 the coupling between MPFL, LR and the bony components is shown).
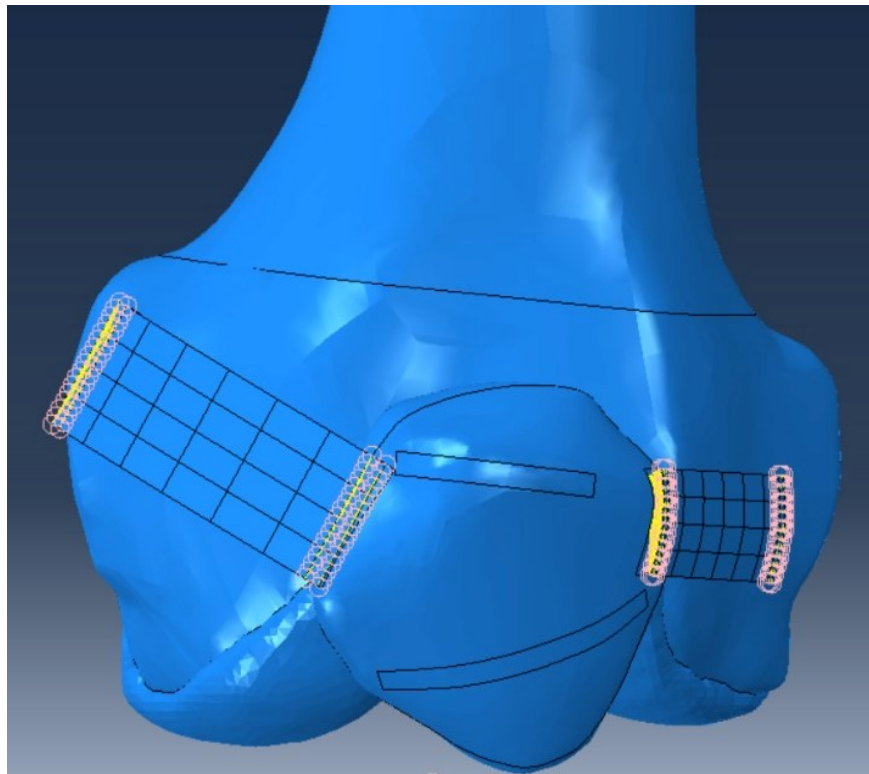
Figure 3.10 - Coupling between the bone components and the MPFL and LR. Highlighted in pink are the nodes used for the constraint.

Instead, for the quadriceps tendon, a reference point was created on its proximal part. This point, where the quadriceps load was applied, was coupled with the nodes of the superior surface of the tendon. The same point was then coupled with the center of rotation of the femur (Figure 3.11), so that the tendon would follow the femur during flexion, allowing the translations in the anterior-posterior and proximal-distal directions.
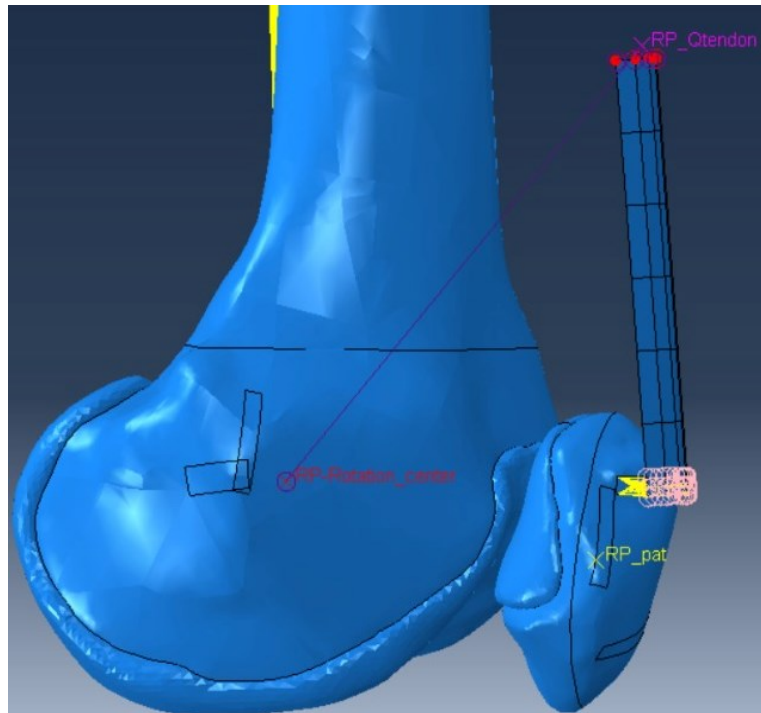
Figure 3.11 - Quadriceps tendon couplings.

3.10 LOADING CONDITION

To simulate the action of the quadriceps, a load was applied at the reference point of the tendon (shown in Figure 3.11). The tabular definition method to define the amplitude curve as a table of values at convenient points on the time scale, in this case from 0 N to 1100 N (Victor J., 2009b), and then Abaqus interpolates linearly between these values. Throughout the entire flexion movement, the force direction remains parallel to the anatomical axis of the femur.

Similarly, an axial force of 2500 N was applied at the reference point of the tibia, directed along its mechanical axis.

3.11 BOUNDARY CONDITION

Boundary conditions for the femur were applied at the center of rotation. Specifically, a single rotation was applied around the flexion-extension axis while fixing rotations around the other two axes and all potential displacements. The flexion was imposed by defining a tabular amplitude of values from 0 to 90 degrees, with a linear increase during the step time.

In contrast, for the tibia, the boundary conditions were applied at its reference point, and all possible rotations and translations were allowed, except rotation in the flexion-extension axis, ensuring complementary degrees of freedom between the two bones.

3.12 CREATION OF PATELLA ALTA AND PATELLA BAJA MODELS

The objective of this study was to analyze the kinematics and contact forces within the knee, specifically focusing on the patellofemoral joint. This analysis was conducted with consideration of both physiological and pathological conditions, as can be the patella baja and patella alta conformation.

Thus, from the native model two other different models were implemented, one for the patella baja and one for the patella alta. As described in Chapter 1, the Blackburne-Peel index was used to define patellar height (Luyckx T. et al., 2009; Blackburne J. S. & Peel T. E., 1977). In particular, Blackburne-Peel indices of 0.59 for patella baja and 1.29 for patella alta were considered.

After the placement of the patella, the same mesh, interactions, constraints, loads, and boundary conditions of the native model were considered for both models and presented above.

The three models are shown in Figure 3.12.
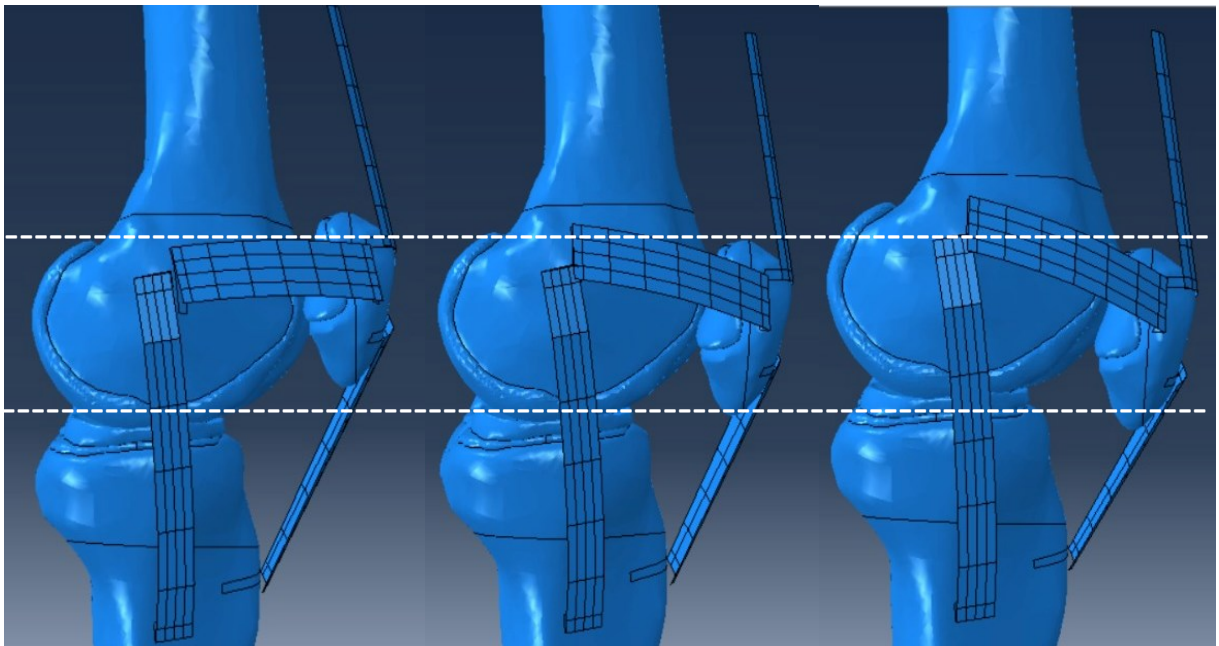
Figure 3.12 - Three models compared: patella alta on the left; native patella in the center; patella baja on the right.

3.13 ANALYZED TASK

The kinematics of the knee joint was studied using an open kinematic chain approach, which simulated three different conditions: a native knee, a knee with patella alta, and a knee with patella baja. In this setup, an open kinematic chain consists of a series of articulated

segments where the proximal part of the extremity is fixed or not free to move, while the distal part is allowed to move freely in space. In this specific model, the femur and tibia represent the two segments of the chain, with the knee joint serving as the articulation point. The simulation began in the full extension reference configuration and the flexion of the femur gradually increased from 0° to 90°, while the tibia remained unconstrained.

3.13.1 Step module

To conduct the analysis, a specific step was defined. The total time period for the analysis was set at 6.2 s. During the initial second of the analysis, no loads were applied, allowing pre-strain of the ligaments.

Within this module, the mass scaling was configured, choosing a value of 10^{-5}. Mass scaling is a parameter used in Abaqus for explicit analysis to adjust the mass of the entire model at the beginning of each step. Complex dynamic models frequently involve a few small elements, which will force Abaqus to employ small time increments. These small elements often result from a difficult mesh generation task. By scaling the masses of these influential elements at the beginning of the step, it is possible to substantially increase the stable time increments. However, this adjustment typically has a negligible impact on the overall dynamic behavior of the model. Therefore, when the mass scaling factor is used, the masses of elements with a time increment smaller than the user-defined time increment are adjusted, making their time increments match the value specified by the user. The aim of mass scaling is to enhance the computational efficiency of the analysis.

CHAPTER 4 RESULTS PRESENTATION AND DISCUSSION

4.1 RESULTS

The objective of this computational study is to examine the biomechanical impact of varying patella height on patellofemoral forces and kinematics. To this end, the following variables were considered and extracted from each test to evaluate the results of the simulations:

- anterior-posterior translation of the femur relative to the tibia;

- internal-external rotation of the tibia (tibial axial rotation);

- internal-external rotation of the patella (patellar tilt);

- flexion-extension of the patella;

- anterior-posterior translation of the patella relative to the femur;

- medio-lateral translation of the patella relative to the femur (patellar shift);

- contact variables (force, area, and pressure) in the articular cartilage of femur, tibia, and patella.

The kinematic results and contact variables obtained from each simulation were compared to assess the range to which the joint function is affected by the alteration of patellar tracking caused by the baja and alta configurations of the patella.

4.1.1 Tibio-femoral kinematics

All of the analyzed cases exhibit a consistent kinematic pattern, although with variations in magnitude compared to the native reference condition. Initially, there is a phase of internal rotation, typically occurring between 0 and 15 degrees of flexion. Subsequently, the tibia undergoes external rotation, accompanied by anterior translation of the femur as flexion progresses. For the three models, native, patella alta, and patella baja, Figure 4.1 and Figure 4.2 show the internal-external rotation of the tibia and the antero-posterior translation of the femur, respectively. During the first 15° of flexion, the tibia rotates internally to a maximum of 2.24°, 1.50° and 1.80° for the native model, patella alta and patella baja, respectively. Then it rotates externally for 6.61°, 5.98° and 4.67°, respectively (Figure 4.1).
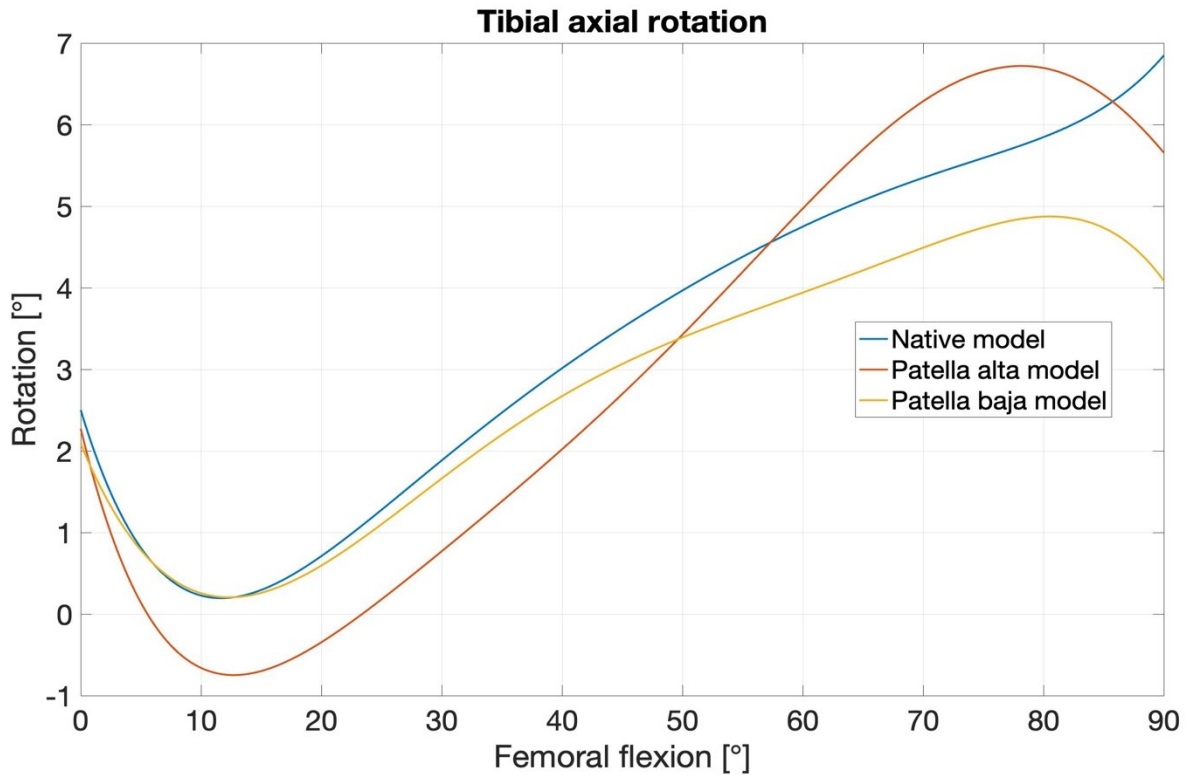
Figure 4.1 - TIbial axial rotation. Decreasing values represent internal rotation and increasing values external rotation.

As for the femur, it moves forward by 8.16 mm, 8.04 mm and 8.54 mm for the native patella, patella alta and patella baja, respectively, followed by a gradual posterior translation (Figure 4.2).
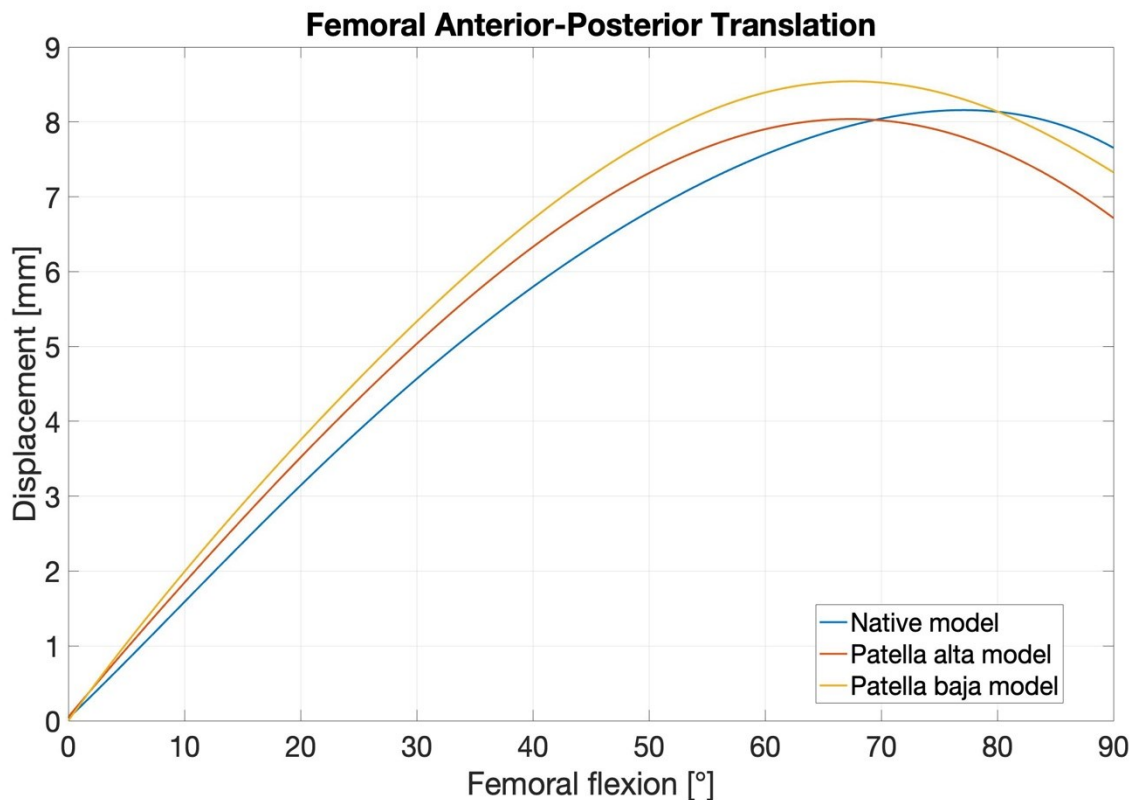

Figure 4.2 - Femoral anterior-posterior translation. Increasing values represent anterior translation, decreasing values represent posterior translation.

The position of the patella (alta or baja) varies in a plane orthogonal to that where antero-posterior translation of the femur occurs. Therefore, different heights of the patella do not induce any effect on this movement.

The differences in the root mean square value (RMS) between the native model and the patella alta kinematics are 0.84° and 0.45 mm for tibia rotation and the femur translation, respectively. While the RMS between the native and patella baja are 0.83° and 0.66 mm.

4.1.2   Patellofemoral kinematics

In terms of PF kinematics, all cases analyzed also showed a consistent trend, although with variations in amplitude from the native reference condition. The patellar shift was not considerably affected by the different patellar heights (Figure 4.6). However, the tilt was more affected by the different heights of the patella (Figure 4.3). In all conditions, the patella consistently translated posteriorly and flexed relative to the femur (Figure 4.4 and Figure 4.5).

The results indicated that the patella baja produced a more lateral tilt, greater than 13° during knee flexion. Regarding the patella alta, in the first 20° of flexion, an internal rotation of 1.7° followed by an external rotation of up to 3.95°. The patella in the native model shows an external rotation of up to 9° (Figure 4.3).
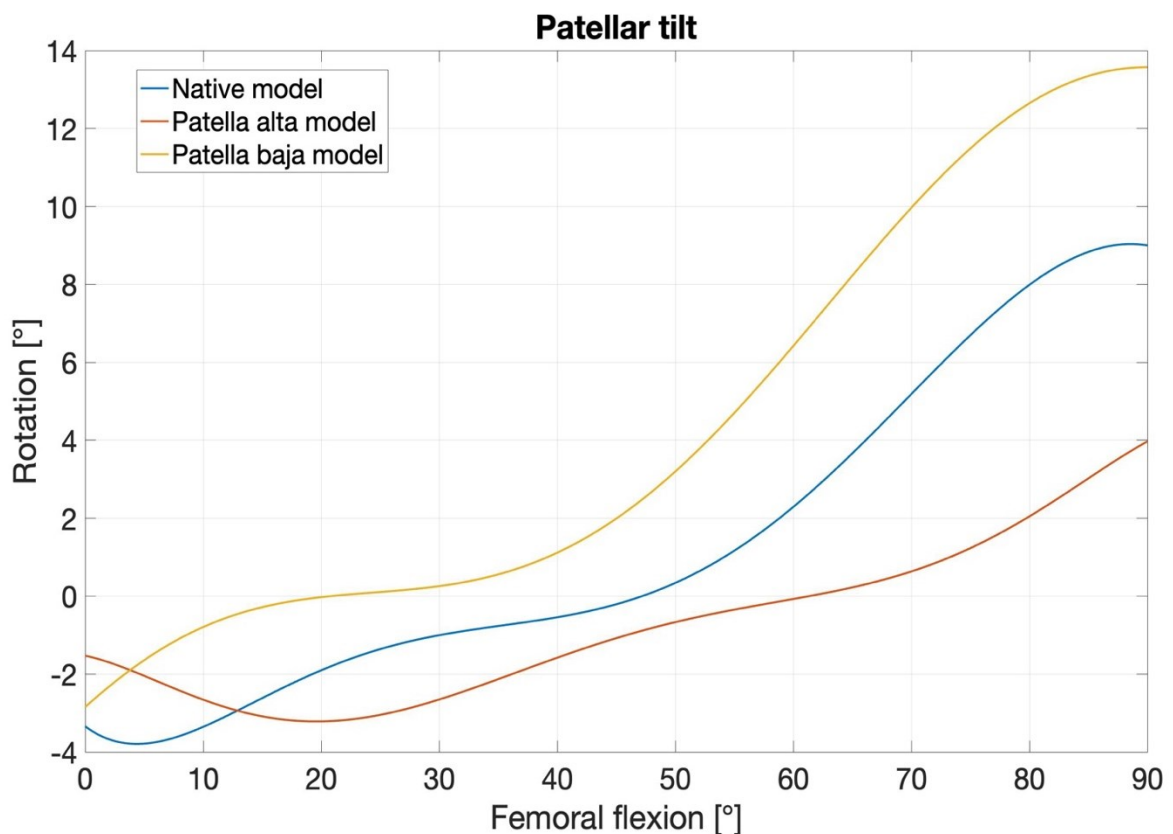

Figure 4.3 - Patellar internal - external rotation (tilt). Negative values represent internal rotation (medial tilt), positive values represent external rotation (lateral tilt).

71

The patellar flexion, for all three models, increases with increasing knee flexion, and the patella is more flexed in the patella alta than in the baja (Figure 4.4).
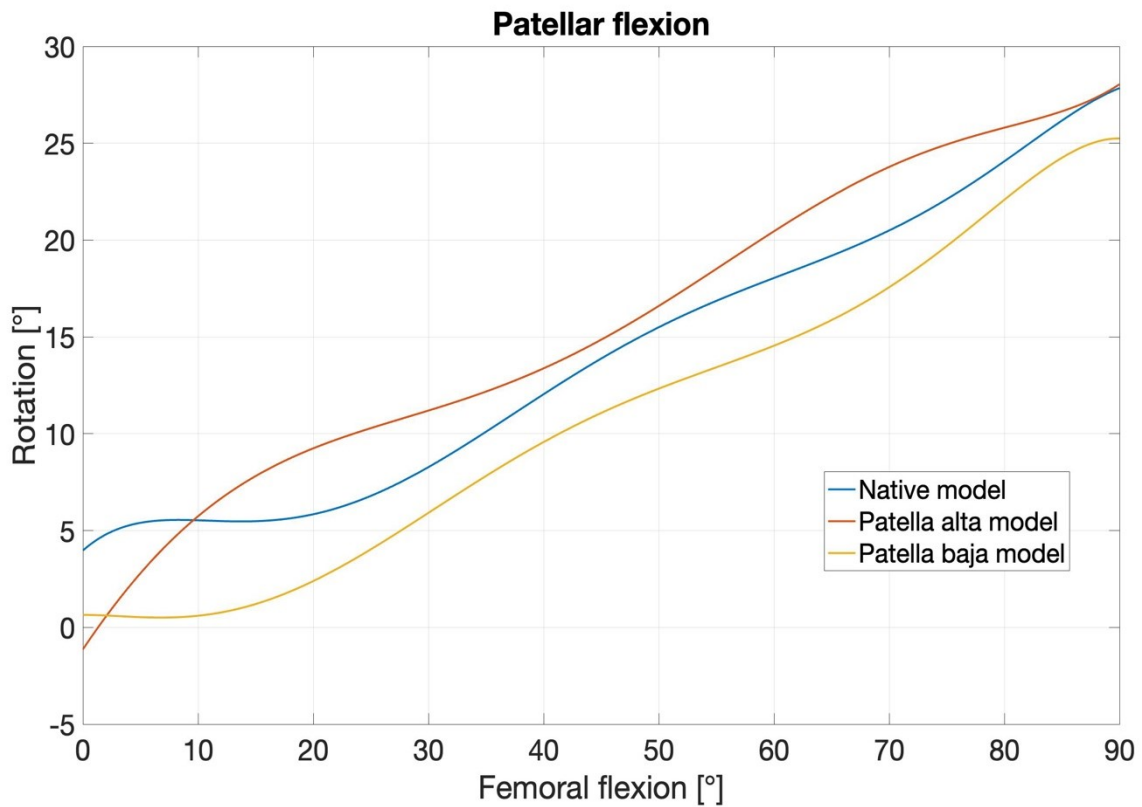

Figure 4.4 - Patellar flexion. Increasing values indicates flexion.

The results show that for all the cases analyzed, the posterior patella translation increases as knee flexion increases (Figure 4.5).
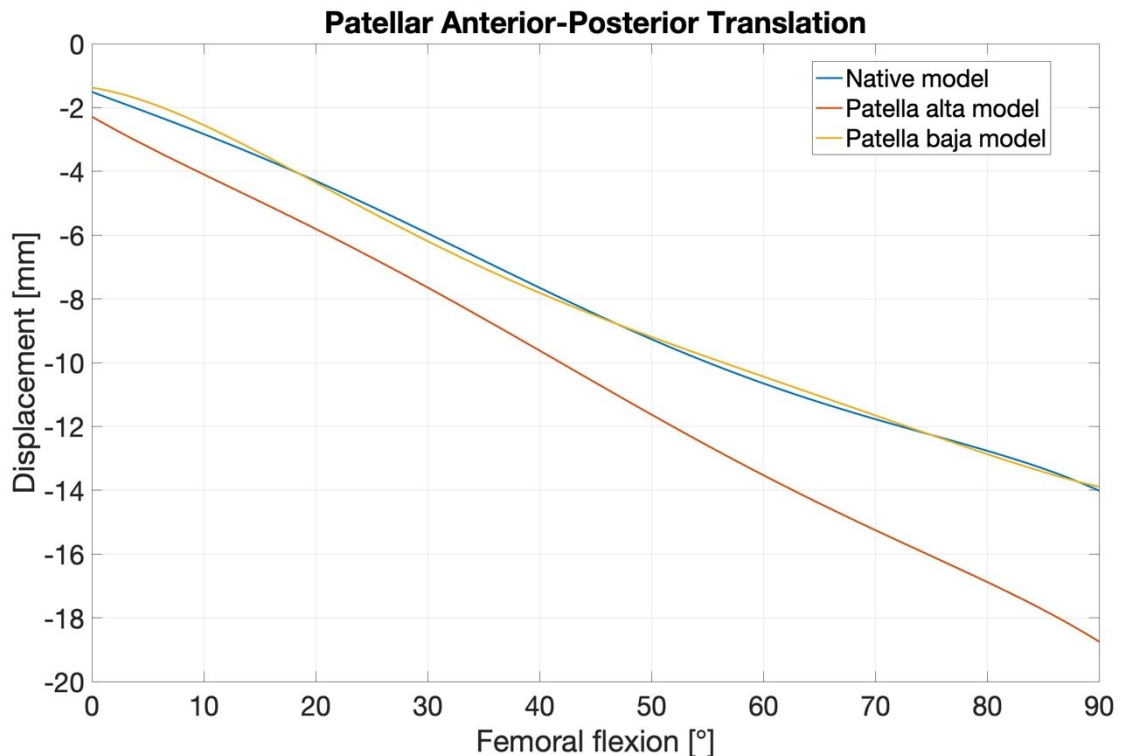

Figure 4.5 - Patellar anterior-posterior translation. Negative values represent posterior translation.

An increasing lateral translation with increasing flexion can also be seen for the medial-lateral translation. The results show a greater lateral translation in the model with the patella alta (Figure 4.6).

The RMS differences between the native model and patella alta kinematics are 2.96°, 2.53°, 2.63 mm and 0.85 mm for patellar tilt, flexion, antero-posterior translation and lateral shift, respectively. The RMS between the native and patella baja are 3.22°, 3.32°, 0.20 mm and 0.84 mm, respectively.
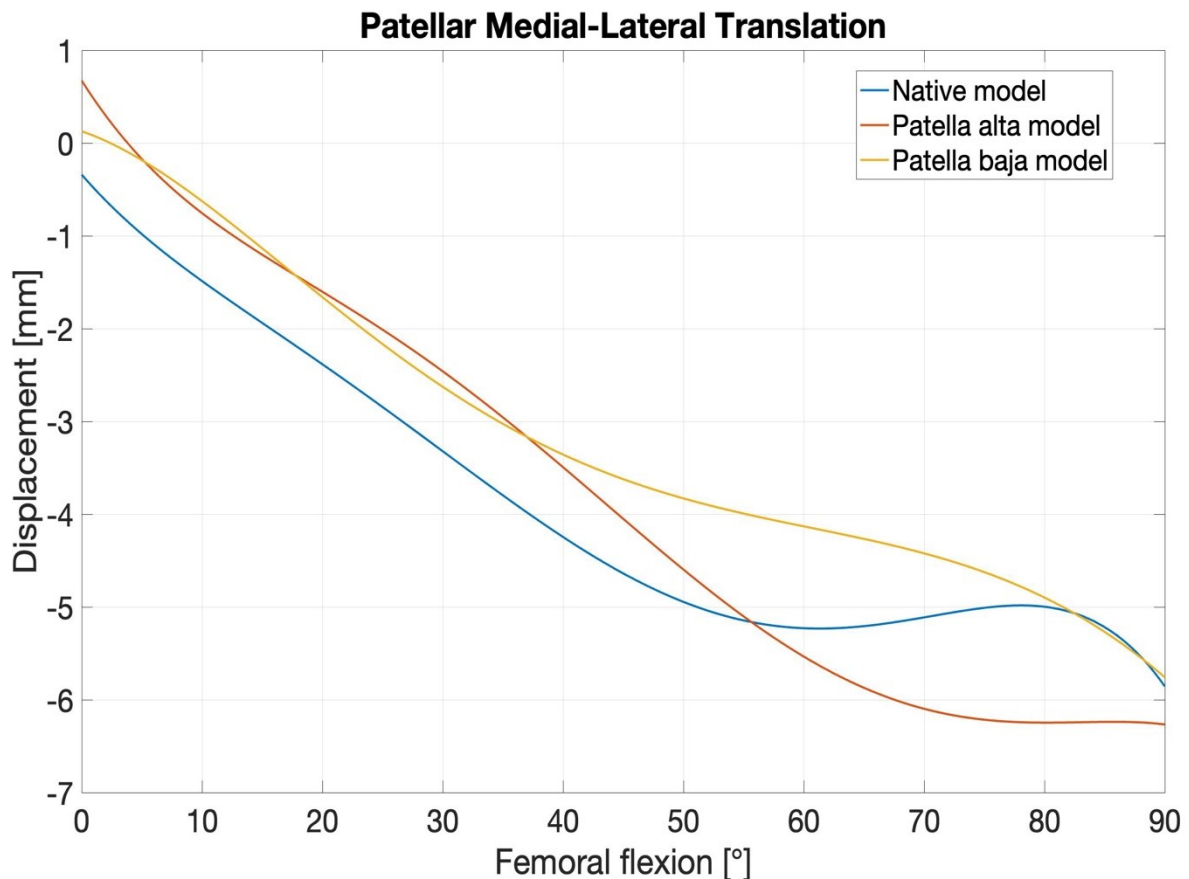

Figure 4.6 - Patellar medial-lateral translation (shift). Positive values represent medial translation, negative values lateral translation.

4.1.3 Results of the contact variables

The total patellofemoral contact area gradually increases with flexion (Figure 4.7). For normal patella height, the contact area reaches a maximum at 90° of flexion. For the first degrees of flexion, a higher patella position corresponds to a lower contact area, whereas a lower position is associated with a higher contact area. After 30° of flexion, the maximum patellofemoral contact area gradually increases with increasing patella height. This may be explained by the higher forces observed in deep flexion (after 90°) for these higher positions.

RMS differences during the flexion cycle averaged less than 170 mm² for the contact area between the native model and the patella alta model, and 55 mm² between the native model and the patella baja model.
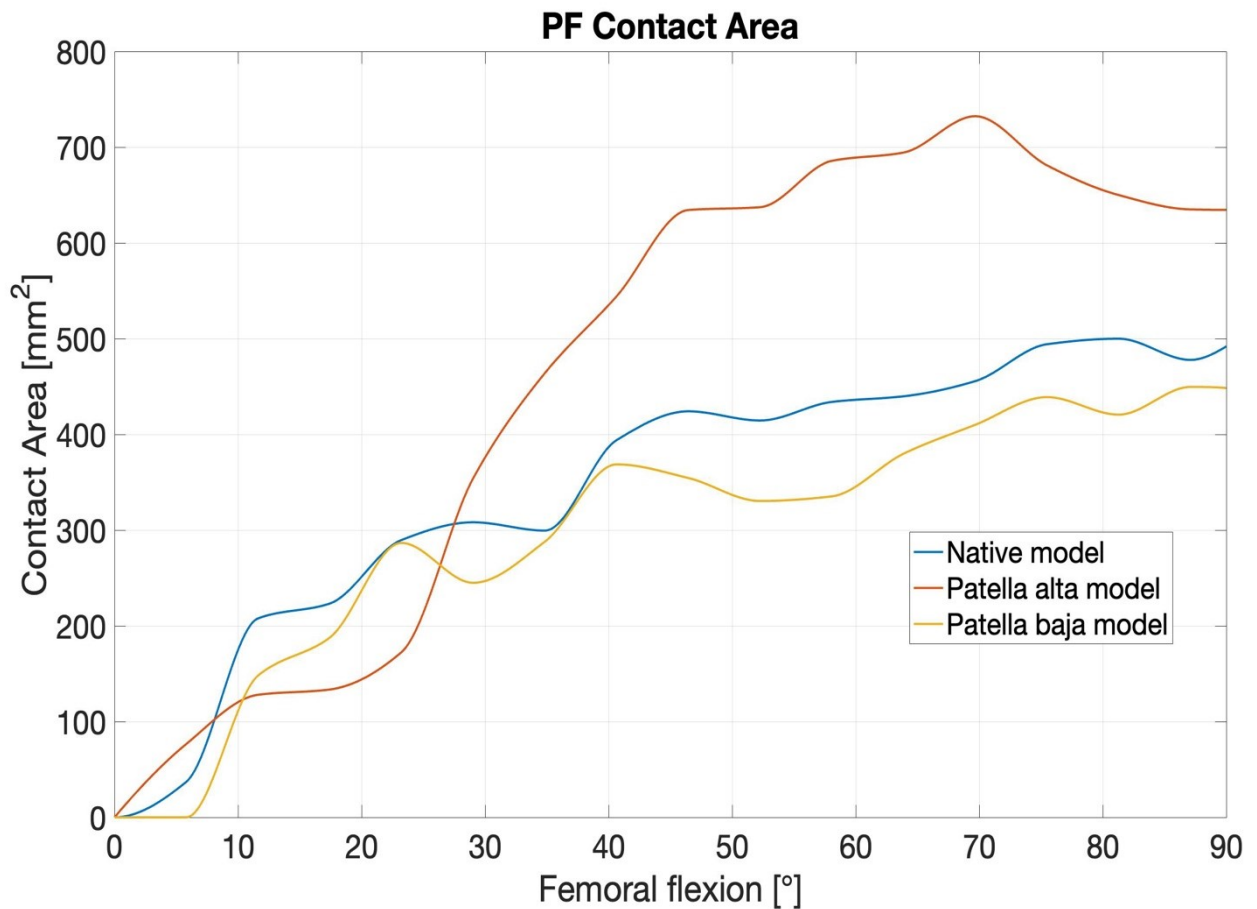

Figure 4.7 - Patellofemoral contact area for the different patellar positions.

The patellofemoral contact force increases as the knee flexes (Figure 4.8), reaching its peak when contact occurs between the quadriceps tendon and the femoral trochlea, resulting in load sharing. However, in cases with a higher patella, this contact is delayed until a deeper flexion angle is reached. During the early stages of flexion, lower patella positions are associated with higher contact forces, while higher positions lead to reduced patellofemoral contact forces in this range of flexion. When the knee is flexed to less than 60°, a higher patella reduces the contact force, and this reduction is directly proportional to the height of the patella. This biomechanical phenomenon is explained by the role of the patella in the extensor mechanism of the knee (Luyckx T. et al., 2008). The patella significantly contributes to knee extension torque by increasing the lever arm of the quadriceps. It also transfers forces from the quadriceps tendon to the patellar tendon. As a result, it can rotate freely around its point of contact with the femoral trochlea in the sagittal plane, acting as a balance beam. Since the point of contact with the femur is initially more distal on the patella during early flexion, the effective moment arm

of the quadriceps tendon becomes greater than that of the patellar tendon. Consequently, in the early stages of flexion, less quadriceps force is needed to generate a given patellar tendon force. The presence of a higher patella enhances this effect by causing a more distal contact point, creating a more efficient knee extensor mechanism. Therefore, the reduction in patellofemoral contact force associated with a higher patella is attributed to the lower required strength of the quadriceps tendon.

The maximum patellofemoral contact forces for the lowest, normal, and highest patella positions are 1614 N, 1657 N, and 1052 N, respectively.
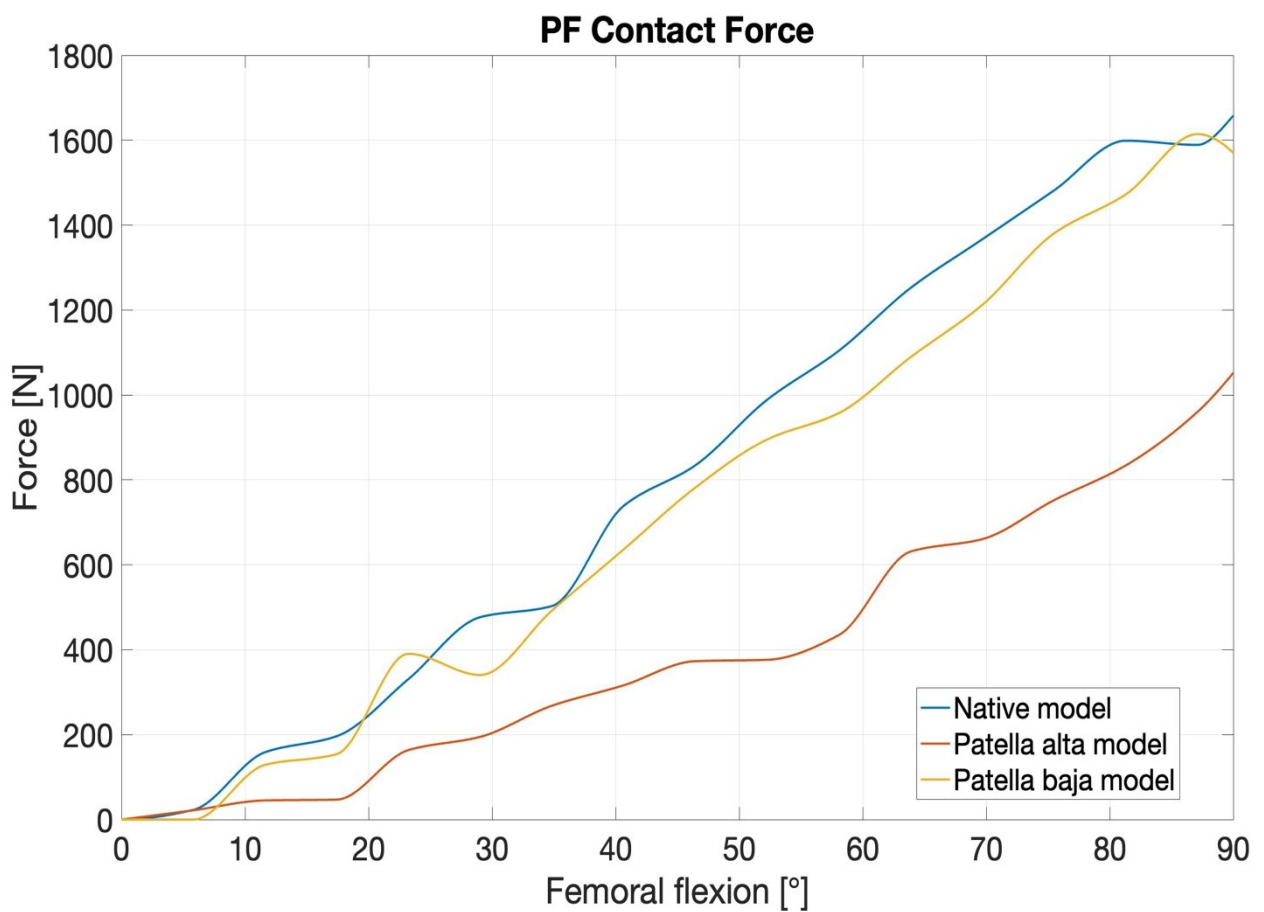

Figure 4.8 - Patellofemoral contact force for the different patellar positions.

Figure 4.9 presents the average contact pressure throughout the flexion. In the normal knee, the maximum patellofemoral contact pressure is reached at about 90 ° of flexion. During the entire range of flexion, the contact pressures are lowest for the higher positions, instead lower positions are associated with higher contact pressures (Figure 4.9).

The RMS between the native and patella alta models, with respect to contact pressure, is 1.43 MPa. The RMS between the native and baja patella is 0.22 MPa.
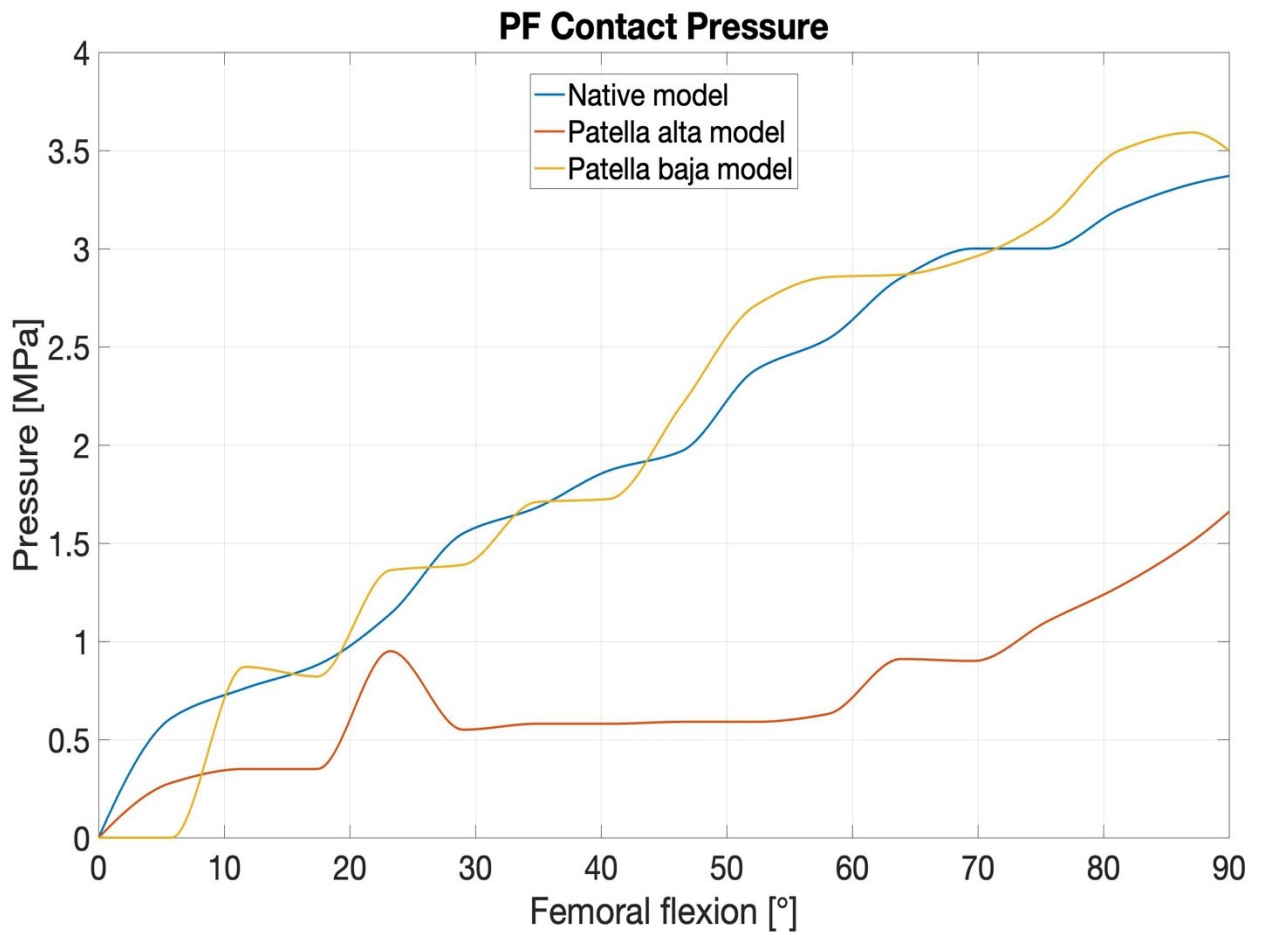

Figure 4.9 - Patellofemoral contact pressure for the different patellar positions.

4.1.3.1 Native knee

In the reference native knee model, Table 4.1 provides contact pressure data for various flexion angles (0°, 30°, 60°, and 90°). As the knee flexes, both the contact areas and the point of highest contact pressure between the tibia and the femur shift to the posterior side of the knee joint. For all degrees of flexion, the tibial cartilage experiences higher loads in the lateral compartment compared to the medial compartment. Maximum contact pressure values, which exceed 14 MPa, are reached at 90° of flexion. Similar trends are observed in the femoral compartment, with the highest pressures occurring at 90° of flexion. The contact between the cartilage of the femur and the patella is observed anteriorly. As the knee flexes, the patellar contact point gradually moves proximally to an area where the cartilage is thicker. The maximal contact interaction is observed in the transition from patellar support by the trochlea to the femoral condyles. This transition corresponds to the shift from one central contact area to two smaller separate areas as the patella moves from the femoral trochlea onto the two condyles at the intercondylar notch, can be seen between 30° and 60°.

These observations illustrate how the patellofemoral contact pressure and contact areas change with knee flexion and provide valuable information on the biomechanics of the knee joint in different flexion states.
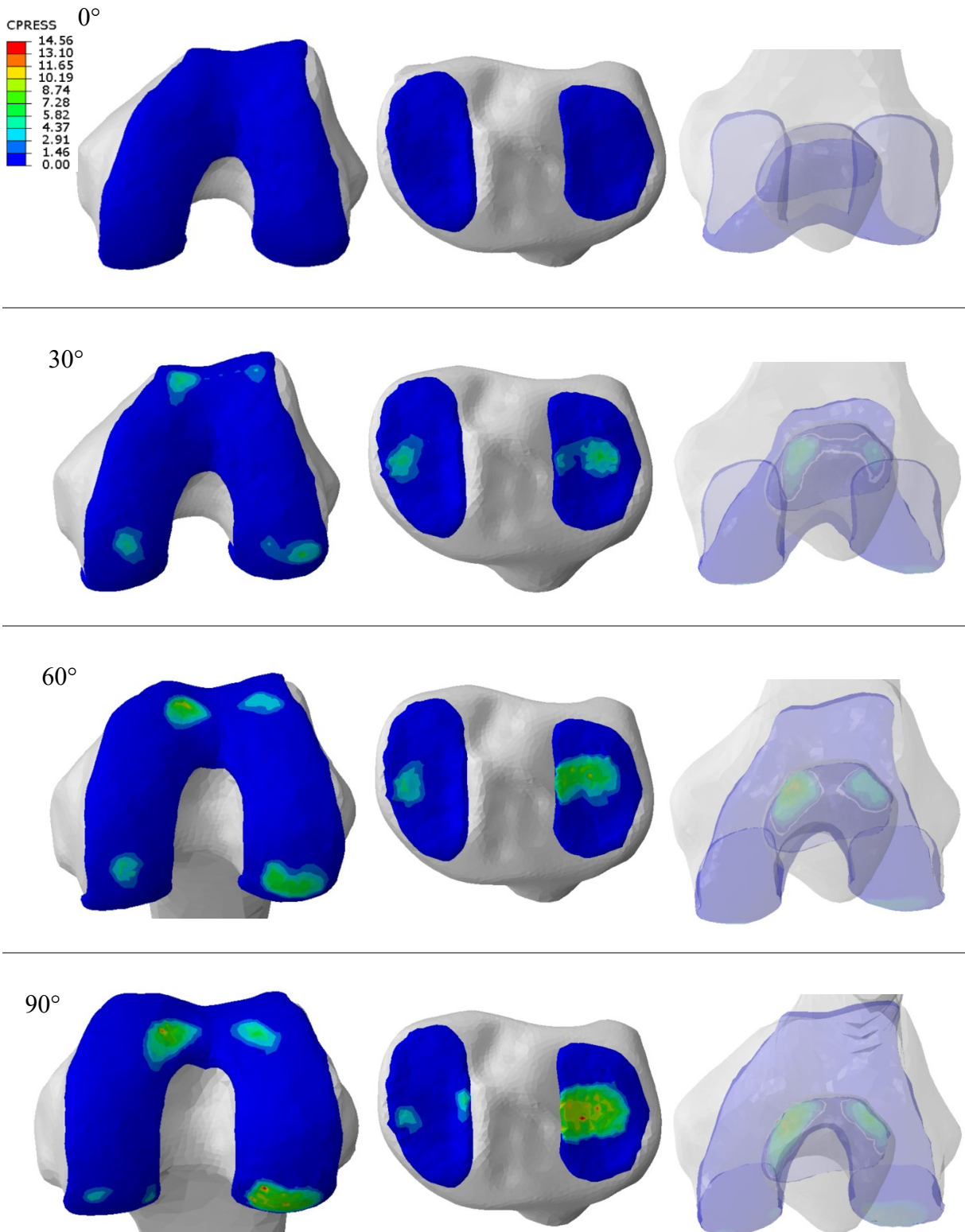
Table 4.4 - Contact pressure, measured in MPa, analysed in femoral, tibial, and patellar cartilage during flexion for the native knee model. In each cell, the left side represents the medial region, whereas the right side represents the lateral region. On the upper left side, contact pressure results are indicated in a legend with colors from blue (0 MPa) to red (14.56 MPa).

4.1.1.1 Patella alta

Compared to the native model, patella alta shifts the contact pressure areas slightly towards the posterior direction, particularly noticeable in the lateral tibial compartment. As previously observed, the maximum contact pressure is still reached at 90° of flexion (Table 4.2). Furthermore, the contact pressure values are lower than those of the native joint model. Concerning the contact between femoral cartilage and patellar cartilage, with patella alta, there is a gradual distal shift in the contact point on the patella as the patellar height increases. This means that in initial flexion, the patella alta is associated with the most distal contact point.
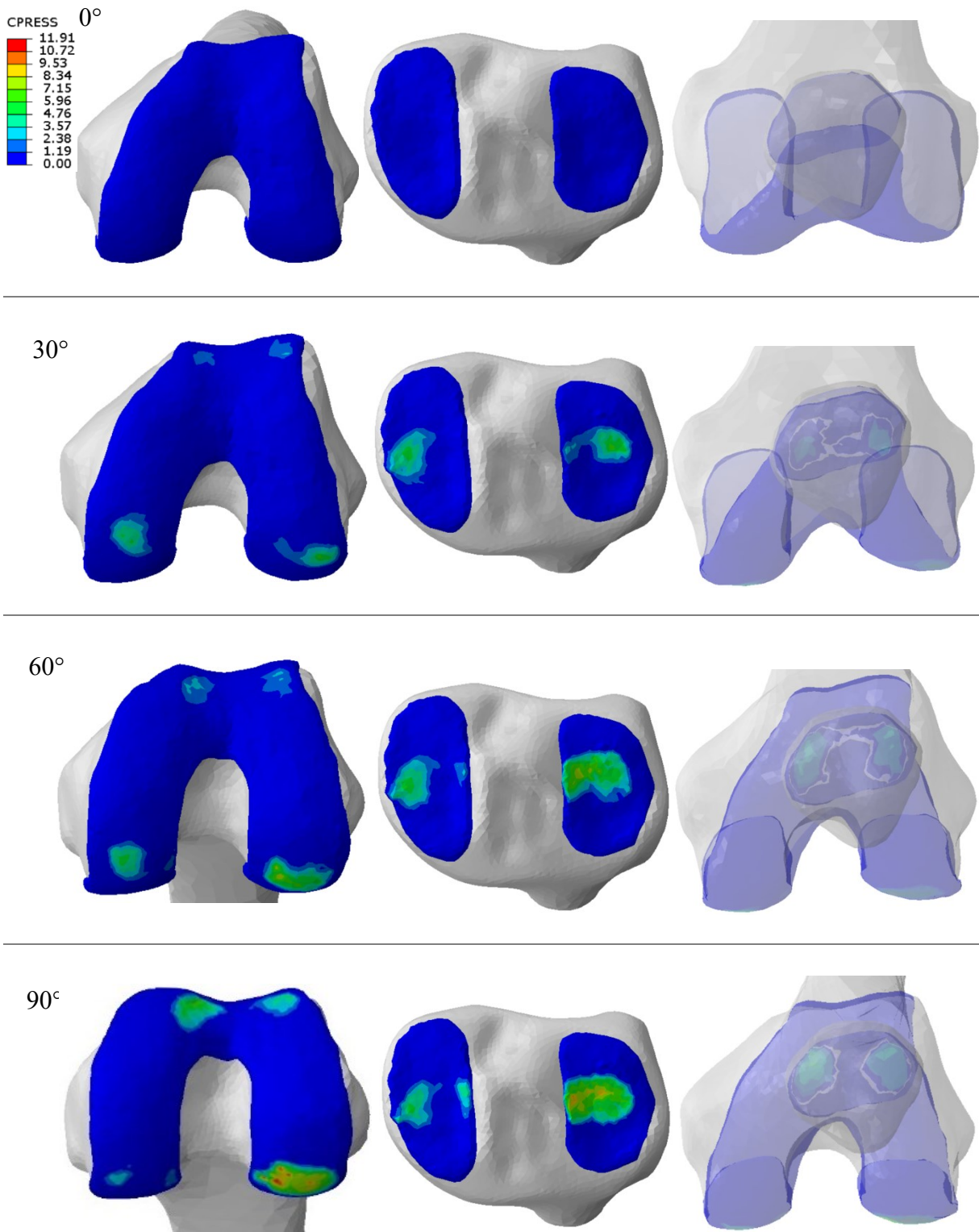
Table 4.5 - Contact pressure, measured in MPa, analyzed in femoral, tibial, and patellar cartilage during flexion for the patella alta model. In each cell, the left side represents the medial region, whereas the right side represents the lateral region. On the upper left side, contact pressure results are indicated in a legend with colors ranging from blue (0 MPa) to red (11.91 MPa).

4.1.1.1 Patella baja

A higher contact pressure is observed in the patella baja model than in the native condition. Table 4.3 provides a comprehensive overview of the contact areas and contact pressures in the femoral, tibial, and patellar compartments at various flexion angles. The tibial cartilage is less loaded in the medial compartment than the native and patella alta models. In femur-patella contact, the patella baja is associated with the most proximal point of patellofemoral contact in early flexion.
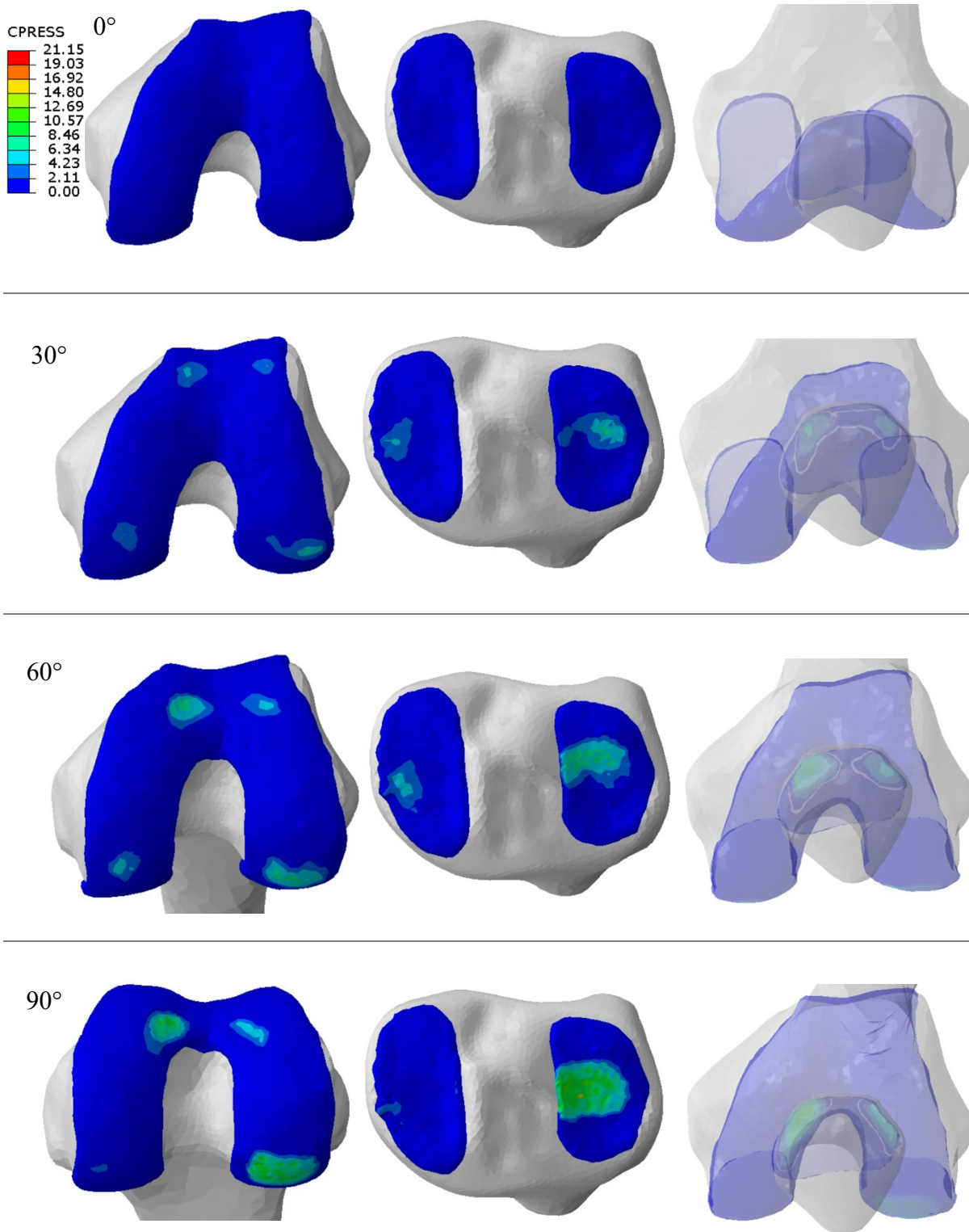
Table 4.6 - Contact pressure, measured in MPa, analyzed in femoral, tibial, and patellar cartilage during flexion for the patella baja model. In each cell, the left side represents the medial region, while the right side represents the lateral region. On the upper left side, the contact pressure results are indicated in a legend with colors from blue (0 MPa) to red (21.15 MPa).

4.2 DISCUSSION

The agreement between the experimental results and the FE model shows that the analysis produces plausible kinematic and mechanical contact results.

It is important to note that comparing the results of this study with those of the existing literature can be difficult. Although similar results can be observed, care must be taken when making such comparisons. Discrepancies may result from variations in constitutive models, material properties, loading conditions, and boundary conditions examined.

The following sections provide a comparative analysis, focusing on patellofemoral (PF) and tibio-femoral (TF) kinematics and contact variables, between the native model developed in this study and results reported in the previous literature. This comparison helps to shed light on the consistency and reliability of the results of the current study compared to established research.

4.2.1 Kinematics

Regarding tibio-femoral kinematics, the comparison results are shown in Figure 4.10 and Figure 4.11, femoral anterior-posterior translation, and tibial axial rotation, respectively. When comparing the results obtained from the literature with those of the present study, it can be seen that the trend is the same, but the values show variations, especially in the axial rotation of the tibia. In any case, all results show an anterior translation of the femur throughout flexion and an overall external rotation of the tibia.
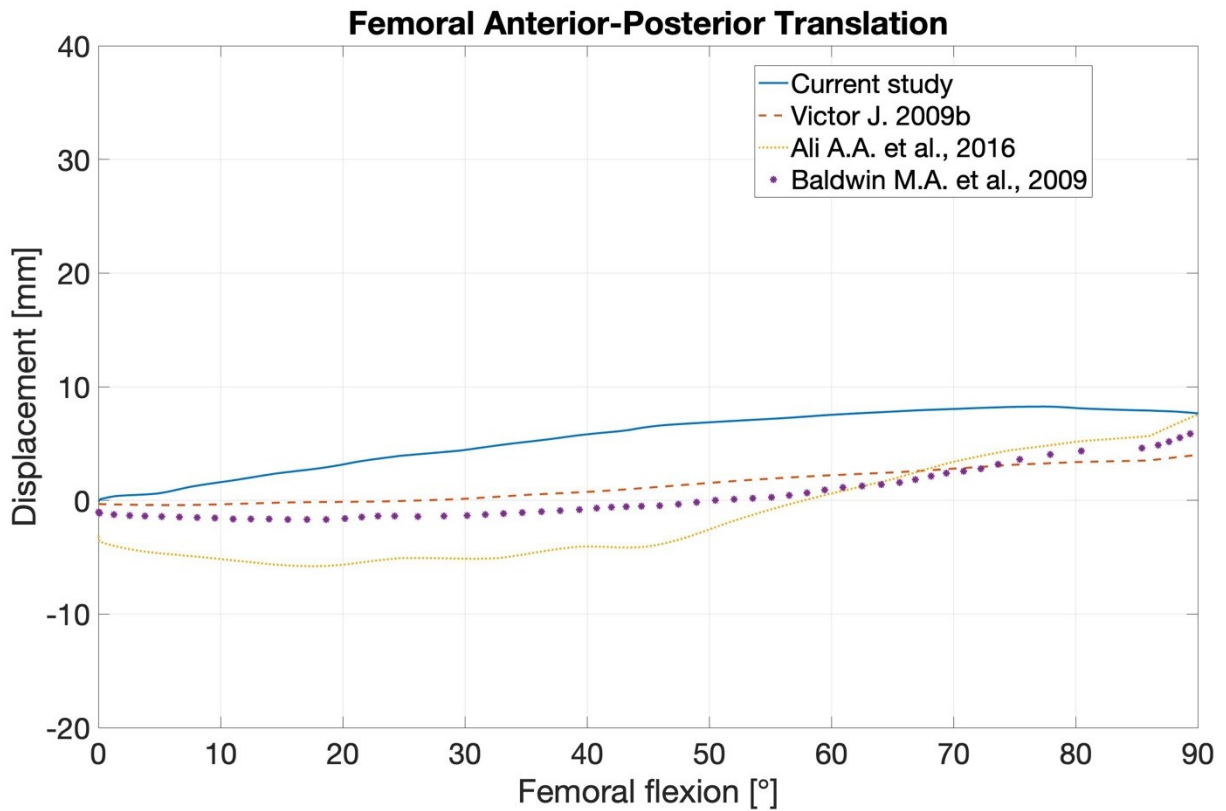
Figure 4.10 - Comparison of femoral anterior-posterior translation between the native model of the current study and the results obtained from the literature. Positive values represent anterior translation, negative value represent posterior translation.
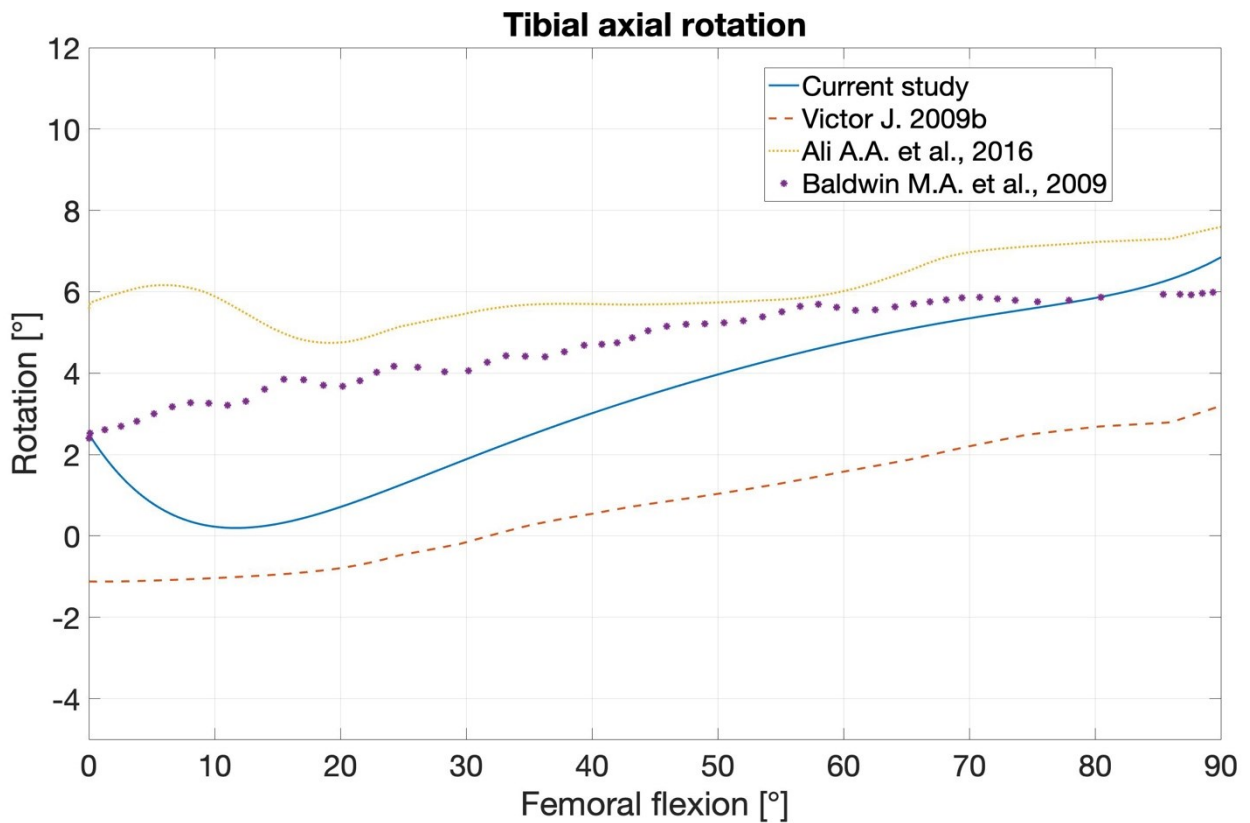

Figure 4.11 - Comparison of tibial axial rotation between the native model of the current study and the results obtained from the literature. Negative values indicates internal rotation, positive external rotation.

84

Similarly to the results of the tibio-femoral kinematics, the patellofemoral kinematics predicted by the native model corresponded well with the trends and magnitudes found in the literature.

Comparisons are shown in Figure 4.12 and Figure 4.13 with respect to patella tilt and medial-lateral translation, respectively.

The patellar tilt in this study corresponds well with the results of the study conducted by Baldwin M. A. et al. (2009). Regarding medio-lateral translation, although all the reported results show lateral translation, the native pattern of this study seems to be very close in both trend and magnitude to the results reported by Fitzpatrick C. K. et al. (2010).
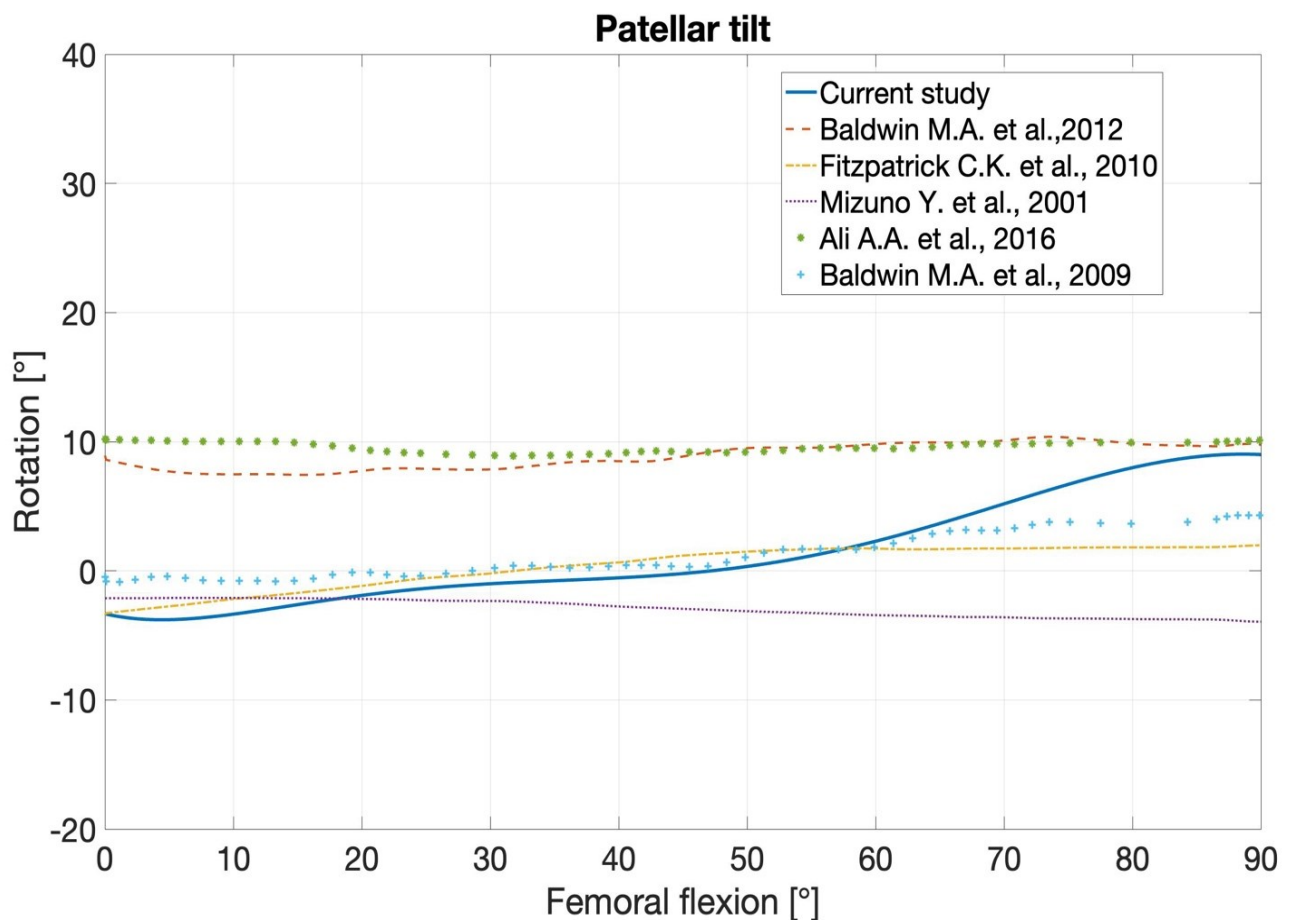

Figure 4.12 - Comparison of patellar tilt between the native model of the current study and the results obtained from the literature. negative values represent internal rotation (medial tilt), positive values represent external rotation (lateral tilt).
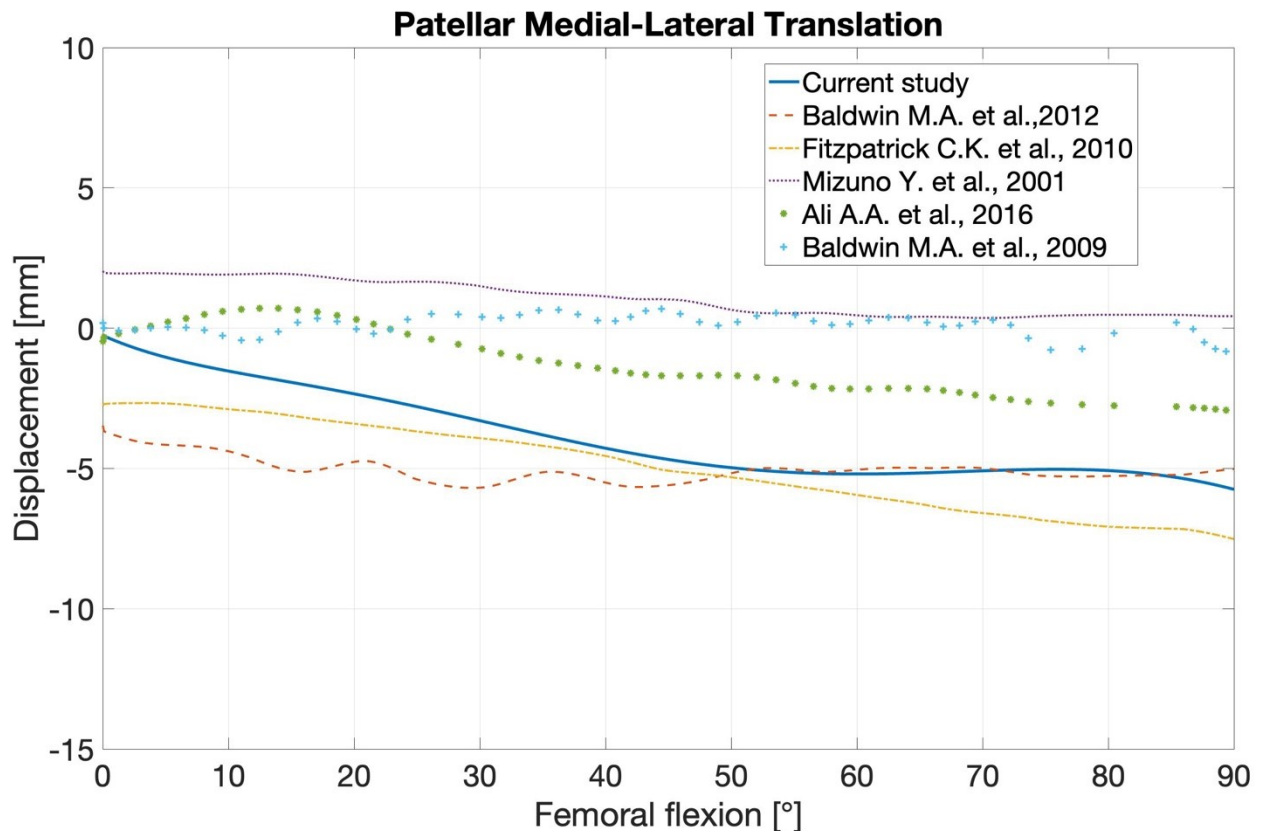
Figure 4.13 - Comparison of patellar medial-lateral translation between the native model of the current study and the results obtained from the literature. Positive values represent medial translation, negative values lateral translation.

4.2.2 Contact variables

Regarding contact variables, few previous studies were found in the literature to compare with the results obtained in this study.

Figures 4.14, 4.15 and 4.16 show the contact area, total force due to contact pressure, and contact pressure, respectively. For all three contact variables, the results of the native model in this study are close to the trend in both the works by Luyckx T. et al. (2008) and Fitzpatrick C. K. et al. (2010).

The differences between the data of the present study and those of Luyckx et al. (2008) may result from the fact that they considered the quadriceps tendon and patella as steel cables. Furthermore, their investigations were initially carried out at a flexion angle greater than 30 ° and the PF ligaments were not considered.

In the present study, the lateral and medial portions of the ligamentous structures surrounding the PF joint (LR and MPFL) were considered, resulting in a trend and magnitude that were consistent with the Fitzpatrick C.K. et al. (2010) study.

Figure 4.14 - Comparison of total patellofemoral contact area between the native model of the current study and the results obtained from the literature.

Figure 4.15 - Comparison of patellofemoral total force due to contact pressure between the native model of the current study and the results obtained from the literature.
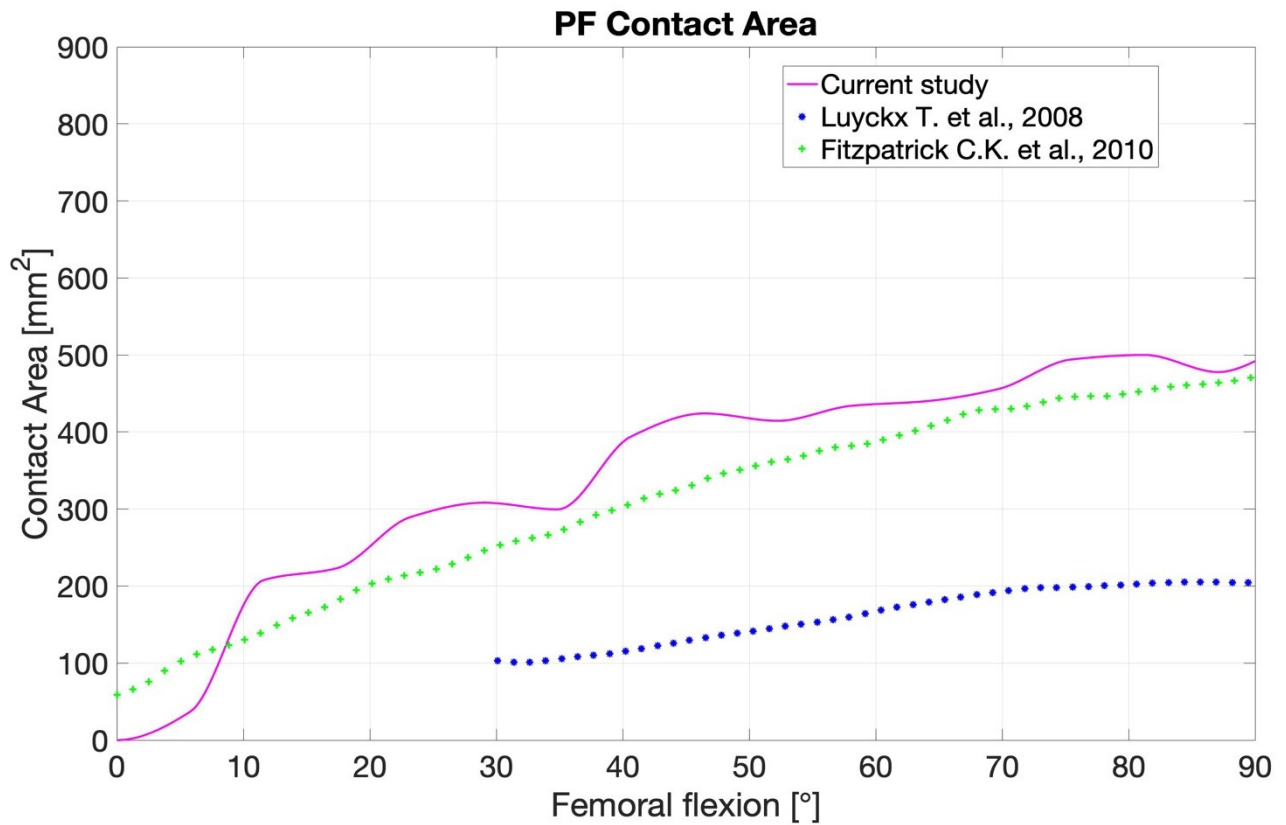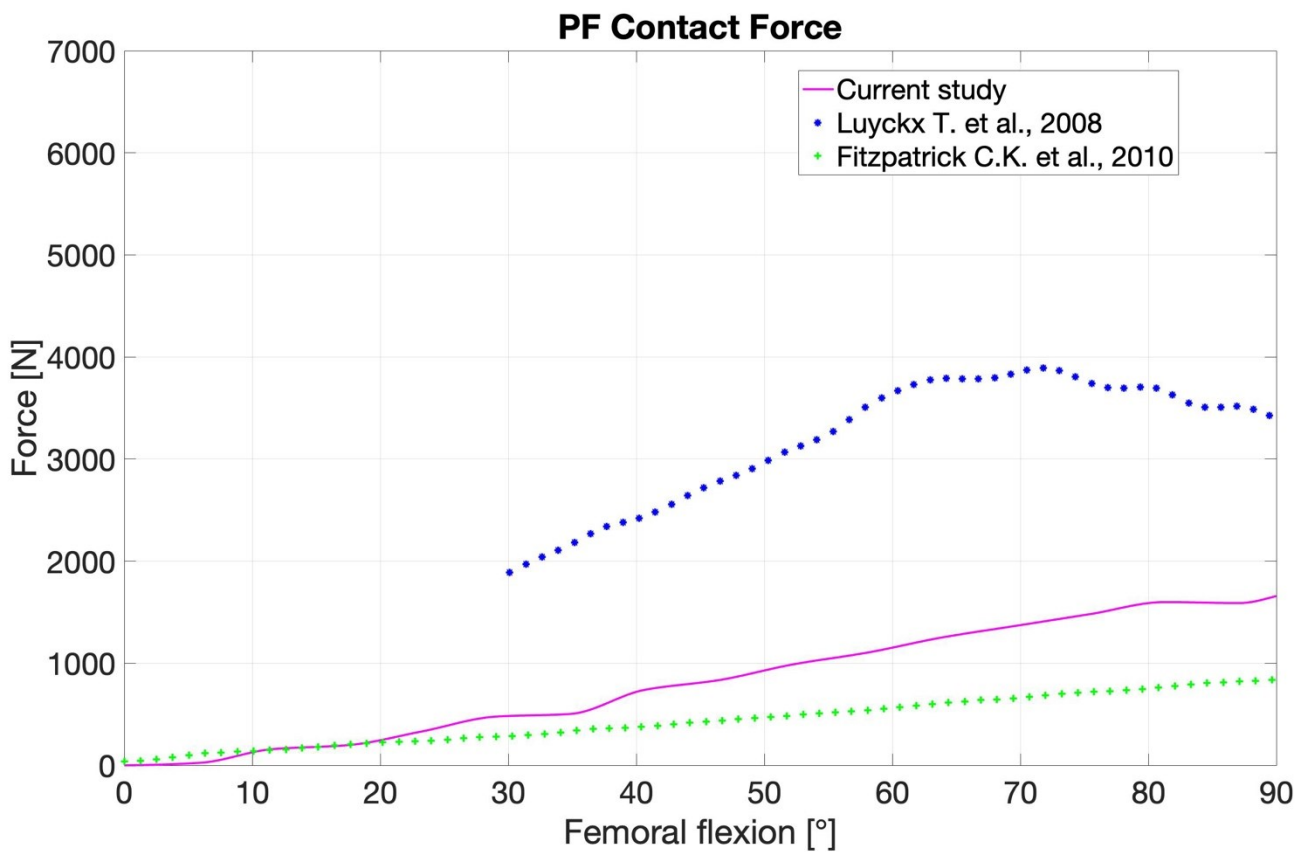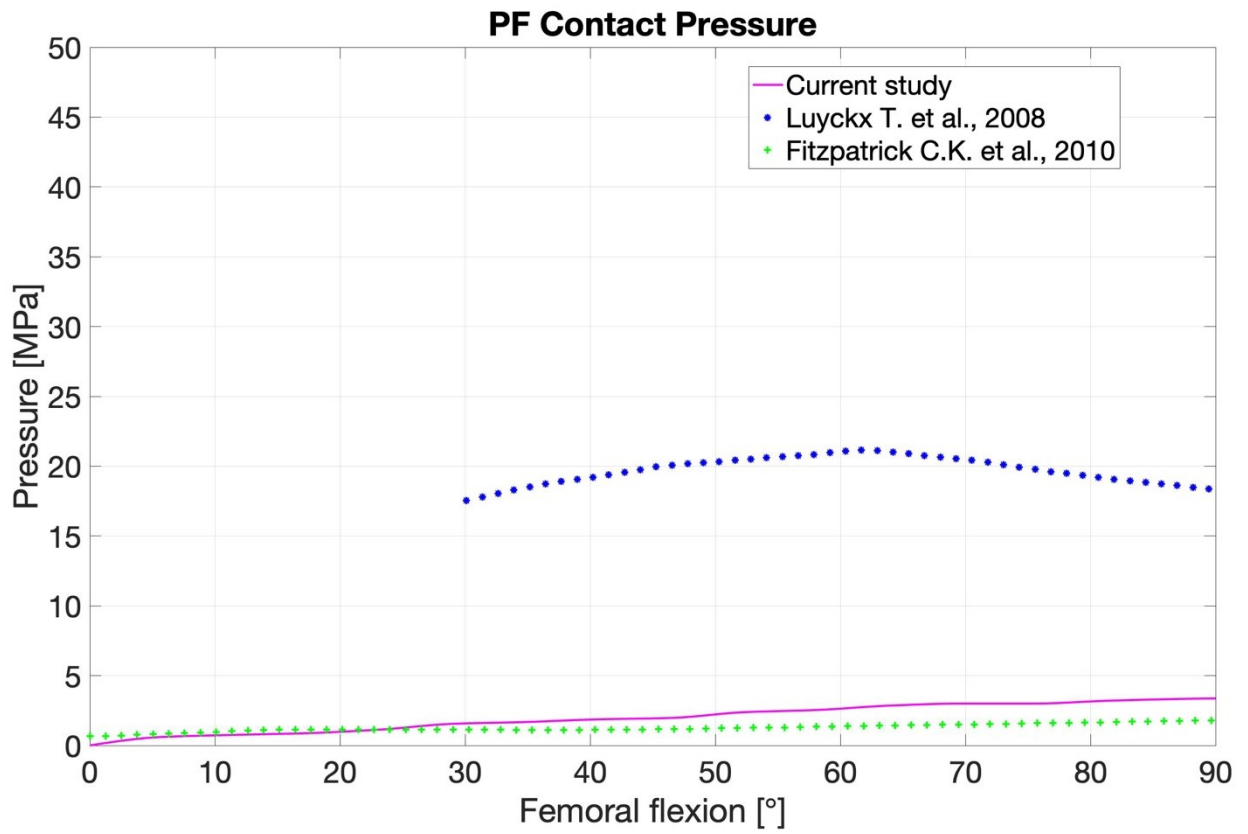
Figure 4.16 - Comparison of patellofemoral contact pressure between the native model of the current study and the results obtained from the literature.

4.3 LIMITATIONS AND PERSPECTIVES

There are several limitations and assumptions associated with the current study.

First, the study was conducted on a morphologically normal knee, but patella alta and baja are components of complex patellofemoral dysplasia in which other factors, such as malalignment and lateral tilt, can influence contact stresses. Second, the constitutive models for menisci and articular cartilage were assumed to be linear elastic isotropic, even though the menisci have transversely isotropic properties and articular cartilage show nonlinear and time-dependent poroviscoelastic behavior.

Moreover, although the shell structures for ligaments and tendons do allow increased fidelity due to wrapping, they were represented as linear elastic isotropic materials, even if they show nonlinear, anisotropic poroviscoelastic behavior. All these approximations were made for the sake of simplicity and because the aim of the study is to evaluate stress conditions due to different heights of the patella and not within soft tissues (ligaments, tendons, menisci, and cartilage).

Another limitation is that the current study was based on one specimen. Therefore it was not possible to take into account age-related effects or underlying diseases. Additionally, the kinematics and contact forces have not been directly compared with the experimental data for the same specimen. Finally, only the functional activity of a flexing motion was considered.

Even if this work is based on several assumptions and limitations, it could be used to facilitate the evalaution of the influence of patella height after a total knee arthroplasty (TKA) on patellofemoral contact forces and kinematics.

To improve this model, more realistic constitutive models for soft tissues should be used. Furthermore, the patellofemoral kinematics performance could be evaluated under a variety of loading and boundary conditions. Lastly, the results obtained must be verified against experimental measurements of the same specimen to evaluate the accuracy of the model predictions.

4.4 CONCLUSIONS

This computational study aims to analyze the biomechanical effect of different patella heights on patellofemoral contact forces and kinematics. Through a FE modeling approach, a native knee model was developed, which served as a reference model. Then, other two models were created, defining the height of the patella through the Blackburne-Peel index. Specifically, Blackburne-Peel indices of 0.59 for the patella baja and 1.29 for the patella alta were considered.

To examine the biomechanical impact of variation in patella height on femoral forces and kinematics, the following were analyzed: internal-external rotation of the tibia, antero-posterior translation of the femur, internal-external rotation of the patella, flexion-extension of the patella, anterior-posterior and medial-lateral translation of the patella relative to the femur and contact areas between the tibio-femoral and patellofemoral joints.

Considering the biomechanical role of the patella within the knee joint, a deviation from its physiological alignment leads to changes in the kinematics and contact forces of the patellofemoral joint. It appears that the patella alta has the largest total contact area and the lowest force due to contact pressure; this is because the point of contact with the femur is more distal than in the native and patella baja configuration and because the engagement of the patella in the trochlear groove occurs at deep degrees of flexion (over 90°).

Although this study is affected by a few limitations, the results obtained may provide new insight into the biomechanical effects of different patella heights on the patellofemoral kinematics.

BIBLIOGRAPHY

Abaqus Analysis User's Guide. [Online]. Available: http://130.149.89.49:2080/v6.14/books/usb/default.htm

Abaqus/CAE User's Guide. [Online]. Available: http://130.149.89.49:2080/v6.14/books/usi/default.htm

Akbar M., Farahmand F., & Arjmand N. (2019). *Mechanical characterization of the ligaments in subject-specific models of the patellofemoral joint using in vivo laxity tests*. The Knee, Vol. 26.

Akbar M., Farahmand F., Jafari A., & Foumani M. S. (2012). *A detailed and validated three dimensional dynamic model of the patellofemoral joint*. Journal of biomechanical engineering, Vol. 134.

Ali A. A., Shalhoub S. S., Cyr A. J., Fitzpatrick C. K., Maletsky L. P., Rullkoetter P. J., & Shelburne K. B. (2016). *Validation of predicted patellofemoral mechanics in a finite element model of the healthy and cruciate-deficient knee.* Journal of biomechanics, Vol. 49.

Amis A.A., Firerc P., Mountneyd J., Senavongsea W., Thomasd N.P. (2003). *Anatomy and biomechanics of the medial patellofemoral ligament.* The knee, Vol.10. Elsevier.

Baldwin M. A., Clary C. W., Fitzpatrick C. K., Deacy J. S., Maletsky L. P., & Rullkoetter P. J. (2012). *Dynamic finite element knee simulation for evaluation of knee replacement mechanics*. Journal of biomechanics, Vol.45.

Baldwin M. A., Clary C., Maletsky L. P., & Rullkoetter P. J. (2009). *Verification of predicted specimen-specific natural and implanted patellofemoral kinematics during simulated deep knee bend*. Journal of biomechanics, Vol. 42.

Bendjaballah MZ., Shirazi-Adl A., Zukor DJ., (1995). *Biomechanics of the human knee joint in compression: reconstruction, mesh generation and finite element analysis*. The Knee.

Blackburne J. S. & Peel T. E. (1977). *A new method of measuring patellar height.* The Journal of bone and joint surgery, Vol. 59.

Blankevoort L., & Huiskes R. (1991). *Ligament-bone interaction in a three-dimensional model of the knee*. Journal of biomechanical engineering, Vol. 113.

Blankevoort L., Kuiper J. H., Huiskes R., & Grootenboer H. J., (1991). *Articular contact in a three-dimensional model of the knee*. Journal of biomechanics.

Bolcos P. O., Mononen M. E., Mohammadi A., Ebrahimi M., Tanaka M. S., Samaan M. A., Souza R. B., Li X., Suomalainen J. S., Jurvelin J. S., Töyräs J., & Korhonen R. K. (2018). *Comparison between kinetic and kinetic-kinematic driven knee joint finite element models*. Scientific reports, Vol. 8.

Cowin S. C. & Doty S. B., (2007). *Tissue Mechanics*. Springer

Cox C. F., Sinkler M. A., Hubbard J. B. (2023). *Anatomy, Bony Pelvis and Lower Limb, Knee Patella*. StatPearls. [Online]. Available: https://www.ncbi.nlm.nih.gov/books/NBK519534/.

Criscenti G., De Maria C., Sebastiani E., Tei M., Placella G., Speziali A., Vozzi G., & Cerulli G. (2016). *Material and structural tensile properties of the human medial patello-femoral ligament*. Journal of the mechanical behaviour of biomedical materials, Vol.54.

Defrate L. E., Nha K. W., Papannagari R., Moses J. M., Gill T. J., & Li G. (2007). *The biomechanical function of the patellar tendon during in-vivo weight-bearing flexion*. Journal of biomechanics, Vol. 40.

DeVries Watson N. A., Duchman K. R., Bollier M. J., & Grosland N. M. (2015). *A Finite Element Analysis of Medial Patellofemoral Ligament Reconstruction*. The Iowa orthopeadic journal, Vol. 35.

Fitzpatrick C. K., Baldwin M. A., & Rullkoetter P. J. (2010). *Computationally efficient finite element evaluation of natural patellofemoral mechanics*. Journal of biomechanical engineering, Vol. 132.

Fox A. J., Wanivenhaus F., Burge A. J., Warren R. F., & Rodeo S. A. (2015). *The human meniscus: a review of anatomy, function, injury, and advances in treatment*. Clinical anatomy, Vol. 28.

Galbusera F., Freutel M., Dürselen L., D'Aiuto M., Croce D., Villa T., Sansone V., & Innocenti B. (2014*). Material models and properties in the finite element analysis of knee ligaments: a literature review*. Frontiers in bioengineering and biotechnology, Vol. 2.

Gao C. & Yang A. (2018). *Patellar Dislocations: Review of Current Literature and Return to Play Potential.* Current Physical Medicine and Rehabilitation Reports, Vol.6. Springer Science+Business Media.

Gilroy A. M., MacPherson B. R. & Ross L. M. (2008). *Atlas of anatomy.* Thieme. [Online]. Available: https://doctorlib.info/medical/anatomy/27.html.

Grood E. S., & Suntay W. J. (1983). *A joint coordinate system for the clinical description of three-dimensional motions: application to the knee.* Journal of biomechanical engineering, Vol. 105.

Guess T. M., Thiagarajan G., Kia M., & Mishra M. (2010). *A subject specific multibody model of the knee with menisci.* Medical engineering & physics, Vol. 32.

Hansen J.T., Netter F.H. & Machado C.A.G. (2019). *Netter's clinical anatomy* 4th edition. Elsevier.

Hashemi J., Chandrashekar N., & Slauterbeck J. (2005). *The mechanical properties of the human patellar tendon are correlated to its mass density and are independent of sex.* Clinical biomechanics (Bristol, Avon), Vol. 20.

Hassebrock J. D., Gulbrandsen M. T., Asprey W. L., Makovicka J. L., & Chhabra A. (2020). *Knee Ligament Anatomy and Biomechanics.* Sports medicine and arthroscopy review, Vol. 28.

Hirschmann M. T., Moser L. B., Amsler F., Behrend H., Leclercq V., & Hess S. (2019). *Phenotyping the knee in young non-osteoarthritic knees shows a wide distribution of femoral and tibial coronal alignment.* Knee surgery, sports traumatology, arthroscopy : official journal of the ESSKA, Vol.27.

Innocenti B. & Galbusera F. (2022). *Human Orthopaedic Biomechanics: Fundamentals, Devices and Applications.* 1th edition. Elsevier.

Innocenti B., Bellemans J., & Catani F. (2016a). *Deviations From Optimal Alignment in TKA: Is There a Biomechanical Difference Between Femoral or Tibial Component Alignment?.* The Journal of arthroplasty, Vol. 31.

Innocenti B., Bilgen Ö. F., Labey L., van Lenthe G. H., Sloten J. V., & Catani F. (2014). *Load sharing and ligament strains in balanced, overstuffed and understuffed UKA. A validated finite element analysis*. The Journal of arthroplasty, Vol. 29.

Innocenti B., Pianigiani S., Labey L., Victor J., & Bellemans J. (2011). *Contact forces in several TKA designs during squatting: A numerical sensitivity analysis*. Journal of biomechanics, Vol. 44.

Innocenti B., Salandra P., Pascale W., & Pianigiani S. (2016b). *How accurate and reproducible are the identification of cruciate and collateral ligament insertions using MRI?*. The Knee, Vol. 23.

Innocenti B., Truyens E., Labey L., Wong P., Victor J., & Bellemans J. (2009). *Can medio-lateral baseplate position and load sharing induce asymptomatic local bone resorption of the proximal tibia? A finite element study*. Journal of orthopedic surgery and research, Vol. 4.

Kayabasi O., Ekici B., (2007). *The effects of static, dynamic and fatigue behaviour on three-dimensional shape optimization of hip prosthesis by finite element method*. Materials & Design, Vol. 28. Elsevier.

Keaveny T.M., Morgan E.F., & Yeh O.C., (2005). Bone Mechanics.

Koshi R. (2017). *Cunningham's manual of practical anatomy.* Oxford University Press, 16th edition, Vol.1.

Kumbhalkar M. A., Rangari D. T., Pawar R. D., Phadtare R. A., Raut K. R., and Nagre A. N. (2021). *Finite Element Analysis of Knee Joint with Special Emphasis on Patellar Implant.* Springer Nature Singapore. E. T. Akinlabi et al. (eds.), *Trends in Mechanical and Biomedical Design* ,Lecture Notes in Mechanical Engineering.

Kwon O. S., Purevsuren T., Kim K., Park W. M., Kwon T. K., & Kim Y. H. (2014). *Influence of bundle diameter and attachment point on kinematic behaviour in double bundle anterior cruciate ligament reconstruction using computational model*. Computational and mathematical methods in medicine.

LaPrade R. F., Engebretsen A. H., Ly T. V., Johansen S., Wentorf F. A., & Engebretsen L. (2007). *The anatomy of the medial part of the knee*. The Journal of bone and joint surgery. American volume, Vol. 89.

Lee D., Stinner D., & Mir H. (2013). *Quadriceps and patellar tendon ruptures*. The journal of knee surgery, Vol. 26.

Loudon J. K. (2016). B*iomechanics and pathomechanics of the patellofemoral joint.* The International Journal of Sports Physical Therapy, Vol. 11.

Luyckx T., Didden K., Vandenneucker H., Labey L., Innocenti B., Bellemans J. (2009). *Is there a biomechanical explanation for anterior knee pain in patients with patella alta?: influence of patellar height on patellofemoral contact force, contact area and contact pressure.* The Journal of bone and joint surgery, Vol. 91.

Markes A. R., Hodax J. D., & Ma C. B. (2020). *Meniscus Form and Function*. Clinics in sports medicine, Vol. 39.

Marques Luís N. & Varatojo R. (2021). *Radiological assessment of lower limb alignment.* EFORT Open Reviews, Vol. 6.

Mesfar W., & Shirazi-Adl A. (2005). *Biomechanics of the knee joint in flexion under various quadriceps forces*. The Knee, Vol.12.

Mizuno Y., Kumagai M., Mattessich S. M., Elias J. J., Ramrattan N., Cosgarea A. J., Chao E. Y. (2001). *Q-angle influences tibiofemoral and patellofemoral kinematics*. Journal of orthopaedic research, Vol. 19. Elsevier.

Moser L. B., Hess S., de Villeneuve Bargemon J. B., Faizan A., LiArno S., Amsler F., Hirschmann M. T., & Ollivier M. (2022). *Ethnical Differences in Knee Phenotypes Indicate the Need for a More Individualized Approach in Knee Arthroplasty: A Comparison of 80 Asian Knees with 308 Caucasian Knees.* Journal of personalized medicine, Vol. 12.

Netter F. H. (2019). *Atlas of human anatomy*. 7th edition. Elsevier.

Peña E., Calvo B., Martínez M. A., & Doblaré M. (2006). *A three-dimensional finite element analysis of the combined behaviour of ligaments and menisci in the healthy human knee joint*. Journal of biomechanics, Vol. 39.

Peña E., Calvo B., Martínez M. A., Palanca D., & Doblaré M. (2005). *Finite element analysis of the effect of meniscal tears and meniscectomies on human knee biomechanics*. Clinical biomechanics, Vol. 20.

Pianigiani S, Croce D, D'Aiuto M, Pascale W, Innocenti B. (2018). *Sensitivity analysis of the material properties of different soft-tissues: implications for a subject-specific knee arthroplasty*. Muscles Ligaments Tendons Journal, Vol. 7.

Shah K.N., DeFroda S.F., Ware J.K., Koruprolu S.C., Owens B.D. (2017). *Lateral Patellofemoral Ligament: An Anatomic Study*. The Orthopaedic Journal of Sports Medicine, Vol. 5.

Shu L., Yamamoto K., Yoshizaki R., Yao J., Sato T., & Sugita N. (2022). *Multiscale finite element musculoskeletal model for intact knee dynamics*. Computers in biology and medicine.

Soenen M., Baracchi M., De Corte R., Labey L., & Innocenti B. (2013). *Stemmed TKA in a femur with a total hip arthroplasty: is there a safe distance between the stem tips?*. The Journal of arthroplasty, Vol. 28.

Standring S., Borley N. R., & Gray H. (2008). *Gray's anatomy: the anatomical basis of clinical practice*. 40th edition, Vol.2, Churchill Livingstone/Elsevier.

Stäubli H. U., Schatzmann L., Brunner P., Rincón L., & Nolte L. P. (1999). *Mechanical tensile properties of the quadriceps tendon and patellar ligament in young adults*. The American journal of sports medicine, Vol. 27.

Steensen R. N., Dopirak R. M., McDonald III W.G. (2004). *The Anatomy and Isometry of the Medial Patellofemoral Ligament. Implications for Reconstruction.* The American Journal of Sports Medicine, Vol. 32, No. 6.

Tecklenburg K., Dejour D., Hoser C., Fink, C. (2006). *Bony and cartilaginous anatomy of the patellofemoral joint*. Knee surgery, sports traumatology, arthroscopy: official journal of the ESSKA, Vol.14. Springer.

Unal B., Hinckel B. B., Sherman S. L., & Lattermann C. (2017). *Comparison of Lateral Retinaculum Release and Lengthening in the Treatment of Patellofemoral Disorders*. American journal of orthopedics (Belle Mead, N.J.), Vol. 46.

van Jonbergen H. P., Innocenti B., Gervasi G. L., Labey L., & Verdonschot N. (2012). *Differences in the stress distribution in the distal femur between patellofemoral joint replacement and total knee replacement: a finite element study*. Journal of orthopaedic surgery and research, Vol. 7.

Vaziri A., Nayeb-Hashemi H., Singh A., & Tafti B. A. (2008). *Influence of meniscectomy and meniscus replacement on the stress distribution in human knee joint*. Annals of biomedical engineering, Vol. 36.

Victor J., Van Doninck D., Labey L., Innocenti B., Parizel P. M., & Bellemans J. (2009a). *How precise can bony landmarks be determined on a CT scan of the knee?*. The Knee, Vol. 16.

Victor, J. (2009b). *A comparative study on the biomechanics of the native human knee joint and total knee arthroplasty* [Doctoral thesis in Medical Sciences]. Katholieke Universiteit Leuven, Group Biomedical Sciences, Faculty of Medicine, Department of Orthopaedics.

Weiss J. A., & Gardiner J. C. (2001). *Computational modeling of ligament mechanics.* Critical reviews in biomedical engineering, Vol. 29.

Xia Y., Momot K. (2017). *Biophysics and Biochemistry of Cartilage by NMR and MRI.* Royal Society of Chemistry Series "New Developments in NMR".

Zielinska B., & Donahue T. L. (2006). *3D finite element model of meniscectomy: changes in joint contact behaviour*. Journal of biomechanical engineering, Vol. 128.